AD-A170 371 LIGHT SCATTERING BY ROUGH SURFACES FULL WAVE SOLUTIONS 1/1
(U) E BAHAR MAY 86 CRDEC-CR-86024 DAAG29-81-D-0100

UNCLASSIFIED F/G 20/14 NL

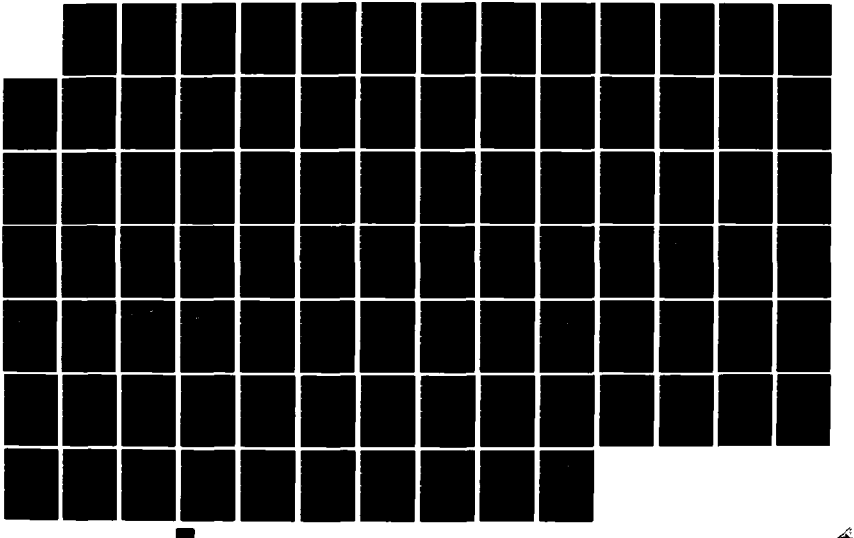

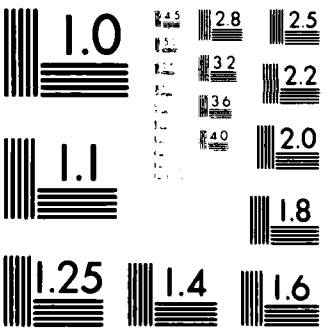

(12)

CHEMICAL
RESEARCH,
DEVELOPMENT &
ENGINEERING
CENTER

CRDEC-CR-86024

LIGHT SCATTERING BY ROUGH SURFACES FULL WAVE SOLUTIONS

by Ezekiel Bahar

E. Z. FULL WAVE ASSOCIATES
Lincoln, NE 68506

May 1986

U.S. ARMY
ARMAMENT
MUNITIONS
CHEMICAL COMMAND

Aberdeen Proving Ground, Maryland 21010-5423

Disclaimer

The findings in this report are not to be construed as an official Department of the Army position unless so designated by other authorizing documents.

Distribution Statement

Cleared for public release; distribution is unlimited.

UNCLASSIFIED
SECURITY CLASSIFICATION OF THIS PAGE

AD-A170 371

REPORT DOCUMENTATION PAGE

1a REPORT SECURITY CLASSIFICATION UNCLASSIFIED	1b RESTRICTIVE MARKINGS
2a SECURITY CLASSIFICATION AUTHORITY	3 DISTRIBUTION/AVAILABILITY OF REPORT Cleared for public release; distribution is unlimited.
2b DECLASSIFICATION/DOWNGRADING SCHEDULE	
4 PERFORMING ORGANIZATION REPORT NUMBER(S) CRDEC-CR-86024	5 MONITORING ORGANIZATION REPORT NUMBER(S)
6a NAME OF PERFORMING ORGANIZATION E.Z. Full Wave Associates 6b OFFICE SYMBOL (If applicable)	7a NAME OF MONITORING ORGANIZATION
6c ADDRESS (City, State, and ZIP Code) 3844 South 39th Street Lincoln, Nebraska 68506	7b ADDRESS (City, State, and ZIP Code)
8a NAME OF FUNDING/SPONSORING ORGANIZATION CRDEC 8b OFFICE SYMBOL (If applicable) SMCCR-RSP-B	9 PROCUREMENT INSTRUMENT IDENTIFICATION NUMBER DAAG29-81-D-0100
8c ADDRESS (City, State, and ZIP Code) Aberdeen Proving Ground, Maryland 21010-5423	10 SOURCE OF FUNDING NUMBERS PROGRAM ELEMENT NO. / PROJECT NO. / TASK NO. D.O. 1854 / WORK UNIT ACCESSION NO.

11 TITLE (Include Security Classification)
Light Scattering By Rough Surfaces Full Wave Solutions

12 PERSONAL AUTHOR(S)
Bahar, Ezekiel

13a TYPE OF REPORT	13b TIME COVERED	14 DATE OF REPORT (Year, Month, Day)	15 PAGE COUNT
Contractor	FROM 85 09 TO 86 02	1986 May	91

16 SUPPLEMENTARY NOTATION
COR: Mr. Robert Frickel, SMCCR-RSP-B, (301) 671-2326

17 COSATI CODES		
FIELD	GROUP	SUB-GROUP
20	03	
20	06	

18 SUBJECT TERMS (Continue on reverse if necessary and identify by block number)
Scattering; Depolarization; Full Wave approach; Diffuse specific intensities; transfer equation
(continued on reverse)

19 ABSTRACT (Continue on reverse if necessary and identify by block number)

Scattering of electromagntic waves in media consisting of random distributions of particles such as atmospheric aerosols, smoke and dust has been investigated extensively using the equation of transfer. The main difficulties in setting up the equation of transfer lies in the determination of the elements of the 4x4 phase (scattering) matrix and the extinction cross sections for the individual particles. Most of the work has been done for particles of idealized shapes such as spheres and cylinders.

In many physical problems of interest, however, the individual scatterers are of irregular shapes such as flakes, spheres and cylinders with random rough surfaces.

In this work the results derived for particles with idealized shapes (spheres) are modified to account for the random surface roughness of the particles. To this end the full wave approach is used to determine the rough surface contributions to the (continued on reverse)

20 DISTRIBUTION/AVAILABILITY OF ABSTRACT	21 ABSTRACT SECURITY CLASSIFICATION
☒ UNCLASSIFIED/UNLIMITED ☐ SAME AS RPT. ☐ DTIC USERS	UNCLASSIFIED
22a NAME OF RESPONSIBLE INDIVIDUAL TIMOTHY E. HAMPTON	22b TELEPHONE (Include Area Code) (301) 671-2914
	22c OFFICE SYMBOL SMCCR-SPD-R

DD FORM 1473, 84 MAR — 83 APR edition may be used until exhausted. All other editions are obsolete.

SECURITY CLASSIFICATION OF THIS PAGE
UNCLASSIFIED

18. SUBJECT TERMS (continued).

albedos
extinction intensities
Stokes parameters

19. ABSTRACT (continued).

like and cross polarized scattering cross sections, and the elements of the phase (scattering) matrix are given in terms of the weighted sum of the Mie solutions and the diffuse scattering terms due to the particle surface roughness. The extinction cross sections are determined through a judicious use of the forward scattering theorem and the very perceptive observation that for the large scatterers compared to a wavelength the forward scattered "shadow forming wave is the same for all surfaces which have the same shadowline."

Linearly polarized waves are assumed to be incident upon a parallel layer consisting of a random distribution of irregular shaped particles. Particles with different complex dielectric coefficients and different surface roughness are considered. The rough surface height is characterized by it surface height spectral density functions (the Fourier transforms of the non-Gaussian surface height autocorrelation functions). The particles with a large range of roughness scales are considered. Special attention is given to determining the effects of varying the mean square height and slope of the particles.

Both single scatter (first order) and multiple scatter results are presented for smooth particles and for particles with rough surfaces. The results are presented for the forward and backward scattered incoherent diffuse scattering intensities as well as the co-polorized and cross polarized intensities. The degree of polarization of the reflected and transmitted intensities are also determined. The Gaussian quadrature technique is used to discritize the equation of transfer and the matrix characteristic value techniques is used to account for multiple scattering.

PREFACE

The work described in this report was authorized under Contract No. DAAG29-81-D-0100. This work was started in September 1985 and completed in February 1986.

The use of trade names or manufacturers' names in this report does not constitute endorsement of any commercial products. This report may not be cited for purposes of advertisement.

This report has been approved for release to the public.

ACKNOWLEDGMENTS

This work was sponsored by the U.S. Army Research Office under Contract Number DAAG29-81-D-0100. The Project Monitor is Robert Frickel, U.S. Chemical Research, Development and Engineering Center, SMCCR-RSP-B, Aberdeen Proving Ground, Maryland 21010-5423.

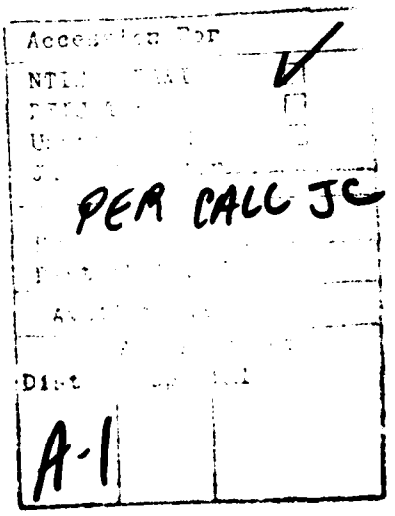

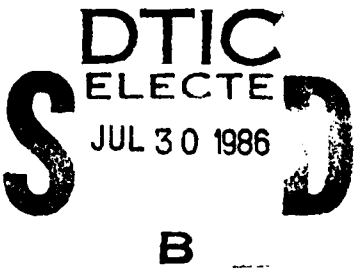

CONTENTS

LIGHT SCATTERING BY ROUGH SURFACES FULL WAVE SOLUTIONS

1. Introduction

1.1 Objectives, Motivation and Background for this Work

Scattering of electromagnetic waves in media consisting of random distributions of particles such as atmospheric aerosols, smoke and dust has been investigated extensively using the equation of transfer (Chandrasekhar 1950, Ishimaru 1978). The main difficulties in setting up the equation of transfer lie in the determination of the elements of the 4x4 phase (scattering) matrix and the extinction cross sections for the individual particles. Most of the work has been done for particles of idealized shapes such as spheres and cylinders (Ruck et al. 1970).

In many physical problems of interest however, the individual scatterers are of irregular shapes such as flakes, spheres and cylinders with random rough surfaces (Scheurman 1980, Bahar and Fitzwater 1983, Bahar and Chakrabarti 1985).

In this work the results derived for particles with idealized shapes (spheres) are modified to account for the random surface roughness of the particles. To this end the full wave approach (Bahar 1981) is used to determine the rough surface contributions to the like and cross polarized scattering cross sections (Bahar and Chakrabarti 1985), and the elements of the phase (scattering) matrix are given in terms of a weighted sum of the Mie solutions and the diffuse scattering terms due to the particle surface roughness. The extinction cross sections are determined through a judicious use of the forward scattering theorem (Born and Wolf 1964) and the very perceptive observation that for large scatterers compared to a wavelength the forward scattered "shadow forming wave is the same for all surfaces which have the same shadowline" (Morse and Feshbach 1953).

Linearly polarized waves are assumed to be incident upon a parallel layer consisting of a random distribution of irregular shaped particles. Particles with different complex dielectric coefficients and different surface roughness are considered. The rough surface height is characterized by its surface height spectral density functions (the Fourier transforms of the non-Gaussian surface height autocorrelation functions). Thus particles with a large range of roughness scales are considered. Special attention is given to determining the effects of varying the mean square height and slope of the particles.

Both single scatter (first order) and multiple scatter results are presented for smooth particles and for particles with rough surfaces. Layers with different optical thicknesses are considered and the results are presented for the forward and backward scattered incoherent diffuse scattering intensities as well as the co-polarized and cross polarized intensities. The degree of polarization of the reflected and transmitted intensities are also determined. The Gaussian quadrature technique is used to discretize the equation of transfer and the matrix characteristic value technique is used to account for multiple scattering (Ishimaru and Cheung 1980). This work is particularly relevant to problems of obscuration by aerosols.

1.2 Principal Elements of the Full Wave Approach

As indicated in Section 1.1, the full wave solutions for the scattered like and cross polarized intensities are determined using the full wave approach which accounts for the specular point (physical optics) scattering and diffuse scattering in a self-consistent manner. Unlike the small perturbation method (Rice 1951, Ruck et al. 1970, Kiehl et al. 1980), the full wave approach is not restricted to surfaces with small roughness

parameters $\beta = 4k_o^2\langle h^2\rangle$ (where $\langle h^2\rangle$ is the mean square height and k_o is the free space wavenumber of the incident electromagnetic wave). The principal elements of the full wave approach (Bahar 1982) are:

(a) The electromagnetic fields are expressed in terms of complete expansions of vertically and horizontally polarized waves. These include the radiation fields, the lateral waves and the surface waves.

(b) Exact boundary conditions are imposed at the irregular surface.

(c) Using the orthogonal properties of the basis functions appearing in the complete expansions of the fields, Maxwell's equations are integrated over the transverse plane. Green's theorems are used to avoid term-by-term differentiation of the field expansions.

(d) Maxwell's equations for the electromagnetic fields are converted into coupled first order ordinary differential equations for the forward and backward traveling wave amplitudes which are only functions of the variable x. (In view of the integration in the transverse plane (y,z), the telegraphists' equations are only functions of x). The coupled equations for the wave amplitudes are referred to the generalized telegraphists' equations.

(e) A variable coordinate system that conforms with the local features of the irregular boundary is introduced and the resulting solutions for the scattered fields are shown to be invariant to coordinate transformations.

(f) Closed form second order iterative solutions for the radiation fields are obtained from the telegraphists' equations on neglecting multiple scattering from the rough surface. These second order iterative solutions account for wave scattering in arbitrary directions.

(g) The full wave solutions are compared with earlier geometric optics physical optics and perturbation solutions. The suitability of the two-scale model is shown to be limited.

2. Outline of this Research

(i) Evaluate the like and cross polarized scattering cross sections for particles of irregular shape. The particles are characterized by their complex permittivities (unperturbed) sizes, rough surface height spectral density functions--(or autocorrelation functions). The full wave approach (see Section 1.2), is used to account for specular point and diffuse scattering in a self-consistent manner.

(ii) Evaluate the extinction cross sections and the albedos for the irregular particles of finite conductivity.

(iii) Solve the transfer equation for the incoherent specific intensities (modified Stokes parameters), and the co-polarized and cross polarized intensities for linearly polarized waves at optical and infrared frequencies incident upon a layer of randomly distributed particles. Compare the results for smooth and rough particles. Present both single scatter and multiple scatter results.

(iv) Evaluate the degree of polarization of the reflected and transmitted intensities.

(v) Document computer programs for inclusion in the final report.

3. Formulation of the Problem

The transfer equation for the diffuse specific intensities (Stokes parameters) can be written as follows in matrix notation (Chandrasekhar 1950, Ishimaru 1978)

$$\mu \frac{d[I]}{d\tau} = -[I] + \int [S][I']d\mu' d\phi' + [I_i] \tag{1}$$

in which τ is the optical distance in the z direction (normal to the plane of a horizontal layer consisting of a random distribution of particles (see Fig. 1)

$$\tau = z\rho[\sigma_t] \equiv z \int \sigma_t \, h(D)dD \tag{2}$$

where D is the diameter of the unperturbed spherical particle, n(D) is the particle size distribution and σ_t is the extinction coefficient (total cross section). The symbol $z[\cdot]$ denotes integration over the size distribution. Since the unperturbed particle is assumed here to be a sphere of diameter D and the surface roughness is assumed to be homogeneous and isotropic, diffuse scattering vanishes in the forward direction (Bahar and Chakrabarti 1985) and the extinction matrix for the rough sphere can be represented by a scalar quantity (Ishimaru and Cheung 1980). The (4x1) column matrices [I] and [I'] are the incoherent diffuse specific intensity matrices (Stokes parameters) for waves scattered by particles in the direction $\theta = \cos^{-1}\mu$ and ϕ and for waves incident in the direction $\theta' = \cos^{-1}\mu'$ and ϕ' respectively. The elements of the matrix [I] are the modified Stokes parameters

$$[I] = \begin{bmatrix} I_1 \\ I_2 \\ U \\ V \end{bmatrix} = \begin{bmatrix} \langle E_1 E_1^* \rangle \\ \langle E_2 E_2^* \rangle \\ 2\mathrm{Re}\langle E_1 E_2^* \rangle \\ 2\mathrm{Im}\langle E_1 E_2^* \rangle \end{bmatrix} \tag{3}$$

in which the symbol $\langle\cdot\rangle$ denotes the statistical average and the symbol * denotes the complex conjugate. An $\exp(i\omega t)$ suppressed time dependent

excitation is assumed. The vertically and horizontally polarized components of the electric field are E_1 and E_2 respectively. The (4x4) scattering (phase) matrix S in the fixed reference coordinate system (see Fig. 1) is expressed in terms of the scattering matrix S' in the scattering plane (which contains the wave normals $\bar{n}^i$ and $\bar{n}^f$ in the direction of the incident and scattered waves) through the following transformation

$$[S] = [\mathcal{L}(-\pi + \alpha)][S'][\mathcal{L}(\alpha')] \tag{4}$$

in which [S'] is the weighted sum of two matrices

$$[S'] = |\chi(\bar{v}\cdot\bar{a}_r)|^2[S_{Mie}] + [S_D] \tag{5}$$

In (4) $[\mathcal{L}]$ is a 4x4 transformation matrix that represents the specific intensities relative to the reference plane of incidence to the intensities relative to the scattering plane and back from the scattering plane to the reference plane of scatter (Chandrasekhar 1950, Ishimaru 1978). The matrix $[S_{Mie}]$ in (5) is the plase matrix for the unperturbed spheres based on the Mie solution (Ruck et al. 1970, Ishimaru 1978). Furthermore, in (5) $\chi(\bar{v}\cdot\bar{a}_r)$ is the particle random rough surface height characteristic function

$$\chi(\bar{v}\cdot\bar{a}_r) = \exp\langle i\bar{v}\cdot\bar{a}_r h\rangle \tag{6}$$

in which h is the rough surface height measured in the direction $\bar{a}_r$, the unit vector in the radial direction (normal to the surface of the unperturbed sphere) and

$$\bar{v} = k_o(\bar{n}^f - \bar{n}^i) \tag{7}$$

In this work the rough surface height probability density function p(h) and joint probability function p(h,h') are assumed to be Gaussian, thus

$$|\chi|^2 = \exp(-\bar{v}\cdot\bar{a}_r\langle h^2\rangle) \tag{8}$$

and the rough surface height joint characteristic function is

$$\chi_2 = \langle \exp[i\bar{v}\cdot\bar{a}_r(h-h')]\rangle = \exp(\bar{v}\cdot\bar{a}_r\langle hh'\rangle)|\chi|^2 \tag{9}$$

Thus in (5) the coefficient $|\chi|^2$ accounts for the degradation of the scattering by the smooth sphere(primarily specular point for spheres with large k_oD) due to surface roughness. The diffuse scattering contribution to the phase matrix [S'] due to surface roughness is

$$[S_D] = \begin{bmatrix} [S_{11}^D] & [S_{12}^D] & 0 & 0 \\ [S_{21}^D] & [S_{22}^D] & 0 & 0 \\ 0 & 0 & [S_{33}^D] & [S_{34}^D] \\ 0 & 0 & [S_{43}^D] & [S_{44}^D] \end{bmatrix} \tag{10}$$

where

$$[S_{ij}^D] = \frac{A_y}{4\pi\rho[\sigma_t]}\,\rho[\langle\sigma^{ij}\rangle_D] \quad \text{for } i,j=1,2 \tag{11}$$

in which $A_y = \pi D^2/4$ is the cross sectional area of the unperturbed particle and $\langle\sigma^{ij}\rangle_D$ in (11) is the like (i=j) or cross ($i\neq j$) cross polarized normalized scattering cross section (Bahar and Chakrabarti 1985). The first and second superscripts i,j denote the polarization (V vertical, H horizontal) of the scattered and incident fields respectively

$$\langle\sigma^{ij}\rangle_D = \int_0^{2\pi}\int_0^{\pi} |k_o D^{ij}|^2 P_2 Q \sin\gamma d\gamma d\delta/\pi^2 \tag{12}$$

in which

$$Q = \int_{-\infty}^{\infty} (\chi_2(\bar{v}\cdot\bar{a}_r) - |\chi(\bar{v}\cdot\bar{a}_r)|^2)\exp(i\bar{v}\cdot\bar{r}_d)dx_d dz_d \tag{13}$$

The surface height autocorrelation function $\langle hh'\rangle$ and therefore the joint characteristic function χ_2 (9) are only functions of distance $r_d=(x_d^2+z_d^2)^{\frac{1}{2}}$ measured along the surface of the unperturbed sphere since the random rough surface is assumed to be isotropic and homogeneous. Furthermore,

$$[S_{ii}^D] = A_y\,\rho[\mathrm{Re}[\langle\sigma_{22}^{11}\rangle_D \pm \langle\sigma_{21}^{12}\rangle_D]]/4\pi\rho[\sigma_t] \tag{14}$$

for i=3 (upper sign) and i=4 (lower sign). For $i\neq j$

$$[S_{ij}^D] = A_y\,\rho[\mathrm{Im}[\pm\langle\sigma_{22}^{11}\rangle_D + \langle\sigma_{21}^{12}\rangle_D]]/4\pi\rho[\sigma_t] \tag{15}$$

where the upper sign is used for i=4, j=3 and the lower sign is used for i=3, j=4. In (14) and (15)

$$\langle \sigma_{k\ell}^{ij} \rangle = \int_0^{2\pi} \int_0^{\pi} k_o^2 D^{ij} D^{k\ell *} P_2 Q \sin\gamma d\gamma d\delta / \pi^2 \tag{16}$$

In (12) and (16) P_2 is the shadow function (Sancer 1969). It is the probability that a point on the surface is both illuminated and visible given the slope of the surface at that point. The scattering coefficients D^{ij} are functions of $\bar{n}^i, \bar{n}^f$ and $\bar{n}$ the normal to the unperturbed surface of the particle as well as the electromagnetic parameters of the material of the particle ε, μ (Bahar 1981). Since D^{ii} and D^{ij} $(i \neq j)$ are symmetric and antisymmetric respectively with respect to the azimuth angle, δ, of the particle, the remaining eight terms of $[S_D]$ vanish.

A linearly polarized wave is assumed to be normally incident upon a parallel layer (of optical thickness τ_o), containing a random distribution of irregular shaped particles. Thus, the incident Stokes matrix at z=0 (see Fig. 1) is

$$[I_{inc}] = \begin{bmatrix} 1 \\ 0 \\ 0 \\ 0 \end{bmatrix} \delta(\mu'-1)\delta(\phi') \equiv [I_o]\delta(\mu'-1)\delta(\phi') \tag{17}$$

in which $\delta(\cdot)$ is the Dirac delta function. Thus, the reduced incident intensity is

$$[I_{ri}] = [I_{inc}]\exp(-\tau) \tag{18}$$

The (4x1) excitation matrix $[I_i]$ in (1) is

$$[I_i] = \int [S][I_{ri}] d\mu' d\phi' = [F]\exp(-\tau) \tag{19}$$

in which [F] can be expressed as

$$[F] = [S][I_o]\Big|_{\substack{\mu'=1 \\ \phi'=o}} \equiv [F]_o + [F]_a \cos 2\phi + [F]_b \sin 2\phi \tag{20}$$

and the matrix $[I_o]$ is defined in (17). The solution of the equation of

transfer (1) for the incoherent specific intensity matrix [I] can be expanded in a Fourier Series (Cheung and Ishimaru 1982). In view of the excitation (20), only the azimuthally independent term (m=o) and the $\cos 2\phi$ and $\sin 2\phi$ terms (m=2) are non-vanishing. Thus, the transfer equation (1) together with the associated boundary conditions

$$[I] = 0 \quad , \quad \text{for } 0 \leq \mu \leq 1 \text{ at } \tau = 0 \tag{21}$$

and

$$[I] = 0 \quad , \quad \text{for } 0 \geq \mu \geq -1 \text{ at } \tau = \tau_o \tag{22}$$

are solved for the specific incoherent diffuse scattering intensities using the Gaussian quadrature method (to discretize the angles $\theta=\cos^{-1}\mu$) and the matrix characteristic value technique (Ishimaru 1978).

The only remaining parameter that needs to be evaluated to solve the equation of transfer (1) is the extinction coefficient (total cross section) σ_t. The "forward scattering theorem" (Born and Wolf 1964) relates the total cross section to the imaginary part of the scattering (complex) amplitude in the forward direction $f_{ii}(\bar{n}^f,\bar{n}^i)$ (Ishimaru 1978). Thus, for a spherical particle, the normalized total cross section (per unit cross sectional area of the sphere of radius a) is

$$\sigma_t = \frac{4}{k_o a^2} \operatorname{Im}[f_{ii}(\bar{n}^f,\bar{n}^i)] \qquad i=1,2 \tag{23}$$

For particles with irregular shape and particles with random rough surfaces, it is very difficult to determind the scattering amplitude f_{ii}. When the surface roughness of the particle is small, such that the roughness parameter $\beta=4k_o^2\langle h^2\rangle \ll 1$, perturbation theory can be used to determine the diffuse scattering contribution (Rice 1951, Ruck et al. 1970). In this case ($\beta \ll 1$) σ_t can be approximated by its unperturbed value since the diffuse scattering contribution $[S_D]$ for large particles vanishes in the forward direction and the shadow boundary is practically the same as that

of the unperturbed particle. However, for the small perturbation case, the effects of particle surface roughness upon the specific intensities is almost negligible. Since in this work particles with very rough surfaces $1 \leq \beta \leq 40$ are considered, small perturbation theory cannot be used to determine the scattering amplitudes f_{ii}, and the effects of surface roughness upon the specific intensities is not negligible. To facilitate the solution to the problem when β is large, judicious use is made of the scattering theorem and the perceptive observation that for large scatterers (physical dimensions large compared to wavelength) the forward scatter "shadow forming wave is the same for all surfaces which have the same shadow line" (Morse and Feshbach 1953). Thus, the albedos A for the particles with random rough surfaces are evaluated as follows

$$A = \frac{\sigma_s}{\sigma_t} = \frac{\sigma_s}{\sigma_{to}} \frac{\sigma_{to}}{\sigma_t} \simeq \frac{\sigma_s}{\sigma_{to}} \left(\frac{\sigma_{to}}{\sigma_t}\right)_{P.C.} \tag{24}$$

In (24) σ_s, the normalized scattering cross sections for the finitely conducting particles, are given by

$$\sigma_s = \frac{1}{\pi a^2} \int |\chi^2| \sigma_M d\Omega + \frac{1}{4\pi} \int \langle\sigma\rangle_D d\Omega$$

$$\equiv \sigma_{s1} + \sigma_{s2} \tag{25}$$

in which χ is the rough surface characteristic function σ_M is the Mie solution for the smooth (unperturbed) sphere (Ruck et al. 1970, Ishimaru 1978) and $d\Omega$ is the elementary solid angle. Thus integrate with respect to the azimuth angle to get (in the notation used by Ishimaru, 1978)

$$\sigma_{s1} = (k_o a)^{-2} \int |\chi|^2 [|S_1(\theta)|^2 + |S_2(\theta)|^2] \sin\theta d\theta \tag{26}$$

The full wave approach is used to obtain the diffuse contribution σ_{s2} to the scattering cross section. Thus

$$\sigma_{s2} = 0.25 \int (\langle\sigma^{VV}\rangle_D + \langle\sigma^{VH}\rangle_D + \langle\sigma^{HV}\rangle_D + \langle\sigma^{HH}\rangle_D) \sin\theta d\theta \tag{27}$$

in which $\langle\sigma^{PQ}\rangle_D$ are the like and cross polarized diffuse differential

scattering cross sections per unit solid angle (Bahar and Fitzwater 1983, Bahar and Chakrabarti 1985). Furthermore, in (24), σ_{to} is the total cross section for the smooth particle. On approximating (σ_{to}/σ_t) by its corresponding, perfectly conducting value $(\sigma_{to}/\sigma_t)_{P.C.}$ use is made of the forward scattering theorem and the fact that for $k_o a \gg 1$, the forward scatter, shadow-forming wave is the same for all surfaces which have the same shadow line. Since for perfectly conducting particles

$$(\sigma_t)_{P.C.} = (\sigma_s)_{P.C.} \tag{28}$$

where $(\sigma_s)_{P.C.}$ is the normalized scattering cross section for the perfectly conducting particle with the same rough surface as the one under consideration. Thus $(\sigma_s)_{P.C.}$ is evaluated using (25) for the corresponding perfectly conducting particle and the expression for the albedo is given by

$$A = [\sigma_s/\sigma_{to}]/[\sigma_s/\sigma_{to}]_{P.C.} = A_1/A_2 \quad . \tag{29}$$

Two limiting cases for the above expression are of particular interest. As the conductivity of the particle increases to infinity $A_1 \to A_2$ and $A \to 1$. As the surface roughness becomes very small $\beta \to 0$, $A_2 \to 1$, (since $(\sigma_s)_{P.C.} \to (\sigma_t)_{P.C.} \to (\sigma_{to})_{P.C.}$) and $A \to A_1 = \sigma_s/\sigma_{to}$. Thus as expected $A \to 1$ for perfectly conducting particles and $A \to A_1$ its corresponding unperturbed value for $\beta \to 0$. The value of the extinction coefficient σ_t is obtained from the relationship $\sigma_t = \sigma_s/A$.

4. Summary of Results and Conclusions

4.1 Illustrative Examples

For the illustrative examples presented in this section, the random rough surface height h (measured normal to the surface of the unperturbed spherical surface of the particle of radius a) is characterized by its surface height spectral density function $W(k_x,k_z)$. Since the random rough surface is assumed to be isotropic and homogeneous, the spectral density function is expressed as a function of $k_T = (k_x^2+k_z^2)^{\frac{1}{2}}$

$$W(k_T) = W(k_x,k_z) = \frac{1}{\pi^2}\int_{-\infty}^{\infty} \langle hh' \rangle \exp(ik_x x_d + ik_z z_d)dx_d dz_d$$

$$= \frac{2}{\pi}\int_{o}^{\infty} \langle hh' \rangle J_o(k_T r_d) r_d dr_d \quad . \tag{29}$$

In (29) $J_o(k_T r_d)$ is the Bessel function of the first kind and $\langle hh' \rangle$ is the rough surface height autocorrelation function which is only a function of distance $r_d = (x_d^2+z_d^2)^{\frac{1}{2}}$ measured along the surface of the unperturbed particle. In view of the Fourier transform relationship between $W(k_T)$ and $\langle hh' \rangle$

$$\langle hh' \rangle = \int_{-\infty}^{\infty} \frac{W(k_x,k_z)}{4} \exp(-ik_x x_d - ik_z z_d)dk_x dk_z$$

$$= \frac{\pi}{2}\int_{o}^{\infty} W(k_T) J_o(k_T r_d) k_T dk_T \tag{30}$$

The following explicit expressions are assumed in this work for the surface height spectral density function

$$W(k_T) = \frac{2C}{\pi}\left[\frac{k_T}{k_T^2+k_m^2}\right]^n \quad , \; k_T > 0 \tag{31}$$

in which the exponent is n = 6 case (a) and n = 8 case (b). The value of $W(k_T)$ is maximum for $k_T = k_m$ (the dominant roughness scale)

$$W(k_m) = 2C/\pi\, k_m^n \tag{32}$$

For n = 8 the scales of roughness are more tightly bound around k_m than for n = 6. The mean square height $\langle h^2 \rangle$ and mean square slope $\langle \sigma_s^2 \rangle$ of the

rough surface are related to k_m and the constant C. Thus

$$\langle h^2 \rangle = \frac{\pi}{2} \int_0^\infty W(k_T) k_T dk_T = \begin{cases} C/210\, k_m^6 & , \quad n = 8 \\ C/40 k_m^4 & , \quad n = 6 \end{cases} \tag{33}$$

and

$$\langle \sigma_s^2 \rangle = \frac{\pi}{2} \int_0^\infty W(k_T) k_T^3 dk_T = \begin{cases} C/84\, k_m^4 & , \quad n = 8 \\ C/10\, k_m^2 & , \quad n = 6 \end{cases} \tag{34}$$

and the surface height correlation distance r_c (where $\langle hh' \rangle = \exp(-1)$ is

$$r_c \simeq 2(\langle h^2 \rangle / \langle \sigma_s^2 \rangle)^{\frac{1}{2}} = \begin{cases} 1.265/k_m & , \quad n = 8 \\ 1/k_m & , \quad n = 6 \end{cases} \tag{35}$$

The autocorrelation functions corresponding to the rough surface height spectral density functions (31) can be written in closed form. Thus for n = 8

$$R(\xi) = \left[1 - \frac{3\xi^2}{8} + \frac{3\xi^4}{32} + \frac{\xi^6}{3072}\right] \xi K_1(\xi) + \left[\frac{1}{2} - \frac{\xi^2}{4} - \frac{\xi^4}{96}\right] \xi^2 K_o(\xi) \tag{36a}$$

and for n = 6

$$R(\xi) = \left[1 - \frac{3\xi^2}{4} - \frac{\xi^4}{96}\right] \xi K_1(\xi) + \left[\frac{1}{2} + \frac{3}{16}\xi^2\right] \xi^2 K_o(\xi) \tag{36b}$$

in which K_o and K_1 are the modified Bessel functions of the second kind or order zero and one respectively (Abramowitz and Stegun 1964) and the dimensionless argument ξ is

$$\xi = k_m r_d \tag{37}$$

The wavelength of the optical excitation is

$$\lambda = 0.555\mu \tag{38}$$

and the diameter of the unperturbed sphere is

$$D = 10\lambda \tag{39}$$

The particles are assumed to be made of (i) aluminum for which the relative dielectric coefficient is (Ehrenreich 1965)

$$\varepsilon_r = -40\text{-}i12 \tag{40a}$$

and (ii) a dissipative dielectric with

$$\varepsilon_r = 1.5\text{-}i8 \tag{40b}$$

Two sets of data for each case n = 6 and n = 8 and each dielectric material are presented graphically in this work. In the first set $k_m D = 4$; thus the correlation length r_c is fixed (35) while both the mean square height and slope vary. The maximum value of $\langle\sigma_s^2\rangle$ is 0.101 corresponding to $\beta_m = 4k_o^2\langle h^2\rangle = 40$ for n = 8 and $\beta_m = 25$ for n = 6. In the second set the mean square slope $\langle\sigma_s^2\rangle$ is set equal to 0.101 while both the mean square height $\langle h^2\rangle$ and k_m (and thus r_c) vary.

In Tables I through VI the value of the scattering cross sections σ_{s1}, σ_{s2} and σ_s (24) as well as A_1, A_2 the albedo A (28) and the extinction coefficient σ_t are listed for different values of the roughness parameter $\beta = 4h_o^2\langle h^2\rangle$. In Tables I and II the relative dielectric coefficient is $\varepsilon_r = -40\text{-}i12$ and for Tables III through VI $\varepsilon_r = 1.5\text{-}i8$. Tables I through IV are for n = 8 while V and VI are for n = 6. In Tables I, III and V $k_m D = 4$ and $\langle\sigma_s^2\rangle$ varies while in Tables II, IV and VI $\langle\sigma_s^2\rangle = 0.101$ and k_m (and the correlation distance r_c) varies.

In Fig. 2 the scattering cross sections σ_s, σ_{s1} and σ_{s2} are plotted as functions of β ($0 < \beta < \beta_m$) and in Fig. 3 the albedo A and the extinction cross section σ_t are plotted as functions of β for the case given in Table I. Similarly, Figs. 4 and 5 correspond to the case given in Table II, Figs. 6 and 7 correspond to the case given in Table III and Figs. 8 and 9 correspond to the case given in Table IV.

It is interesting to note that while σ_s the scattering cross section is primarily dependent on the roughness parameter β, the absorption cross section $\sigma_a = \sigma_t - \sigma_s$ depends both upon β and the mean square slope $\langle\sigma_s^2\rangle$. Thus for particles with the same roughness parameter β, the

absorption cross section σ_a increases (and the albedo decreases) as the mean square slope increases. In the next set of 24 plots, the (differential) like and cross polarized normalized diffuse scattering cross sections $\langle\sigma^{PQ}\rangle_D$ are plotted as functions of the angle θ between the incident and scattered wave normals $\bar{n}^i$ and $\bar{n}^f$ respectively. In Figures 10 through 18 the surface height spectral density function W is given by (31) with n = 8. The constant parameter for the different curves is $\beta = 4k_o^2\langle h^2\rangle$. In this set of curves $k_m D = 4$ thus the correlation length r_c is constant while the mean square slope $\langle\sigma_s^2\rangle$ is different for different values of β. The relative dielectric coefficient, for Figures 10, 11 and 12 is $\epsilon_r = 40\text{-}i12$ for Figures 13, 14 and 15 it is $\epsilon_r = 1.5\text{-}i8$, and for Figures 16, 17 and 18 the particle is assumed to be perfectly conducting ($|\epsilon_r| \to \infty$). In Figures 19 through 27 n = 8 however the mean square slope is constant, $\langle\sigma_s^2\rangle = 0.101$ thus for different values of the roughness parameter β the correlation distance r_c is different. In Figures 28 through 33 $\langle\sigma^{PQ}\rangle_D$ is given for n = 6 and $\epsilon = 1.5\text{-}i8$. For Figures 28, 29 and 30, $k_m D = 4$ while the mean square height and mean square slope are parameters and for Figures 31, 32 and 33 $\langle\sigma_s^2\rangle = 0.101$ while the mean square height and correlation distance r_c are parameters.

In order to facilitate comparison between the different data for the case n = 8, the data corresponding to $\beta = 40$ is common to the set $k_m D = 4$ and the set $\langle\sigma_s^2\rangle = 0.101$. Similarly, for the case n = 6, the data corresponding to $\beta = 25$ is common to the set $k_m D = 4$ and the set $\langle\sigma_s^2\rangle = 0.101$.

For the case $\langle\sigma_s^2\rangle$ constant the diffuse scattering terms merge for $\beta > 5$ except for scattering in the near forward direction where the parameter β (and r_c) has a very significant effect on $\langle\sigma^{PQ}\rangle_D$. For the

case $k_m D = 4$ (r_c = const), the parameter β (and $\langle\sigma_s^2\rangle$) has an effect on the diffuse scattering cross sdction $\langle\sigma^{PQ}\rangle_D$ for all θ.The main differences are in the backscattered ($\theta \approx 0$) and the forward scattered ($\theta = 180^\circ$) directions. The effects of particle conductivity (absorption) on the scattering cross sections are also evident from the plots in these figures. The level of the diffuse scattering terms decreases as the absorption of the particle increases. The differences between the results for cases n = 8 and n = 6 are most significant for scattering in the forward direction.

Note in particular that there is a significant like polarized backscatter enhancement due to the surface roughness of the particle. The cross polarized diffuse cross sections have sharp nulls in the backscatter direction. This is due to the symmetry of the particle and the fact that the particle surface roughness is assumed to be isotropic.

In the last set of figures, solutions of the transfer equation (1) are presented for a parallel layer consisting of a random distribution of particles with rough surfaces. The incident wave is linearly polarized and normally incident upon the layer of optical thickness τ_o. The special cases considered in detail are for particles with very rough surfaces $\beta = 40$, $k_m D = 4$, $\langle\sigma_s^2\rangle = 0.101$, n = 8, $\lambda = 0.555\mu$. Both aluminum particles $\epsilon_r = -40\text{-}i12$ and dissipative dielectric particles $\epsilon_r = 1.5\text{-}i8$ are considered.

In Figures 34 and 35 the transmitted diffuse incoherent specific intensities I_1 (copolarized) and I_2 (cross polarized) are plotted as functions of θ ($0 < \theta < 90^\circ$) and in Figures 36 and 37 the reflected diffuse specific intensities are plotted as functions of θ ($90^\circ < \theta < 180^\circ$). The optical thickness of the layer is $\tau_o = 2$ and the relative dielectric coefficient is $\epsilon_r = -40\text{-}i12$. Single scatter and multiple scatter results are shown for both (except for single scatter cross polarized intensity

for the smooth particles). Similarly, in Figures 38 through 41, the copolarized and cross polarized transmitted and reflected specific intensities are plotted as functions of θ for $\tau_o = 2$ and $\epsilon_r = 1.5\text{-}i8$. In Figures 42 through 47 the copolarized incoherent specific intensity I_x (scattered electric field parallel to incident electric field) and cross polarized incoherent specific intensity I_y (scattered electric field perpendicular to incident electric field) (Ishimaru 1978) are plotted as functions of the azimuth angle ϕ. The optical thickness $\tau_o = 2$ and $\epsilon_r = -40\text{-}i12$. In Figures 42 and 43, I_x and I_y are plotted for $\theta = 9.7^\circ$. Similarly in Figures 44 and 45, I_x and I_y are plotted for $\theta = 170.3^\circ$, and in Figures 46 and 47 I_x and I_y are plotted for $\theta = 175.8^\circ$. Here, too, both the single scatter and multiple scatter results are given for both the smooth and the rough particles.

In Figures 48 through 50, the degree of polarization m (Ishimaru 1978) is plotted as a function of the azimuth angle ϕ. The optical thickness is $\tau_o = 2$ and the relative dielectric coefficient is $\epsilon_r = -40\text{-}i12$. In Figure 48 $\theta = 4.2^\circ$ and 9.7°, in Figure 49 $\theta = 15.3^\circ$ and 20.8° and in Figure 50 $\theta = 170.3^\circ$ and $\theta = 175.8^\circ$.

4.2 Computer Data and Programs

The tapes contain all the computer programs needed in this work as well as the computed data for the following 12 cases. Surface height spectral density function W (31) with n=6 and n=8. Complex dielectric coefficient $\epsilon_r = -40\text{-}i12$, $\epsilon_r = 1.5\text{-}i8$ and $|\epsilon_r| \to \infty$. The mean square slope $\langle\sigma_s^2\rangle$ is a constant parameter (β and r_c vary) in one set of data while the correlation length r_c is a constant parameter (β and $\langle\sigma_s^2\rangle$ vary) in the other set of data. Data for layers of different optical thickness $\tau_o = 0.1,1,2,10$ are computed. Selected data are plotted in Figures 2 through 50.

References

1. Abramowitz, M. and I. A. Stegun (1964), Handbook of Mathematical Functions, Applied Math. Series 55, National Bureau of STandards, Washington, D.C.

2. Bahar, E. (1981), "Scattering Cross Sections for Composite Random Surfaces--Full Wave Analysis," Radio Sci., 16, 1327.

3. Bahar, E. (1982), "Scattering and Depolarization by Rough Surfaces--Full Wave Approach," Proceedings of SPIE Conference on Mathematics in Modern Optics, Vol. 358, No. 28, pp. 1-14.

4. Bahar, E., and S. Chakrabarti (1985), "Scattering and Depolarization by Large Conducting Spheres with Rough Surfaces," Applied Optics, 24, No. 12, 1820.

5. Bahar, E., and M. A. Fitzwater (1983), "Backscatter Cross Sections for Randomly Oriented Metallic Flakes at Optical Frequencies--Full Wave Approach," Applied Optics, Vol. 23, pp. 3813-3819.

6. Born, M., and E. Wolf (1964), Principles of Optics, Pergamon Press, New York.

7. Chandrasekhar, S. (1950), Radiative Transfer. Dover, Publ., New York.

8. Cheung, R.L.-T., and A. Ishimaru (1982),"Transmission, Backscattering and Depolarization of Waves in Randomly Distributed Spherical Particles," Applied Optics, Vol. 21, No. 20, 3792.

9. Ehrenreich, H. (1965), "The Optical Properties of Metals," IEEE Spectrum, Vol. 2, p. 162.

10. Ishimaru, A. (1978), Wave Propagation and Scattering in Random Media, Academic, New York.

11. Ishimaru, A., and R.L.-T. Cheung (1980), "Multiple Scattering Effects in Wave Propagation Due to Rain," Ann. Telecommun., 35, 373.

12. Kiehl, J. T., M. W. Ko, A. Mugnai and Petr Chylek (1980), Perturbation Approach to Light Scattering by Non-Spherical Particles, Chapter in Light Scattering by Irregular Shaped Particles, Editor, D. W. Scheurman, Plenum Press, New York.

13. Morse, P. M., and H. Feshbach (1953), Methods of Theoretical Physics, McGraw-Hill, New York.

14. Rice, S. O. (1951), "Reflection of Electromagnetic Waves from a Slightly Rough Surface ," Communication of Pure and Applied Math., Vol. 4, pp. 351-378.

15. Ruck, G. T., D. E. Barrick, W. D. Stuart and C. K. Krichbaum (1970), "Radar Cross Section Handbook," Plenum Press, New York.

16. Sancer, M. H. (1969), "Shadow-Corrected Electromagnetic Scattering from a Randomly Rough Surface," IEEE Transaction on Antennas and Propagation, AP-15, p. 668.

17. Scheurman, D. W. (1980), Editor, Light Scattering by Irregular Shaped Particles, Plenum Press, New York.

BLANK

APPENDIX A

BLANK

TABLE I. Extinction Cross Section and Albedos

for Spheres with Rough Surfaces

β	0	1	5	10	15	20	40
σ_{s1}	2.114	1.747	1.306	1.190	1.142	1.112	1.047
σ_{s2}	0	0.334	0.720	0.805	0.830	0.840	0.854
σ_s	2.114	2.081	2.026	1.995	1.972	1.952	1.898
A_1	0.936	0.921	0.897	0.883	0.872	0.864	0.840
A_2	1.000	0.998	0.991	0.987	0.985	0.983	0.979
$A = A_1/A_2$	0.936	0.923	0.904	0.895	0.886	0.879	0.858
$\sigma_t = \sigma_s/A$	2.26	2.26	2.24	2.23	2.23	2.22	2.21
$\langle\sigma_s^2\rangle$	0	0.0025	0.0125	0.0253	0.0380	0.0506	0.1013

$\lambda = 0.555\mu$ $\quad D = 10\lambda$ $\quad \varepsilon_r = -40\text{-}i12$

$$W = \frac{2C}{\pi}\left[\frac{k_T}{k_T^2 + k_m^2}\right]^8$$

$k_m D = 4$ $\quad r_c/\pi D = 0.101$

APPENDIX A

TABLE II. Extinction Cross Section and Albedos

for Spheres with Rough Surfaces

β	1	5	10	15	20	40
σ_{s1}	1.747	1.306	1.190	1.141	1.112	1.047
σ_{s2}	0.334	0.717	0.798	0.824	0.836	0.851
σ_s	2.081	2.023	1.989	1.965	1.948	1.898
A_1	0.921	0.895	0.880	0.870	0.862	0.840
A_2	1.023	1.017	1.009	1.003	0.997	0.979
$A = A_1/A_2$	0.899	0.880	0.871	0.867	0.864	0.858
$\sigma_t = \sigma_s/A$	2.31	2.30	2.28	2.27	2.25	2.21
$k_m D$	25.16	11.24	7.96	6.52	5.64	4.0
$r_c/\pi D$	0.016	0.036	0.050	0.062	0.072	0.101

$\lambda = 0.555\mu$ $\quad D = 10\lambda$ $\quad \epsilon_r = -40 - i12$

$$W = \frac{2C}{\pi}\left[\frac{k_T}{k_T^2 + k_m^2}\right]^8 \quad , \quad \langle\sigma_s^2\rangle = 0.101$$

For $\beta = 0$

$\sigma_{so} = 2.114$, $\sigma_{to} = 2.259$, $A_o = 0.936$

APPENDIX A

TABLE III. Extinction Cross Section and Albedos

for Spheres with Rough Surfaces

β	0	1	5	10	15	20	40
σ_{s1}	1.482	1.345	1.171	1.117	1.090	1.072	1.025
σ_{s2}	0	0.130	0.281	0.312	0.320	0.321	0.316
σ_s	1.482	1.475	1.452	1.429	1.410	1.393	1.341
A_1	0.661	0.657	0.647	0.637	0.629	0.621	0.597
A_2	1.00	0.998	0.992	0.988	0.985	0.983	0.979
$A = A_1/A_2$	0.661	0.659	0.652	0.645	0.638	0.632	0.611
$\sigma_t = \sigma_a/A$	2.243	2.24	2.23	2.22	2.21	2.21	2.20
$\langle\sigma_s^2\rangle$	0	0.0025	0.0125	0.0253	0.0380	0.0506	0.1013

$\lambda = 0.555\mu$ $\quad D = 10\lambda$ $\quad \varepsilon_r = 1.5\text{-}i8$

$$W = \frac{2C}{\pi}\left[\frac{k_T}{k_T^2 + k_m^2}\right]^8$$

$k_m D = 4$ $\quad r_c/\pi D = 0.101$

APPENDIX A

TABLE IV. Extinction Cross Section and Albedos

for Spheres with Rough Surfaces

β	1	5	10	15	20	40
σ_{s1}	1.345	1.171	1.117	1.090	1.072	1.025
σ_{s2}	0.115	0.262	0.294	0.305	0.309	0.316
σ_s	1.460	1.433	1.411	1.395	1.381	1.341
A_1	0.651	0.639	0.629	0.622	0.616	0.597
A_2	1.024	1.017	1.009	1.003	0.997	0.979
$A = A_1/A_2$	0.636	0.628	0.623	0.619	0.617	0.611
$\sigma_t = \sigma_s/A$	2.30	2.28	2.27	2.25	2.24	2.20
$k_m D$	25.16	11.24	7.96	6.52	5.64	4.0
$r_c/\pi D$	0.016	0.036	0.050	0.062	0.072	0.101

$\lambda = 0.555\mu$ $\quad D = 10\lambda$ $\quad \epsilon_r = 1.5\text{-}i8$

$$W = \frac{2C}{\pi}\left[\frac{k_T}{k_T^2 + k_m^2}\right]^8 , \quad \langle\sigma_s^2\rangle = 0.101$$

For $\beta = 0$

$$\sigma_{so} = 1.482 , \quad \sigma_{to} = 2.243 , \quad A_o = 0.661$$

APPENDIX A

TABLE V. Extinction Cross Section and Albedos

for Spheres with Rough Surfaces

β	0	1	5	10	15	20	25
σ_{s1}	1.482	1.345	1.171	1.117	1.090	1.072	1.057
σ_{s2}	0	0.129	0.279	0.308	0.314	0.315	0.314
σ_s	1.482	1.474	1.450	1.425	1.404	1.387	1.371
A_1	0.661	0.657	0.646	0.635	0.626	0.618	0.611
A_2	1.00	0.998	0.994	0.992	0.991	0.991	0.992
$A = A_1/A_2$	0.661	0.658	0.650	0.640	0.632	0.624	0.616
$\sigma_t = \sigma_s/A$	2.24	2.24	2.23	2.23	2.22	2.22	2.22
$\langle\sigma_s^2\rangle$	0	0.0040	0.020	0.0404	0.0606	0.0808	0.101

$\lambda = 0.555\mu$ $\quad D = 10\lambda$ $\quad \varepsilon_r = 1.5\text{-}i8$

$$W = \frac{2C}{\pi}\left[\frac{k_T}{k_T^2 + k_m^2}\right]^8$$

$k_m D = 4$ $\quad r_c/\pi D = 0.08$

APPENDIX A

TABLE VI. Extinction Cross Section and Albedos

for Spheres with Rough Surfaces

β	1	5	10	15	20	25
σ_{s1}	1.345	1.171	1.117	1.090	1.072	1.057
σ_{s2}	0.116	0.263	0.296	0.306	0.311	0.314
σ_s	1.461	1.434	1.413	1.396	1.383	1.371
A_1	0.651	0.639	0.629	0.622	0.617	0.611
A_2	1.020	1.016	1.009	1.003	0.997	0.992
$A = A_1/A_2$	0.638	0.629	0.624	0.621	0.618	0.616
$\sigma_t = \sigma_s/A$	2.29	2.28	2.26	2.25	2.24	2.23
$k_m D$	19.88	8.92	6.32	5.16	4.44	4.0
$r_c/\pi D$	0.016	0.036	0.05	0.062	0.072	0.080

$\lambda = 0.555\mu$ $\quad D = 10\lambda$ $\quad \varepsilon_r = 1.5\text{-}i8$

$$W = \frac{2C}{\pi}\left[\frac{k_T}{k_T^2 + k_m^2}\right]^6 \quad , \quad \langle\sigma_s^2\rangle = 0.101$$

For $\beta = 0$

$\sigma_{so} = 1.482$, $\sigma_{to} = 2.243$, $A_o = 0.661$

APPENDIX A

APPENDIX B

BLANK

8. Figure Captions

Fig. 1. Scattering geometry indicating incident and scatter wave normals $\bar{n}^i$ and $\bar{n}^f$ and corresponding field components E_1 parallel (vertical) and E_2 perpendicular (horizontal) polarizations.

Fig. 2. Scattering cross sections σ_{s1}, σ_{s2} and σ_s versus the roughness parameter β (Table I).

Fig. 3. Extinction cross sections σ_t and albedo A versus the roughness parameter β (Table I).

Fig. 4. Scattering cross sections σ_{s1}, σ_{s2} and σ_s versus the roughness parameter β (Table II).

Fig. 5. Extinction cross sections σ_t and albedo A versus the roughness parameter β (Table II).

Fig. 6. Scattering cross sections σ_{s1}, σ_{s2} and σ_s versus the roughness parameter β (Table III).

Fig. 7. Extinction cross sections σ_t and albedo A versus the roughness parameter β (Table III).

Fig. 8. Scattering cross sections σ_{s1}, σ_{s2} and σ_s versus the roughness parameter β (Table IV).

Fig. 9. Extinction cross sections σ_t and albedo A versus the roughness parameter β (Table IV).

Fig. 10. $\langle\sigma^{VV}\rangle_D$ versus θ, $n = 8$, $k_m D = 4$, $\epsilon_r = -40\text{-}i12$
$\beta = 1$ (0), 5 (Δ), 10 (+), 20 (x), 40 ($\diamond$).

Fig. 11. $\langle\sigma^{HH}\rangle_D$ versus θ, $n = 8$, $k_m D = 4$, $\epsilon_r = -40\text{-}i12$
$\beta = 1$ (0), 5 (Δ), 10 (+), 20 (x), 40 ($\diamond$).

Fig. 12. $\langle\sigma^{VH}\rangle_D = \langle\sigma^{HV}\rangle D$ versus θ, $n = 8$, $k_m D = 4$, $\epsilon_r = -40\text{-}i12$
$\beta = 1$ (0), 5 (Δ), 10 (+), 20 (x), 40 ($\diamond$).

Fig. 13. $\langle\sigma^{VV}\rangle_D$ versus θ, $n = 8$, $k_m D = 4$, $\epsilon_r = 1.5\text{-}i8$
$\beta = 1$ (0), 5 (Δ), 10 (+), 20 (x), 40 ($\diamond$).

Fig. 14. $\langle\sigma^{HH}\rangle_D$ versus θ, $n = 8$, $k_m D = 4$, $\epsilon_r = 1.5\text{-}i8$
$\beta = 1$ (0), 5 (Δ), 10 (+), 20 (x), 40 ($\diamond$).

Fig. 15. $\langle\sigma^{VH}\rangle_D = \langle\sigma^{HV}\rangle_D$ versus θ, $n = 8$, $k_m D = 4$, $\epsilon_r = 1.5\text{-}i8$
$\beta = 1$ (0), 5 (Δ), 10 (+), 20 (x), 40 ($\diamond$).

APPENDIX B

Fig. 16. $\langle\sigma^{VV}\rangle_D$ versus θ, n = 8, $k_m D = 4$, perfect conductor
β = 1 (0), 5 (Δ), 10 (+), 20 (x), 40 ($\diamond$).

Fig. 17. $\langle\sigma^{HH}\rangle_D$ versus θ, n = 8, $k_m D = 4$, perfect conductor
β = 1 (0), 5 (Δ), 10 (+), 20 (x), 40 ($\diamond$).

Fig. 18. $\langle\sigma^{VH}\rangle_D = \langle\sigma^{HV}\rangle_D$ versus θ, n = 8, $k_m D = 4$, perfect conductor
β = 1 (0), 5 (Δ), 10 (+), 20 (x), 40 ($\diamond$).

Fig. 19. $\langle\sigma^{VV}\rangle_D$ versus θ, n = 8, $\langle\sigma_s^2\rangle = 0.101$, $\varepsilon_r = -40\text{-}i12$
β = 1 (0), 5 (Δ), 10 (+), 20 (x), 40 ($\diamond$).

Fig. 20. $\langle\sigma^{HH}\rangle_D$ versus θ, n = 8, $\langle\sigma_s^2\rangle = 0.101$, $\varepsilon_r = -40\text{-}i12$
β = 1 (0), 5 (Δ), 10 (+), 20 (x), 40 ($\diamond$).

Fig. 21. $\langle\sigma^{VH}\rangle_D = \langle\sigma^{HV}\rangle_D$ versus θ, n = 8, $\langle\sigma_s^2\rangle = 0.101$, $\varepsilon_r = -40\text{-}i12$
β = 1 (0), 5 (Δ), 10 (+), 20 (x), 40 ($\diamond$).

Fig. 22. $\langle\sigma^{VV}\rangle_D$ versus θ, n = 8, $\langle\sigma_s^2\rangle = 0.101$, $\varepsilon_r = 1.5\text{-}i8$
β = 1 (0), 5 (Δ), 10 (+), 20 (x), 40 ($\diamond$).

Fig. 23. $\langle\sigma^{HH}\rangle_D$ versus θ, n = 8, $\langle\sigma_s^2\rangle = 0.101$, $\varepsilon_r = 1.5\text{-}i8$
β = 1 (0), 5 (Δ), 10 (+), 20 (x), 40 ($\diamond$).

Fig. 24. $\langle\sigma^{VH}\rangle_D = \langle\sigma^{HV}\rangle_D$ versus θ, n = 8, $\langle\sigma_s^2\rangle = 0.101$, $\varepsilon_r = 1.5\text{-}i8$
β = 1 (0), 5 (Δ), 10 (+), 20 (x), 40 ($\diamond$).

Fig. 25. $\langle\sigma^{VV}\rangle_D$ versus θ, n = 8, $\langle\sigma_s^2\rangle = 0.101$, perfect conductor
β = 1 (0), 5 (Δ), 10 (+), 20 (x), 40 ($\diamond$).

Fig. 26. $\langle\sigma^{HH}\rangle_D$ versus θ, n = 8, $\langle\sigma_s^2\rangle = 0.101$, perfect conductor
β = 1 (0), 5 (Δ), 10 (+), 20 (x), 40 ($\diamond$).

Fig. 27. $\langle\sigma^{VH}\rangle_D = \langle\sigma^{HV}\rangle_D$ versus θ, n = 8, $\langle\sigma_s^2\rangle = 0.101$, perfect conductor
β = 1 (0), 5 (Δ), 10 (+), 20 (x), 40 ($\diamond$).

Fig. 28. $\langle\sigma^{VV}\rangle_D$ versus θ, n = 6, $k_m D = 4$, $\varepsilon_r = 1.5\text{-}i8$
β = 1 (0), 5 (Δ), 10 (+), 20 (x), 40 ($\diamond$).

Fig. 29. $\langle\sigma^{HH}\rangle_D$ versus θ, n = 6, $k_m D = 4$, $\varepsilon_r = 1.5\text{-}i8$
β = 1 (0), 5 (Δ), 10 (+), 20 (x), 40 ($\diamond$).

Fig. 30. $\langle\sigma^{VH}\rangle_D = \langle\sigma^{HV}\rangle_D$ versus θ, n = 6, $k_m D = 4$, $\varepsilon_r = 1.5\text{-}i8$
β = 1 (0), 5 (Δ), 10 (+), 20 (x), 40 ($\diamond$).

Fig. 31. $\langle\sigma^{VV}\rangle_D$ versus θ, n = 6, $\langle\sigma_s^2\rangle = 0.1$, $\varepsilon_r = 1.5\text{-}i8$
β = 1 (0), 5 (Δ), 10 (+), 20 (x), 40 ($\diamond$).

Fig. 32. $\langle\sigma^{HH}\rangle_D$ versus θ, n = 6, $\langle\sigma_s^2\rangle$ = 0.1, ε_r = 1.5-i8
β = 1 (0), 5 (Δ), 10 (+), 20 (x), 40 ($\diamond$).

Fig. 33. $\langle\sigma^{VH}\rangle_D = \langle\sigma^{HV}\rangle_D$ versus θ, n = 6, $\langle\sigma_s^2\rangle$ = 0.1, ε_r = 1.5-i8
β = 1 (0), 5 (Δ), 10 (+), 20 (x), 40 ($\diamond$).

Fig. 34. Specific incoherent intensity I_1 for a linearly polarized wave. Normal incidence, β = 40, $k_m D$ = 4, $\langle\sigma_s^2\rangle$ = 0.101, n = 8 (31) λ = 0.555μ, ε_r = -40-i12, D = 10λ. Transmitted τ_o = 2, ϕ = 0. First order (—), smooth and rough particles. Multiple scatter (+) smooth (Δ) rough.

Fig. 35. Specific incoherent intensity (I_2) for a linearly polarized wave. Normal incidence, β = 40, $k_m D$ = 4, $\langle\sigma_s^2\rangle$ = 0.101, n = 8 (31) λ = 0.555μ, ε_r = -40-i12, D = 10λ. Transmitted τ_o = 2, ϕ = 0. First order (—), smooth and rough particles. Multiple scatter (+) smooth (Δ) rough.

Fig. 36. Specific incoherent intensity I_1 for a linearly polarized wave. Normal incidence, β = 40, $k_m D$ = 4, $\langle\sigma_s^2\rangle$ = 0.101, n = 8 (31) λ = 0.555μ, ε_r = -40-i12, D = 10λ. Reflected τ_o = 2, ϕ = 0. First order (—), smooth and rough particles. Multiple scatter (+) smooth (Δ) rough.

Fig. 37. Specific incoherent intensity (I_2) for a linearly polarized wave. Normal incidence, β = 40, $k_m D$ = 4, $\langle\sigma_s^2\rangle$ = 0.101, n = 8 (31) λ = 0.555μ, ε_r = -40-i12, D = 10λ. Reflected τ_o = 2, ϕ = 0. First order (—), smooth and rough particles. Multiple scatter (+) smooth (Δ) rough.

Fig. 38. Specific incoherent intensity I_1 for a linearly polarized wave. Normal incidence, β = 40, $k_m D$ = 4, $\langle\sigma_s^2\rangle$ = 0.101, n = 8 (31) λ = 0.555μ, ε_r = 1.5-i8, D = 10λ. Transmitted τ_o = 2, ϕ = 0. First order (—), smooth and rough particles. Multiple scatter (+) smooth (Δ) rough.

Fig. 39. Specific incoherent intensity I_2 for a linearly polarized wave. Normal incidence, β = 40, $k_m D$ = 4, $\langle\sigma_s^2\rangle$ = 0.101, n = 8 (31) λ = 0.555μ, ε_r = 1.5-i8, D = 10λ. Transmitted τ_o = 2, ϕ = 0. First order (—), smooth and rough particles. Multiple scatter (+) smooth (Δ) rough.

APPENDIX B

Fig. 40. Specific incoherent intensity I_1 for a linearly polarized wave. Normal incidence, $\beta = 40$, $k_m D = 4$, $\langle\sigma_s^2\rangle = 0.101$, $n = 8$ (31) $\lambda = 0.555\mu$, $\epsilon_r = 1.5\text{-}i8$, $D = 10\lambda$. Reflected $\tau_o = 2$, $\phi = 0$. First order (—), smooth and rough particles. Multiple scatter (+) smooth (Δ) rough.

Fig. 41. Specific incoherent intensity (I_2) for a linearly polarized wave. Normal incidence, $\beta = 40$, $k_m D = 4$, $\langle\sigma_s^2\rangle = 0.101$, $n = 8$ (31) $\lambda = 0.555\mu$, $\epsilon_r = 1.5\text{-}i8$, $D = 10$. Reflected $\tau_o = 2$, $\phi = 0$. First order (—), smooth and rough particles. Multiple scatter (+) smooth (Δ) rough.

Fig. 42. Specific incoherent intensity I_x for a linearly polarized wave. Normal incidence, $\beta = 40$, $k_m D = 4$, $\langle\sigma_s^2\rangle = 0.101$, $n = 8$ (31), $\lambda = 0.555\mu$, $\epsilon_r = -40\text{-}i12$, $D=10\lambda$. Transmitted $\tau_o = 2$, $\theta = 9.7^\circ$. First order (—), smooth and rough particles. Multiple scatter ($\bar{X}$) smooth (X) rough.

Fig. 43. Specific incoherent intensity I_y for a linearly polarized wave. Normal incidence, $\beta = 40$, $k_m D = 4$, $\langle\sigma_s^2\rangle = 0.101$, $n = 8$ (31), $\lambda = 0.555\mu$, $\epsilon_r = -40\text{-}i12$, $D = 10\lambda$. Transmitted $\tau_o = 2$, $\theta = 9.7^\circ$. First order (—), smooth and rough particles. Multiple scatter ($\bar{X}$) smooth (X) rough.

Fig. 44. Specific incoherent intensity I_x for a linearly polarized wave. Normal incidence, $\beta = 40$, $k_m D = 4$, $\langle\sigma_s^2\rangle = 0.101$, $n = 8$ (31), $\lambda=0.0555\mu$, $\epsilon_r = -40\text{-}i12$, $D = 10\lambda$. Reflected $\tau_o = 2$, $\theta = 170.3^\circ$. First order (—), smooth and rough particles. Multiple scatter ($\bar{X}$) smooth (X) rough.

Fig. 45. Specific incoherent intensity I_y for a linearly polarized wave. Normal incidence, $\beta = 40$, $k_m D = 4$, $\langle\sigma_s^2\rangle = 0.101$, $n = 8$ (31), $\lambda = 0.555u$, $\epsilon_r = -40\text{-}i12$, $D - 10\lambda$. Reflected $\tau_o = 2$, $\theta = 170.3^\circ$. First order (—), smooth and rough particles. Multiple scatter ($\bar{X}$) smooth (X) rough.

Fig. 46. Specific incoherent intensity I_x for a linearly polarized wave. Normal incidence, $\beta = 40$, $k_m D = 4$, $\langle\sigma_s^2\rangle = 0.101$, $n = 8$ (31) $\lambda = 0.555\mu$, $\epsilon_r = -40\text{-}i12$, $D = 10\lambda$. Reflected $\tau_o = 2$, $\theta = 175.8^\circ$. First order (—), smooth and rough particles. Multiple scatter ($\bar{X}$) smooth (X) rough.

Fig. 47. Specific incoherent intensity I_y for a linearly polarized wave. Normal incidence, $\beta = 40$, $k_m D = 4$, $\langle\sigma_s^2\rangle = 0.101$, $n = 8$ (31), $\lambda = 0.555\mu$, $\varepsilon_r = -40\text{-}i12$, $D = 10\lambda$. Reflected $\tau_o = 2$, $\theta = 175.8^\circ$. First order (—), smooth and rough particles. Multiple scatter (X) smooth (X) rough.

Fig. 48. Degree of polarization m. Normal incidence, linearly polarized wave, $\beta = 40$, $k_m D = 4$, $\langle\sigma_s^2\rangle = 0.101$, $n = 8$ (31), $\lambda = 0.555\mu$, $\varepsilon_r = -40\text{-}i12$, $D = 10\lambda$, $\tau_o = 2$. $\theta = 4.2^\circ$ (+) smooth (X) rough; $\theta = 9.7^\circ$ (0) smooth (Δ) rough.

Fig. 49. Degree of polarization m. Normal incidence, linearly polarized wave, $\beta = 40$, $k_m D = 4$, $\langle\sigma_s^2\rangle = 0.101$, $n = 8$ (31), $\lambda = 0.555\mu$, $\varepsilon_r = -40\text{-}i12$, $D = 10\lambda$, $\tau_o = 2$. $\theta = 15.3^\circ$ (+) smooth (X) rough $\theta = 20.8^\circ$ (0) smooth (Δ) rough.

Fig. 50. Degree of polarization m. Normal incidence, linearly polarized wave, $\beta = 40$, $k_m D = 4$, $\langle\sigma_s^2\rangle = 0.101$, $n = 8$ (31), $\lambda = 0.555\mu$, $\varepsilon_r = -40\text{-}i12$, $D = 10\lambda$, $\tau_o = 2$. $\theta = 170.3^\circ$ (+) smooth (X) rough $\theta = 175.8^\circ$ (0) smooth (Δ) rough.

APPENDIX B

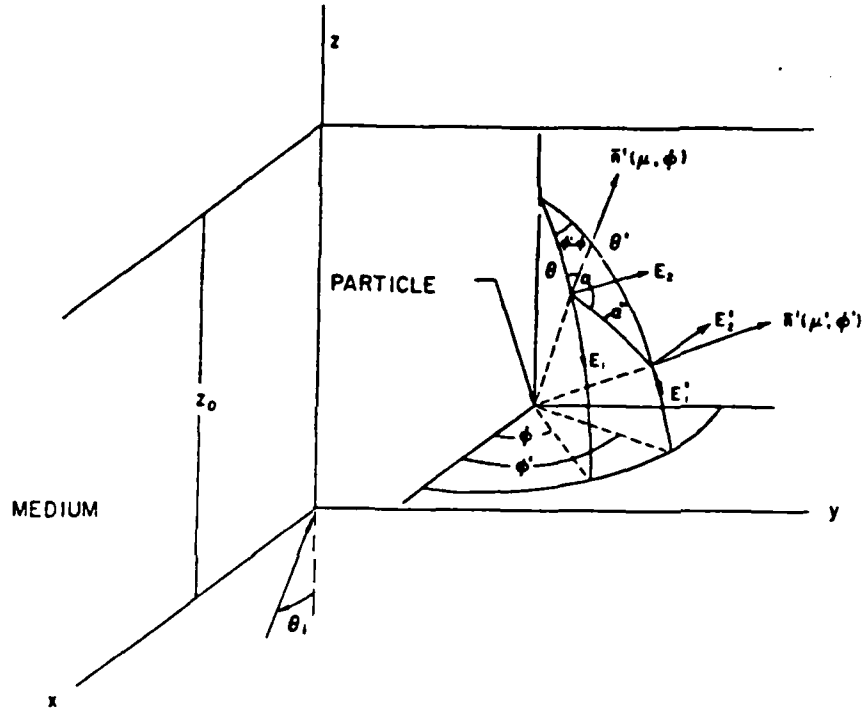

Fig. 1.

APPENDIX B

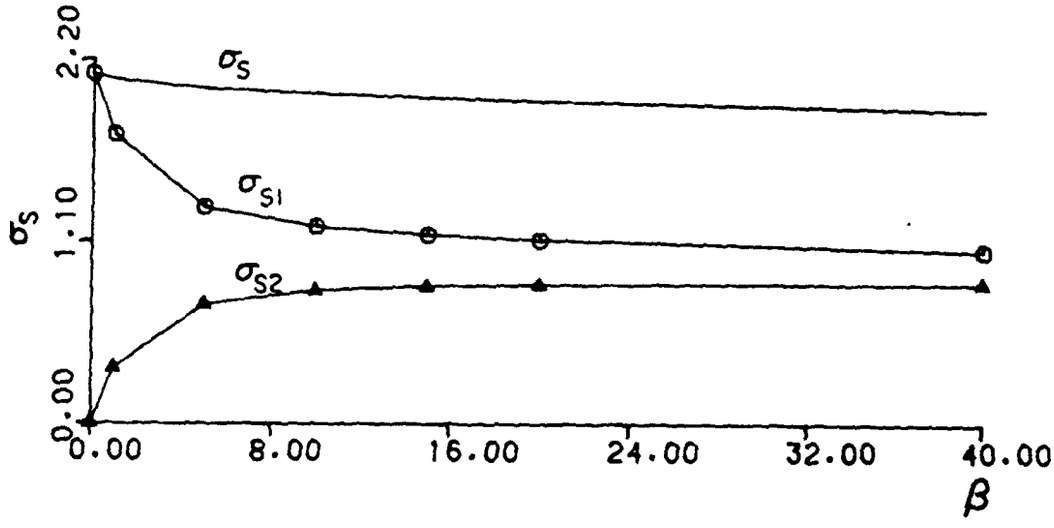

Fig. 2

APPENDIX B

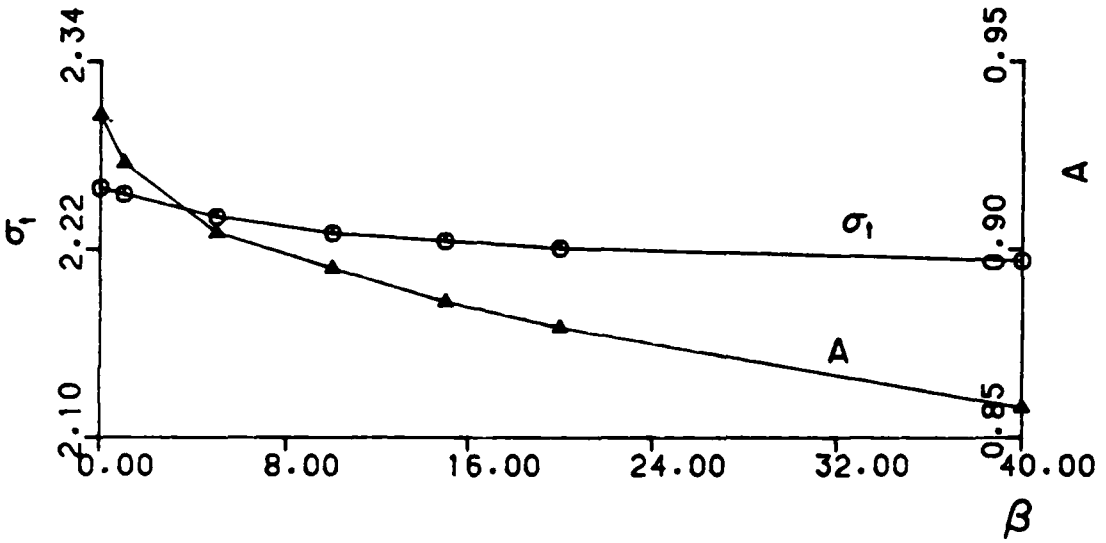

Fig. 3

APPENDIX B

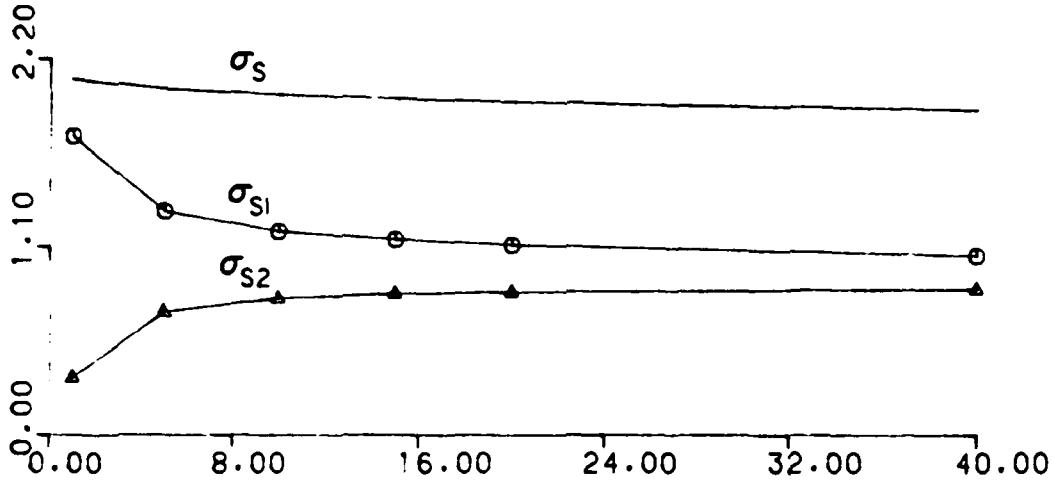
2.20
1.10
0.00
σ_S
σ_{S1}
σ_{S2}
0.00
8.00
16.00
24.00
32.00
40.00

Fig. 4

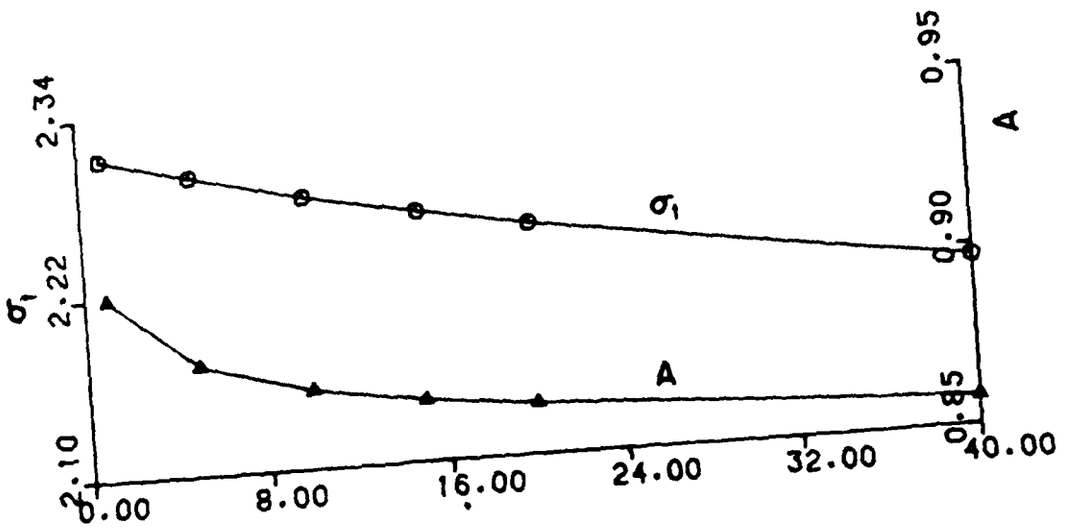
2.34
2.22
2.10
σ_1
σ_1
A
A
0.95
0.90
0.85
0.00
8.00
16.00
24.00
32.00
40.00

Fig. 5

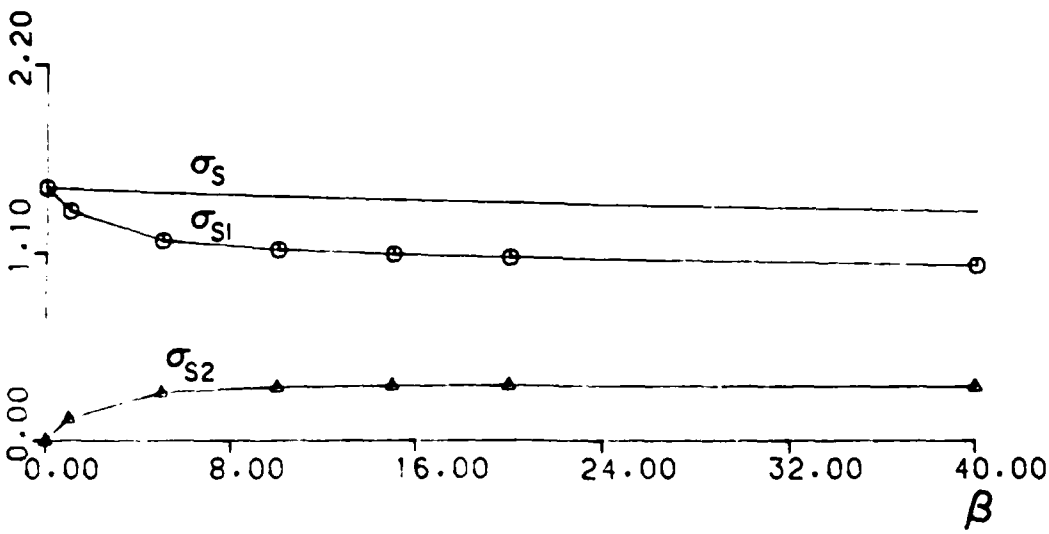

Fig. 6

APPENDIX B

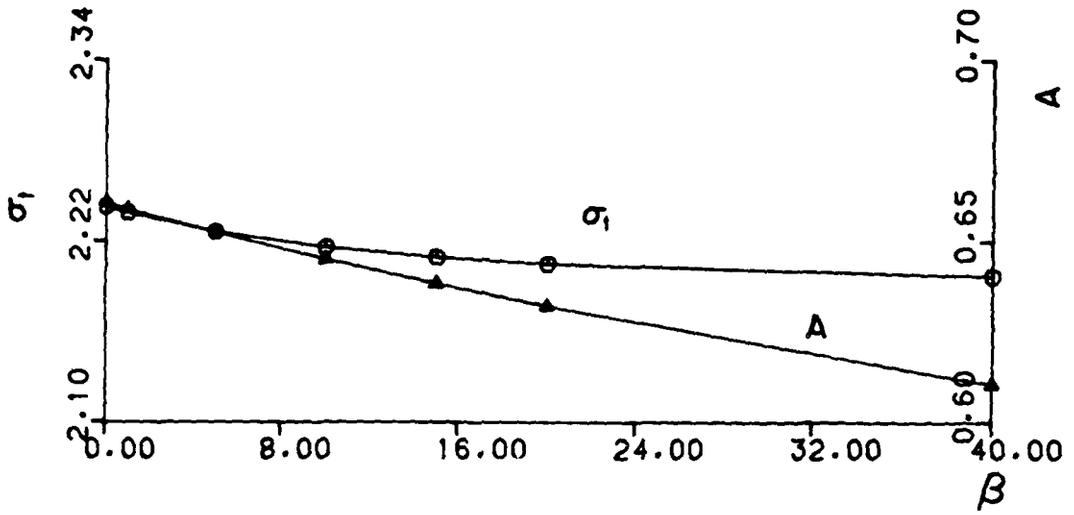

Fig. 7

APPENDIX B

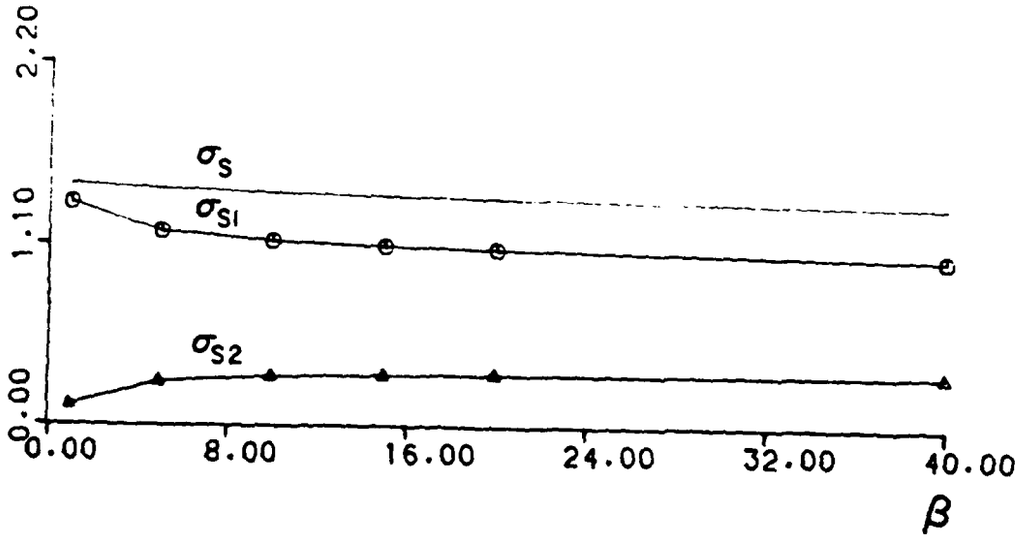

Fig. 8

APPENDIX B

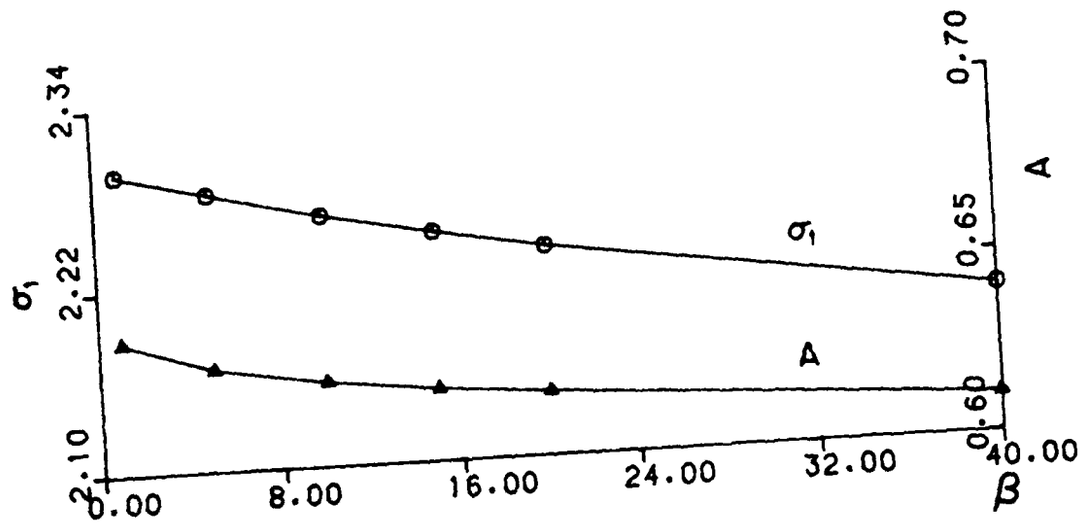
2.34
2.22
2.10
σ_1
0.70
0.65
0.60
A
σ_1
A
0.00
8.00
16.00
24.00
32.00
40.00
β

Fig. 9

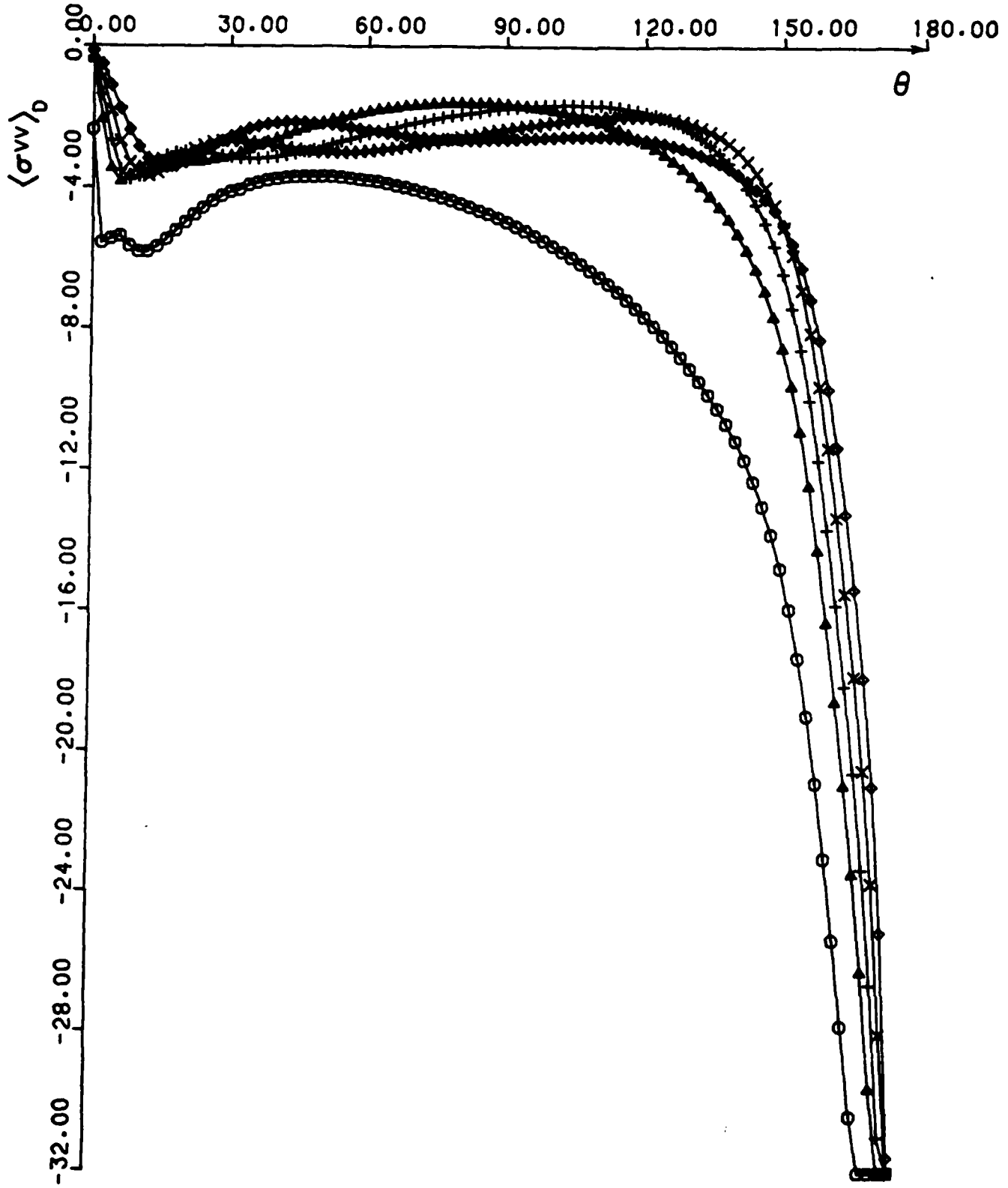

Fig. 10

APPENDIX B

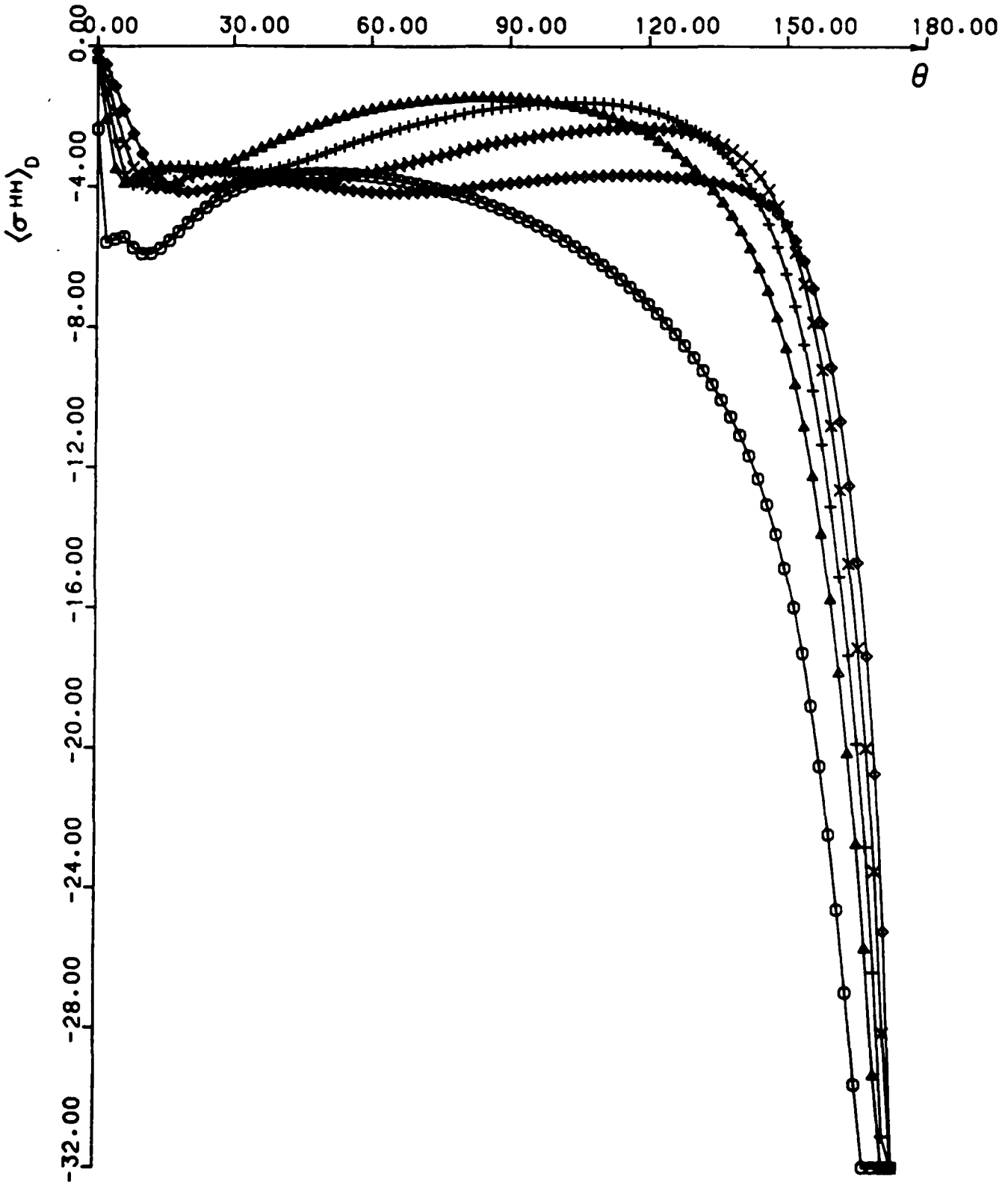

Fig. 11

APPENDIX B

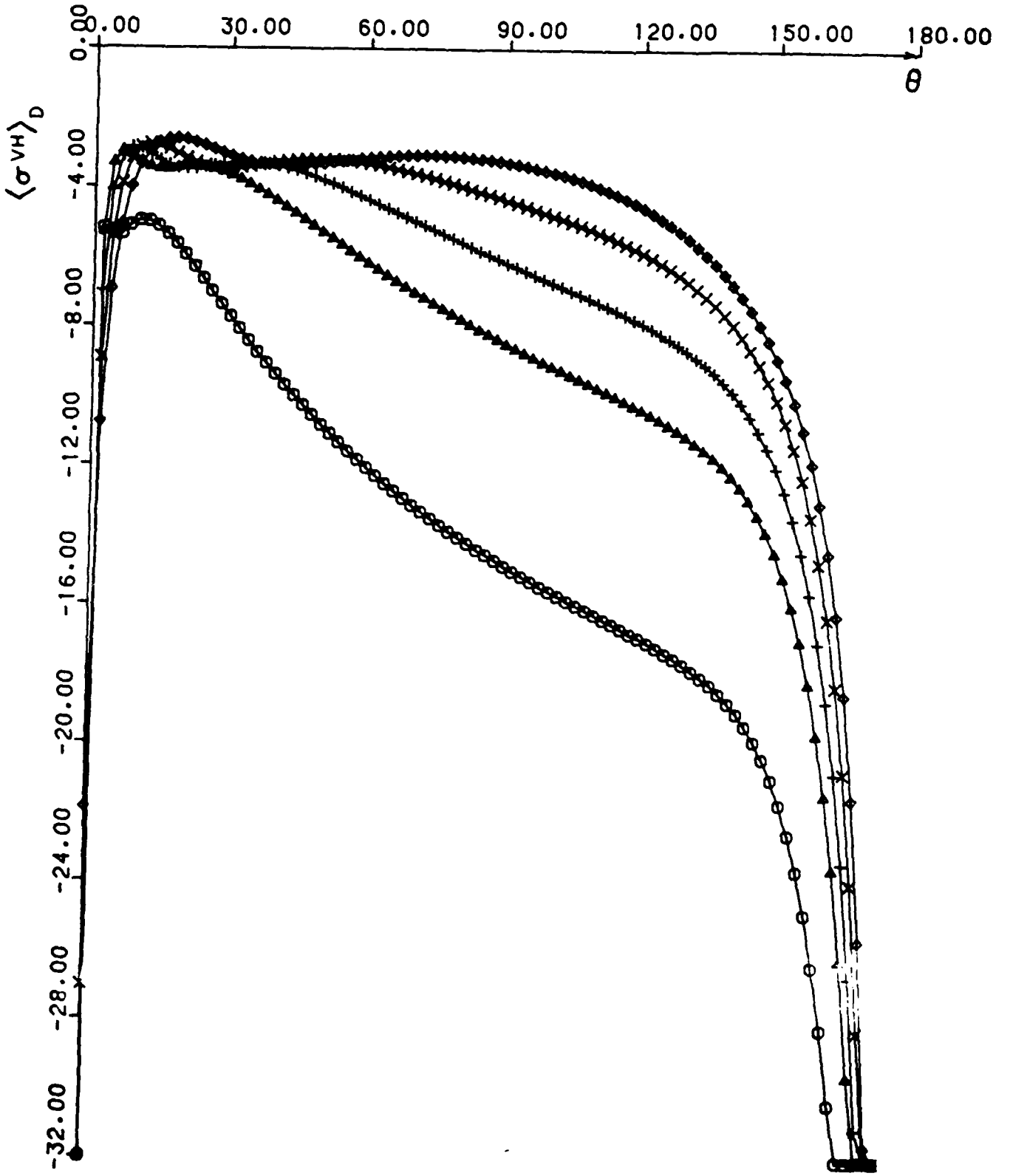

Fig. 12

APPENDIX B

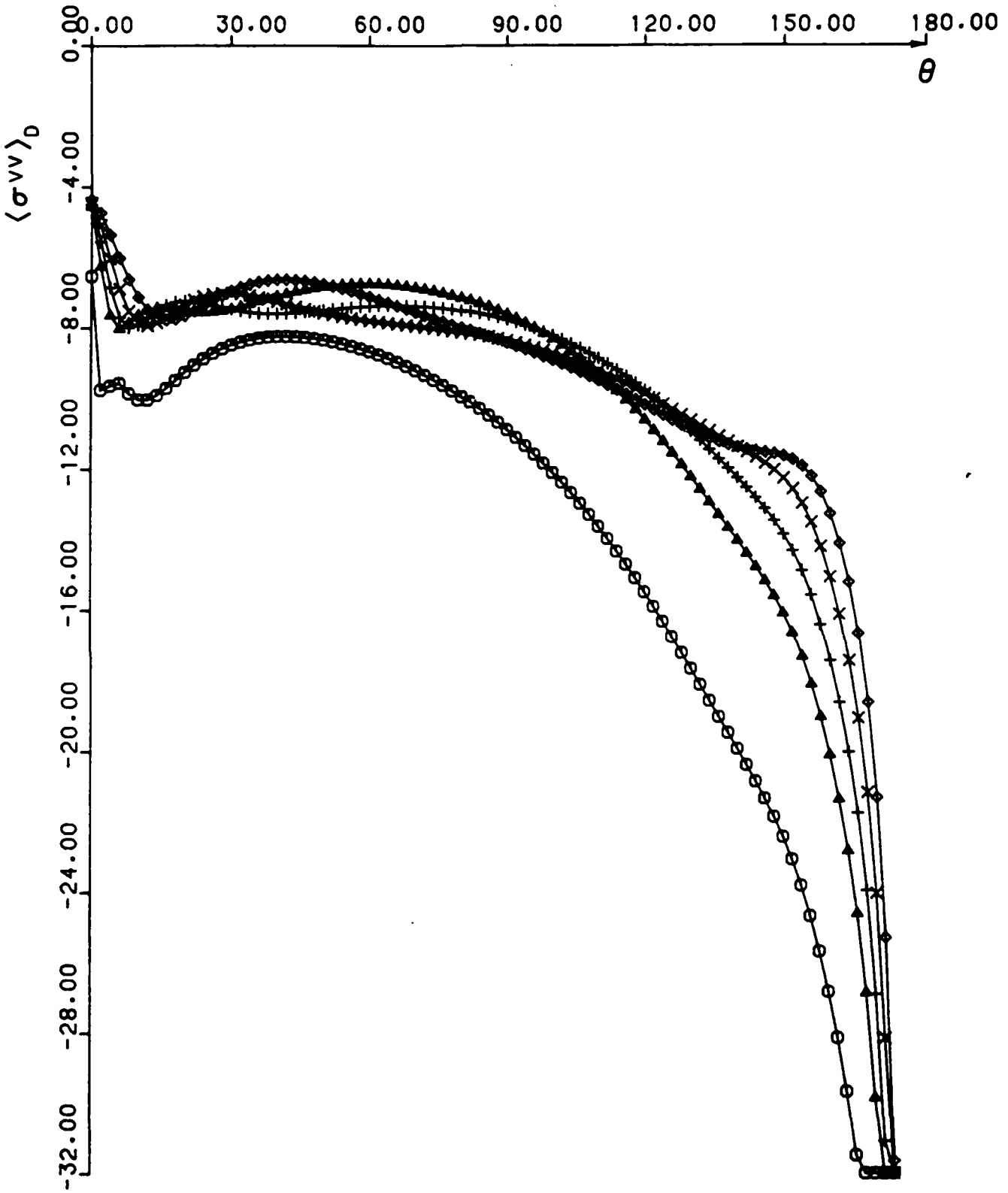
0.00
30.00
60.00
90.00
120.00
150.00
180.00
θ
$\langle \sigma^{vv} \rangle_D$
0.00
-4.00
-8.00
-12.00
-16.00
-20.00
-24.00
-28.00
-32.00

Fig. 13

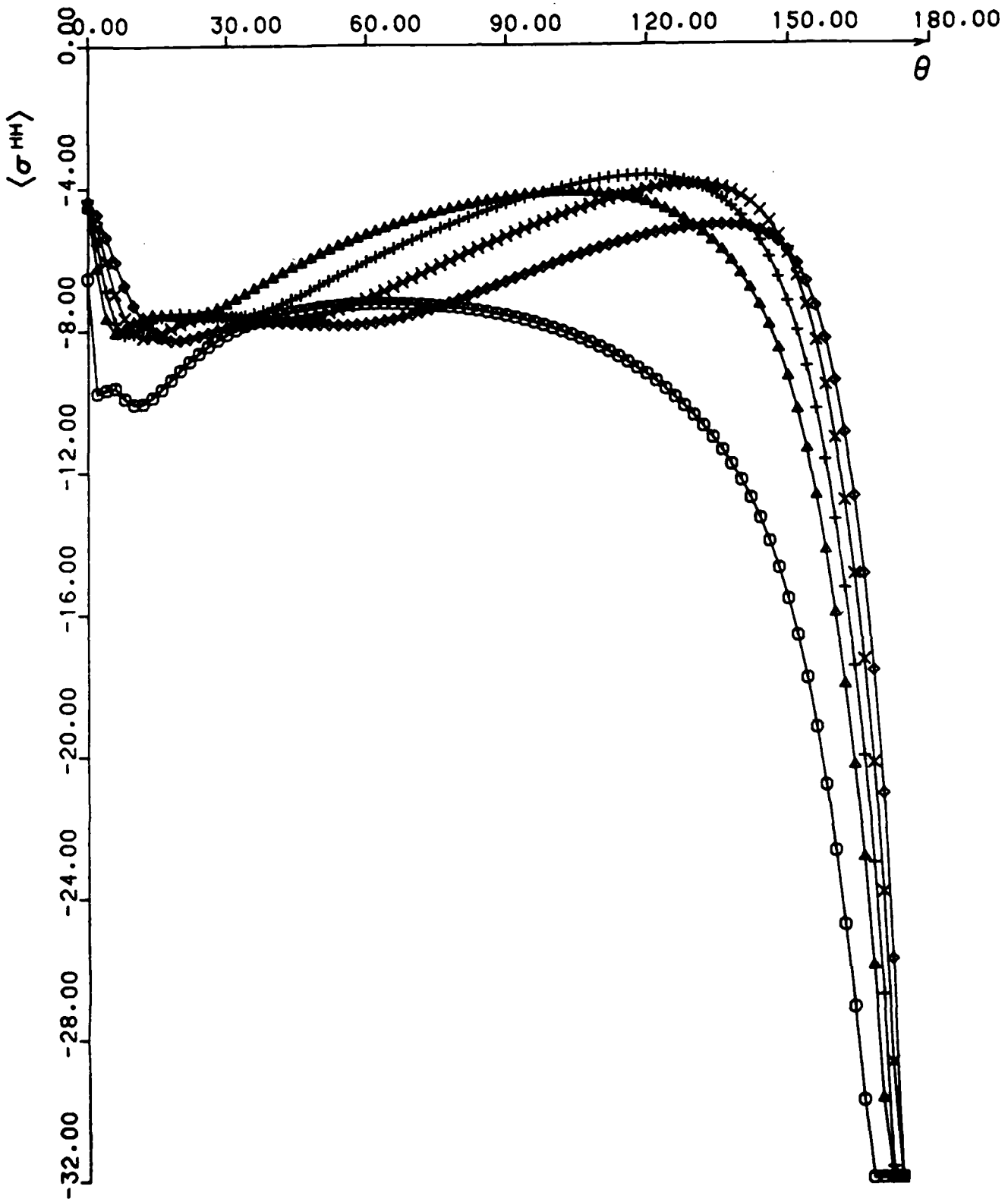
0.00
30.00
60.00
90.00
120.00
150.00
180.00
θ
⟨σ HH⟩
0.00
-4.00
-8.00
-12.00
-16.00
-20.00
-24.00
-28.00
-32.00

Fig. 14

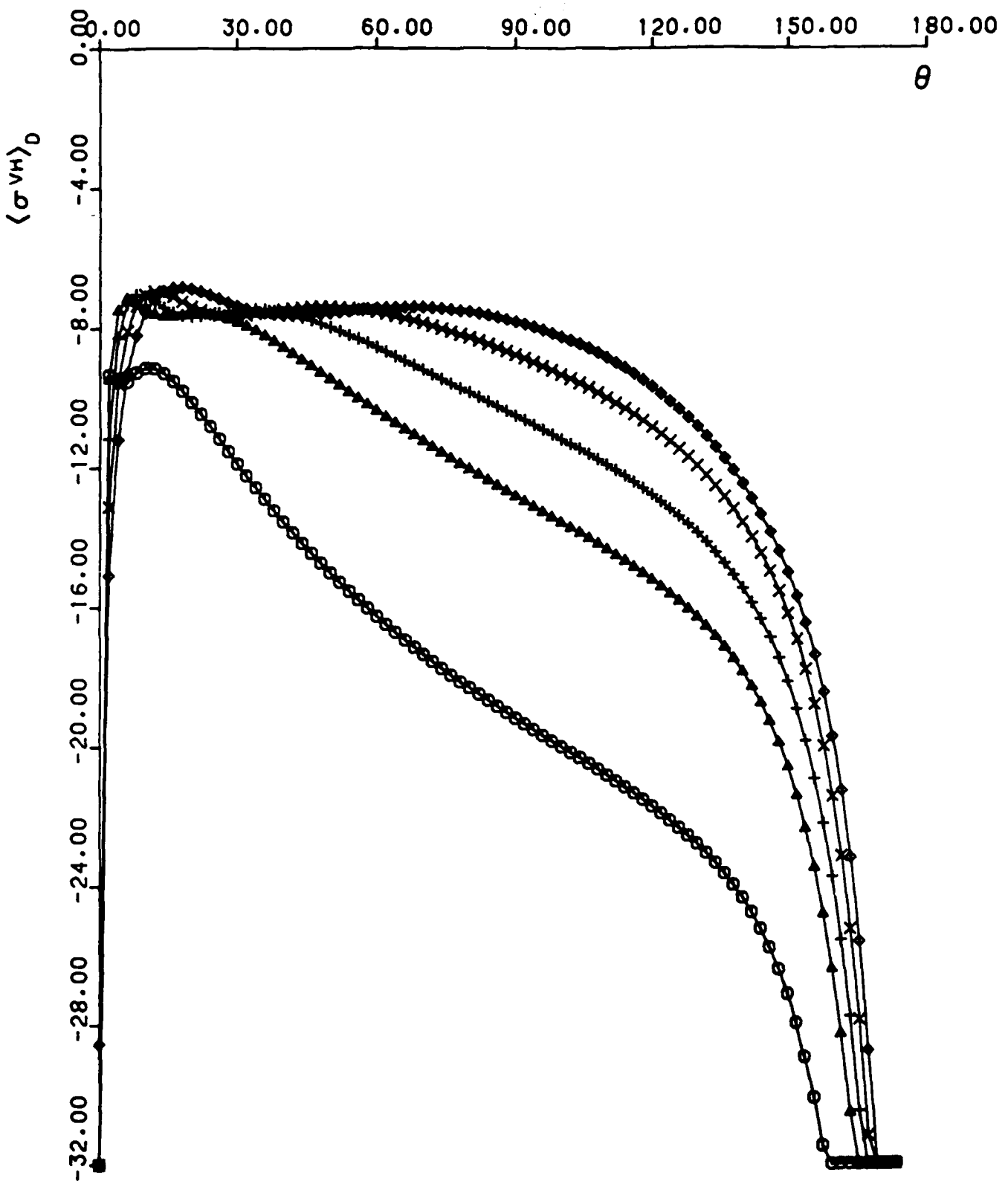

Fig. 15

APPENDIX B

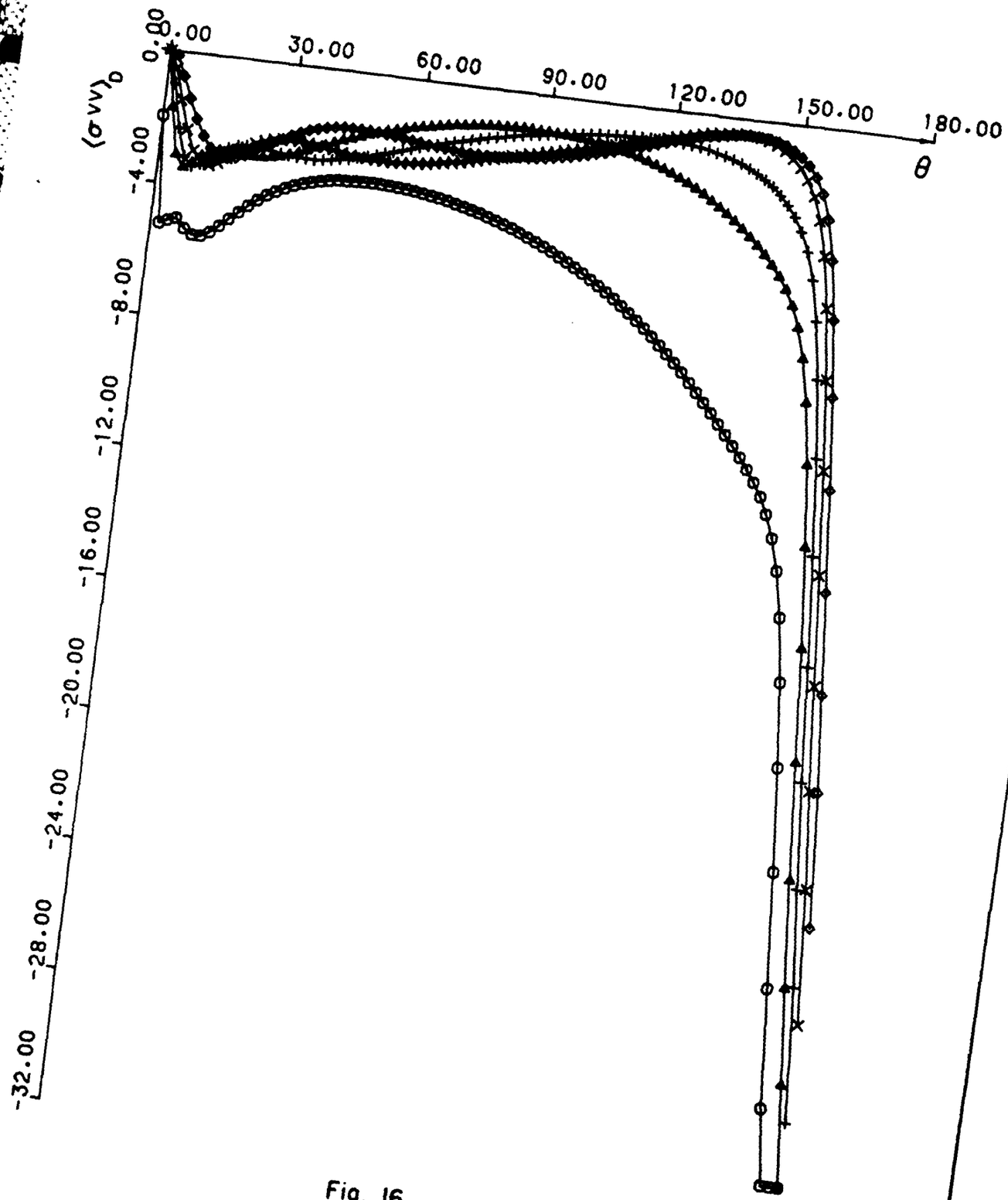

Fig. 16

APPENDIX B

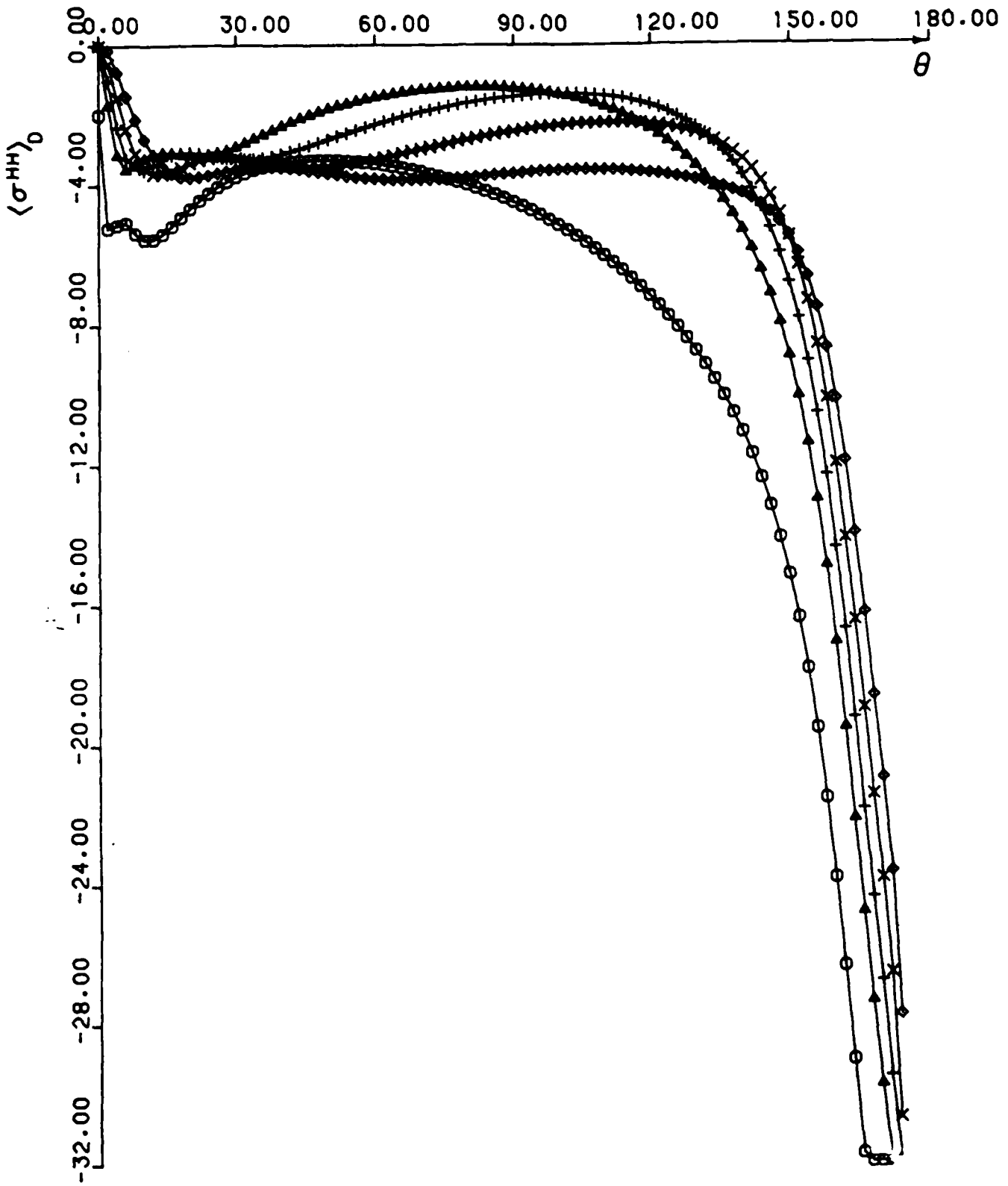

Fig. 17

APPENDIX B

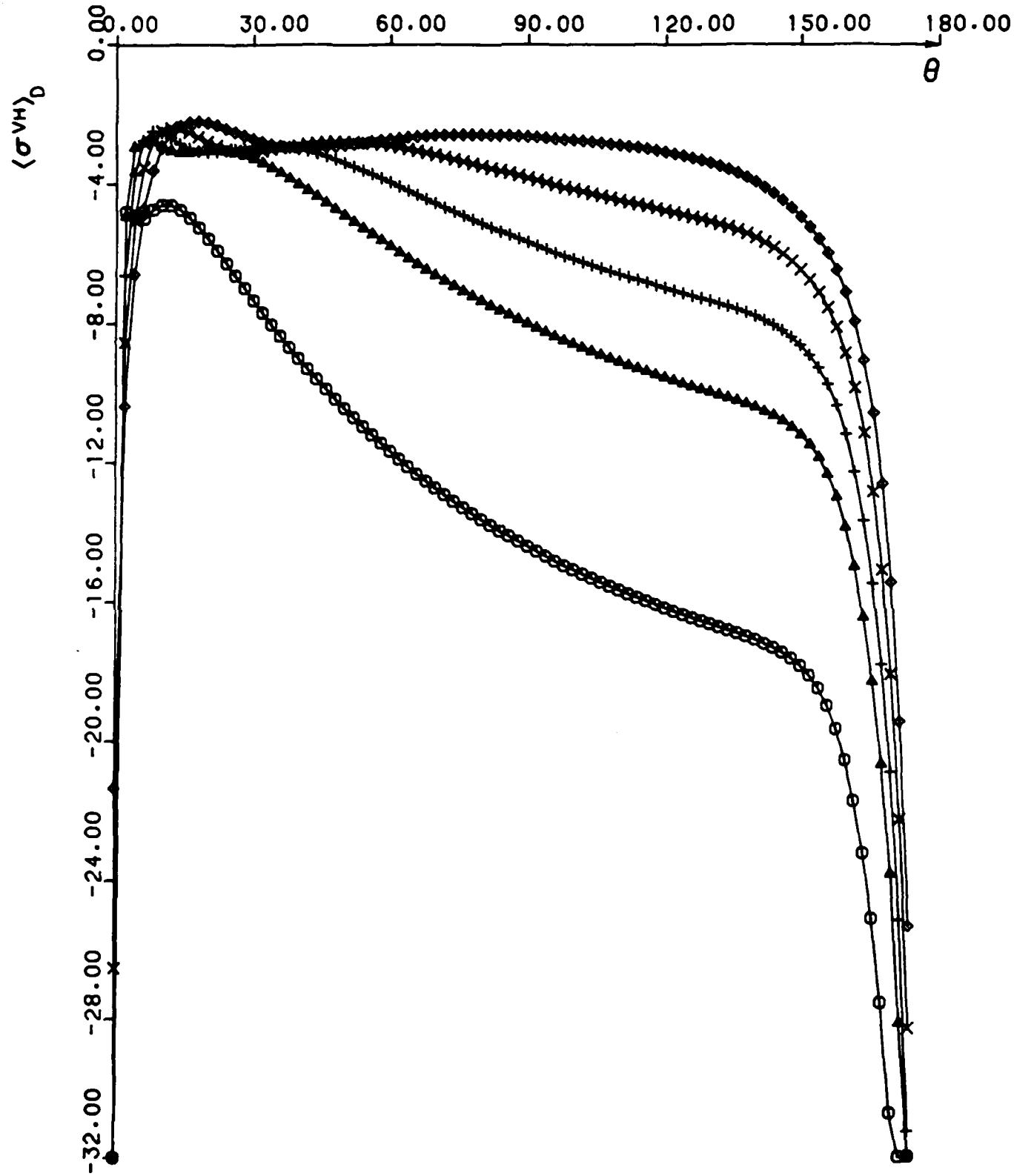

Fig. 18

APPENDIX B

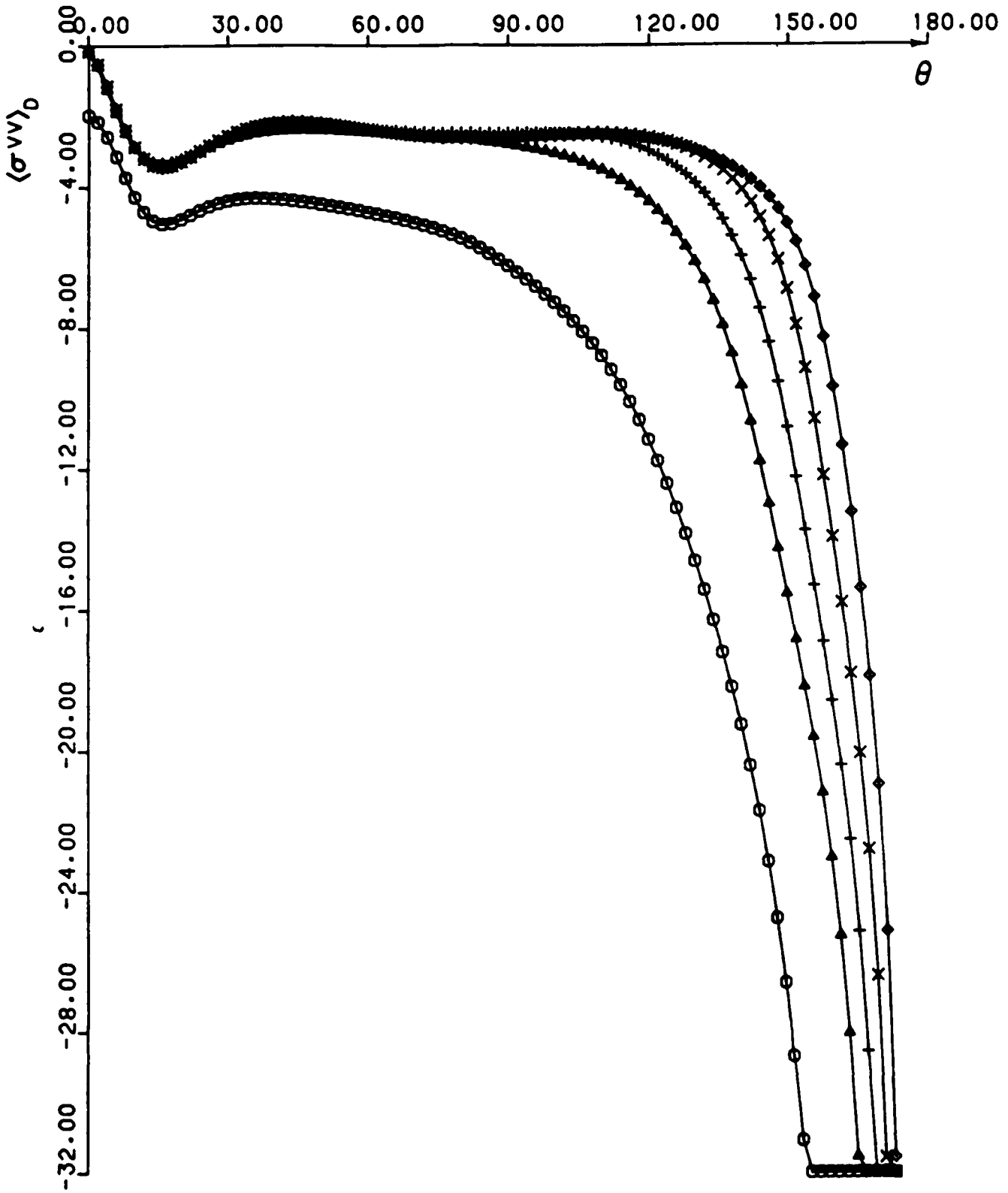

Fig. 19

APPENDIX B

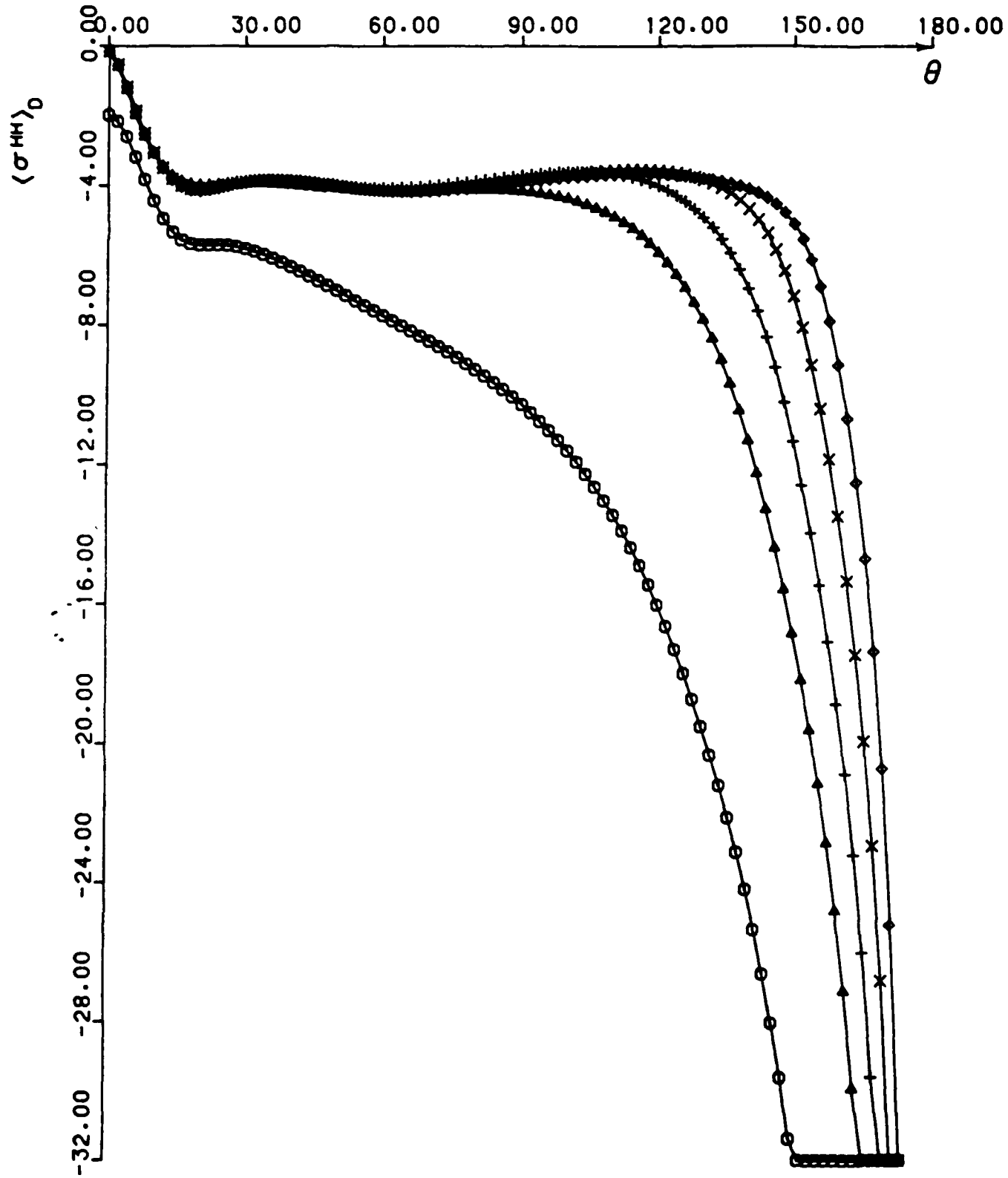

Fig. 20

APPENDIX B

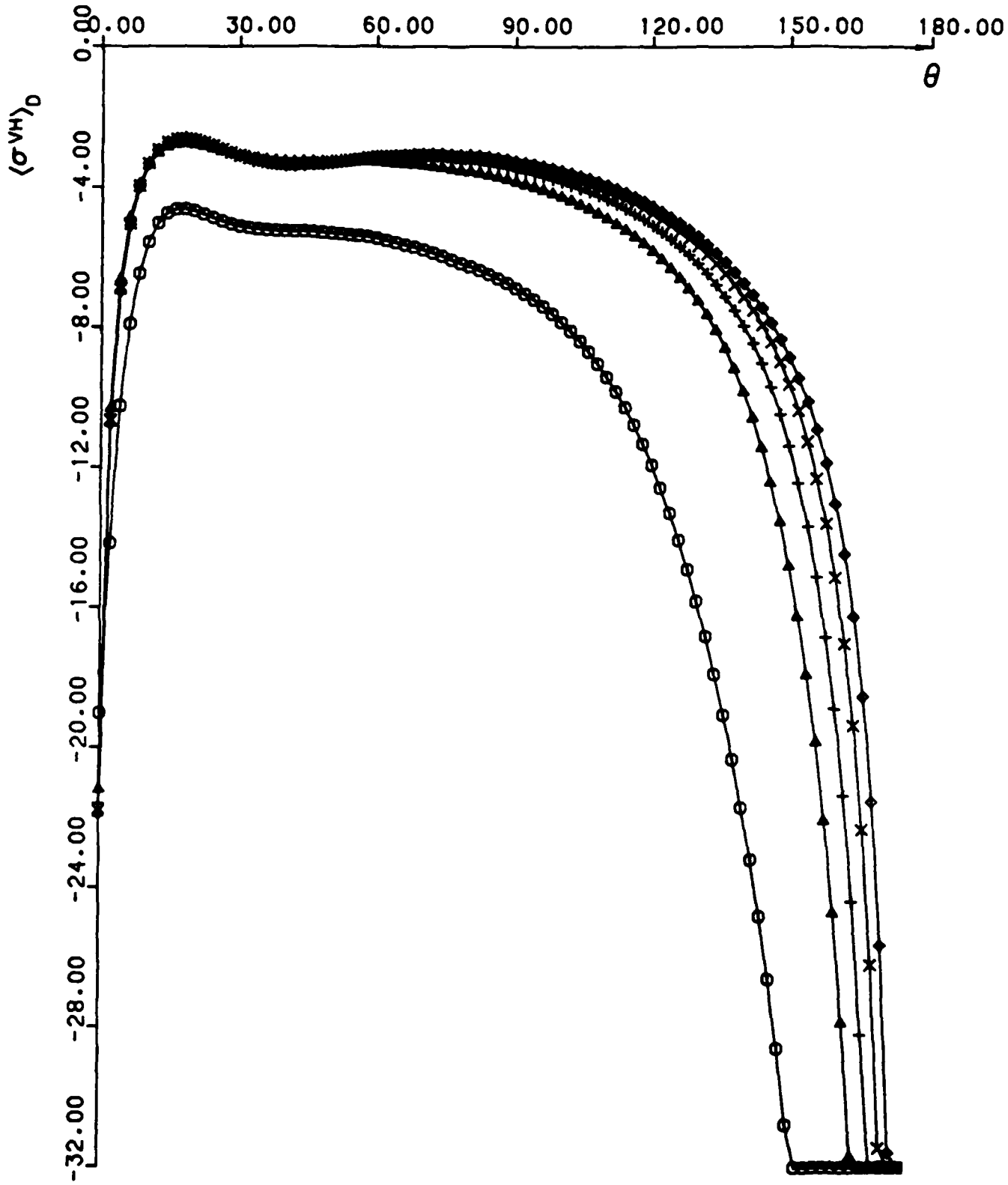
0.00
30.00
60.00
90.00
120.00
150.00
180.00
θ
$(\sigma^{VH})_0$
0.00
-4.00
-8.00
-12.00
-16.00
-20.00
-24.00
-28.00
-32.00

Fig. 21

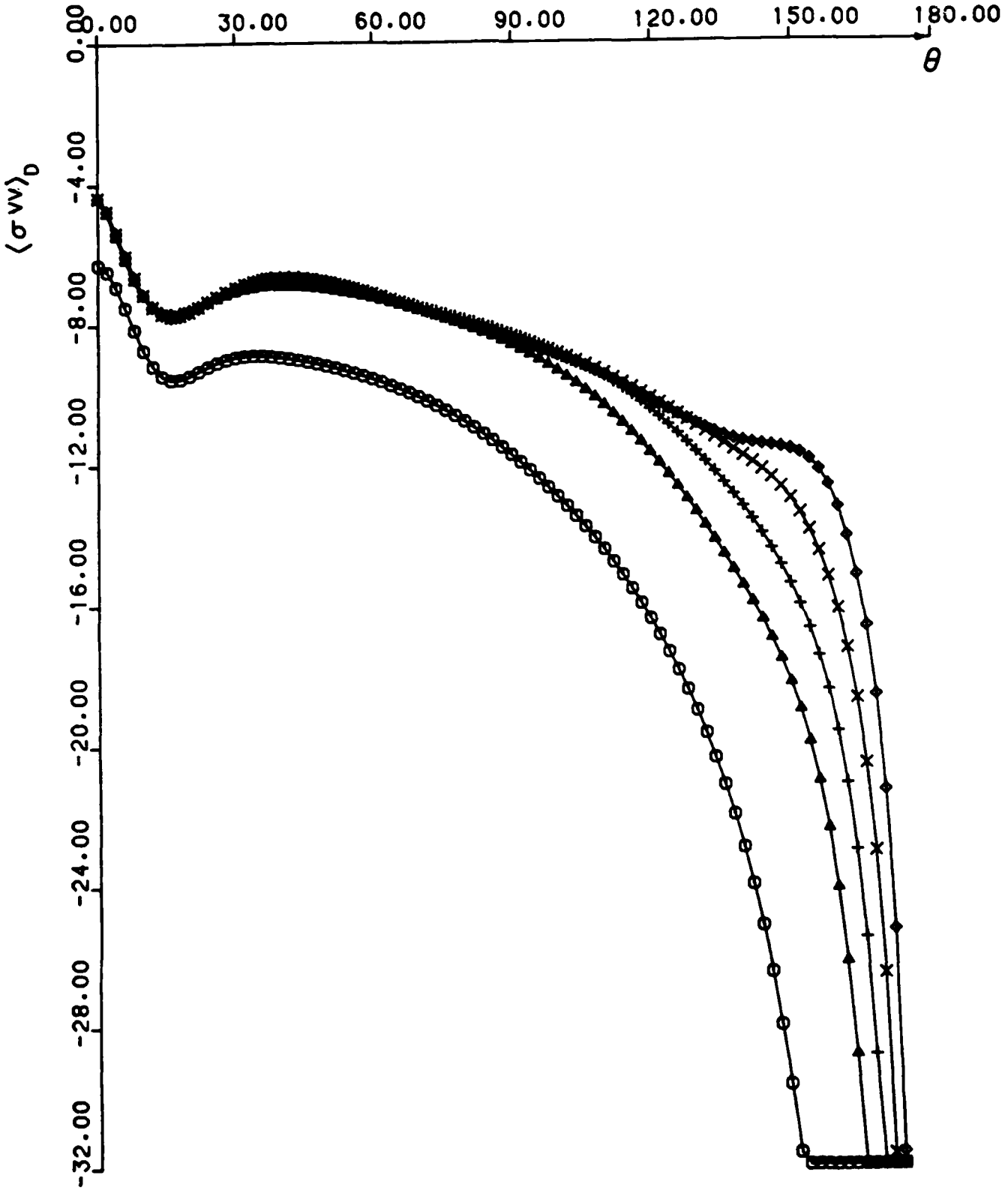

Fig. 22

APPENDIX B

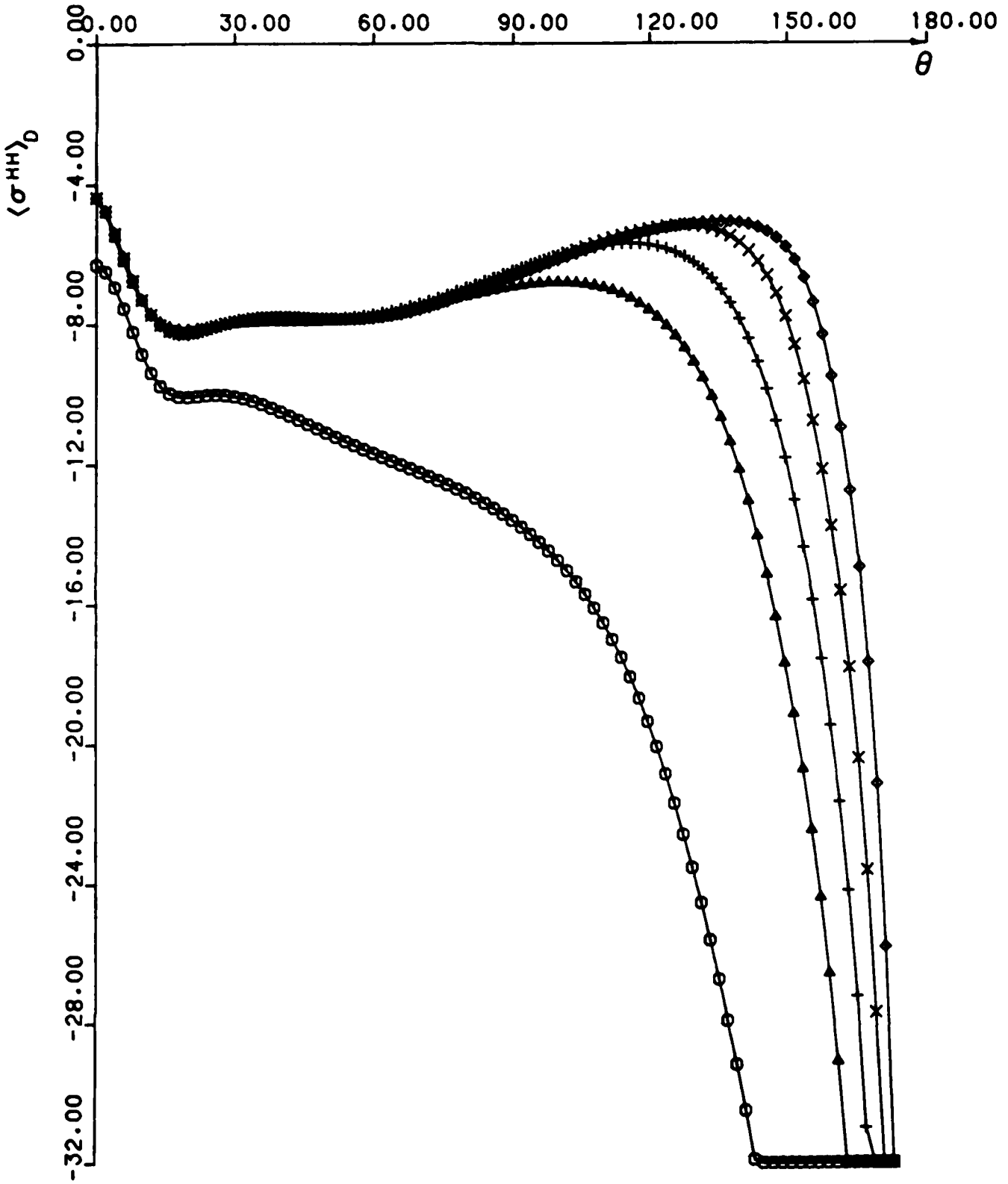

Fig. 23

APPENDIX B

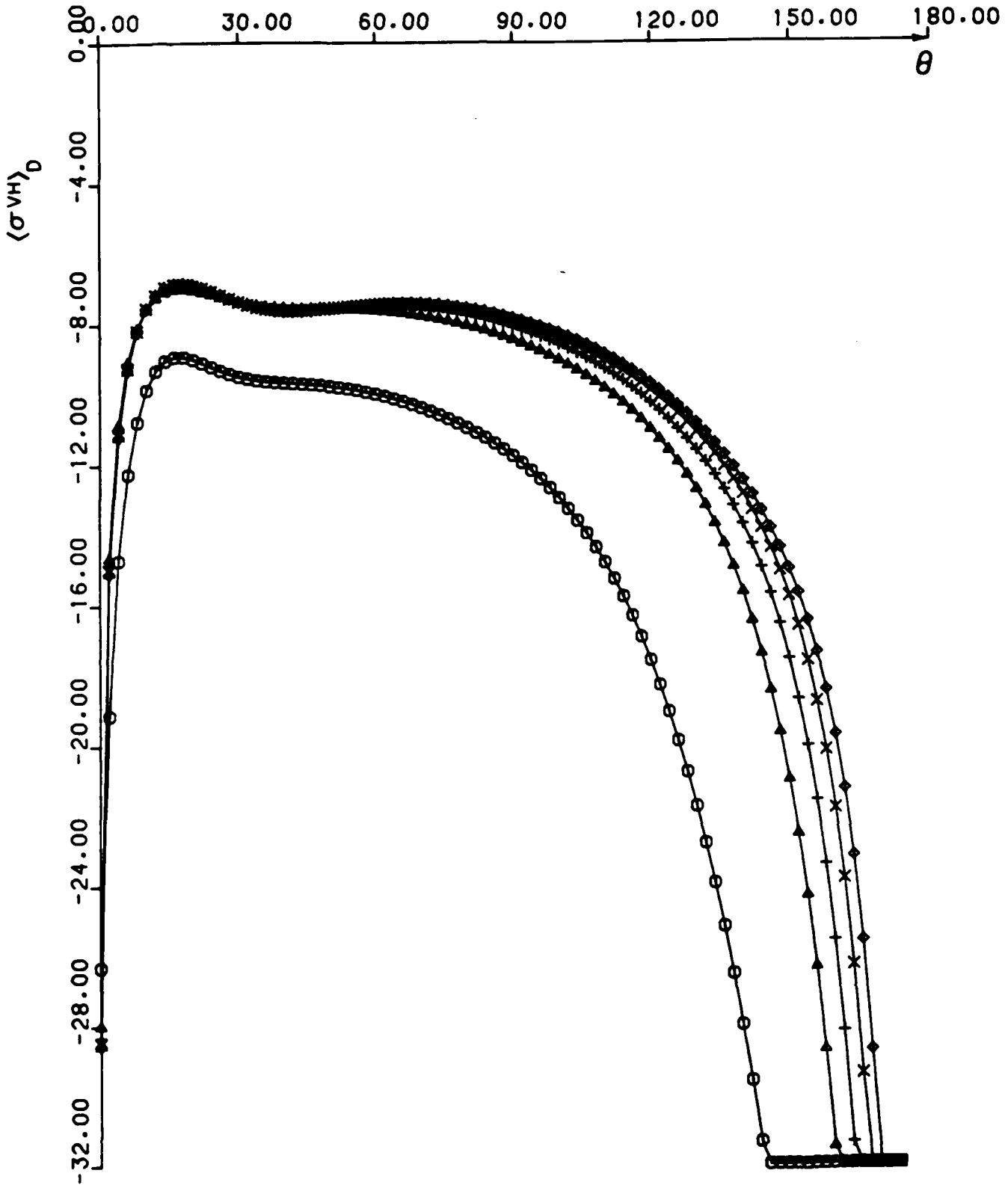

Fig. 24

APPENDIX B

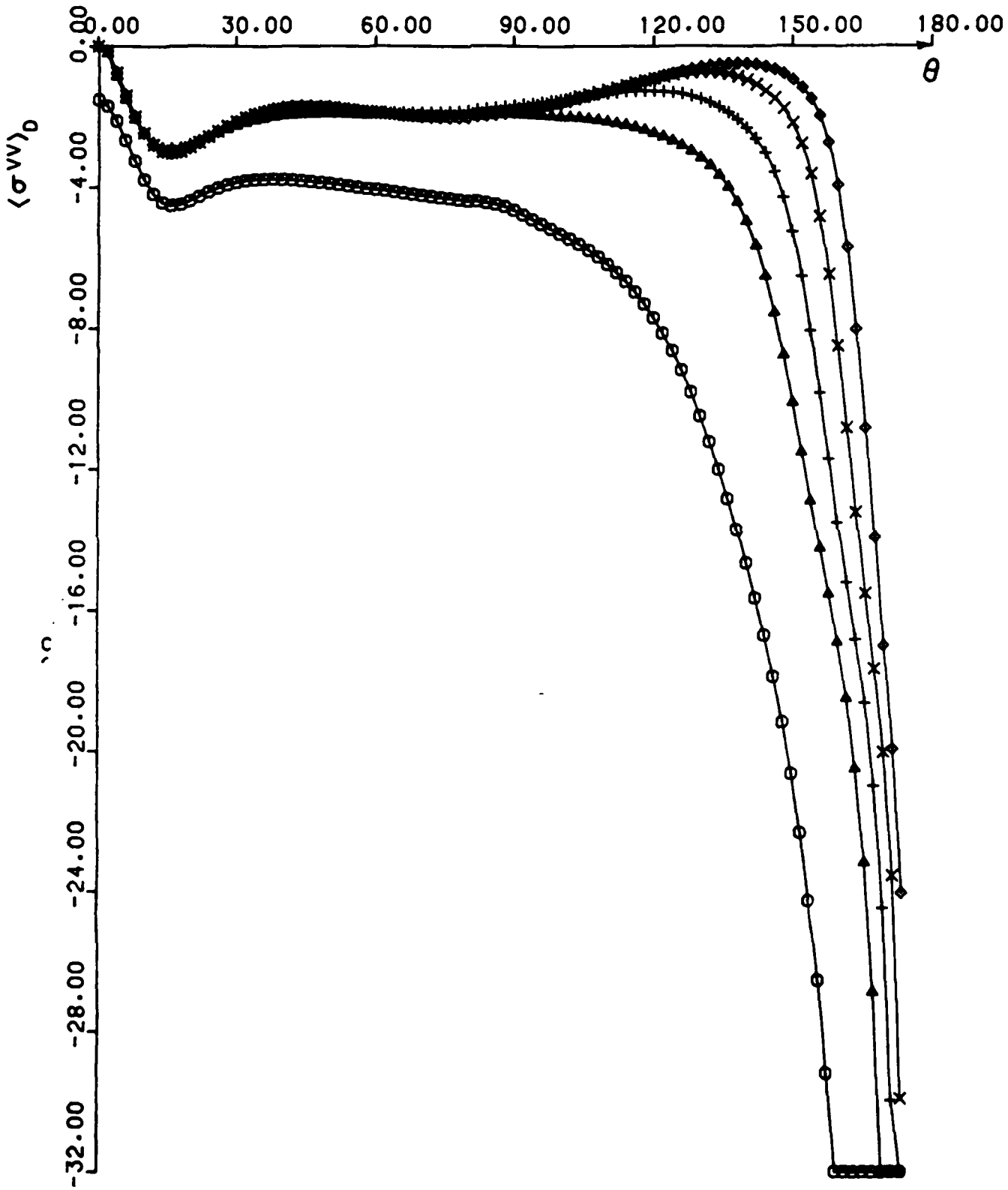

APPENDIX B

Fig. 25

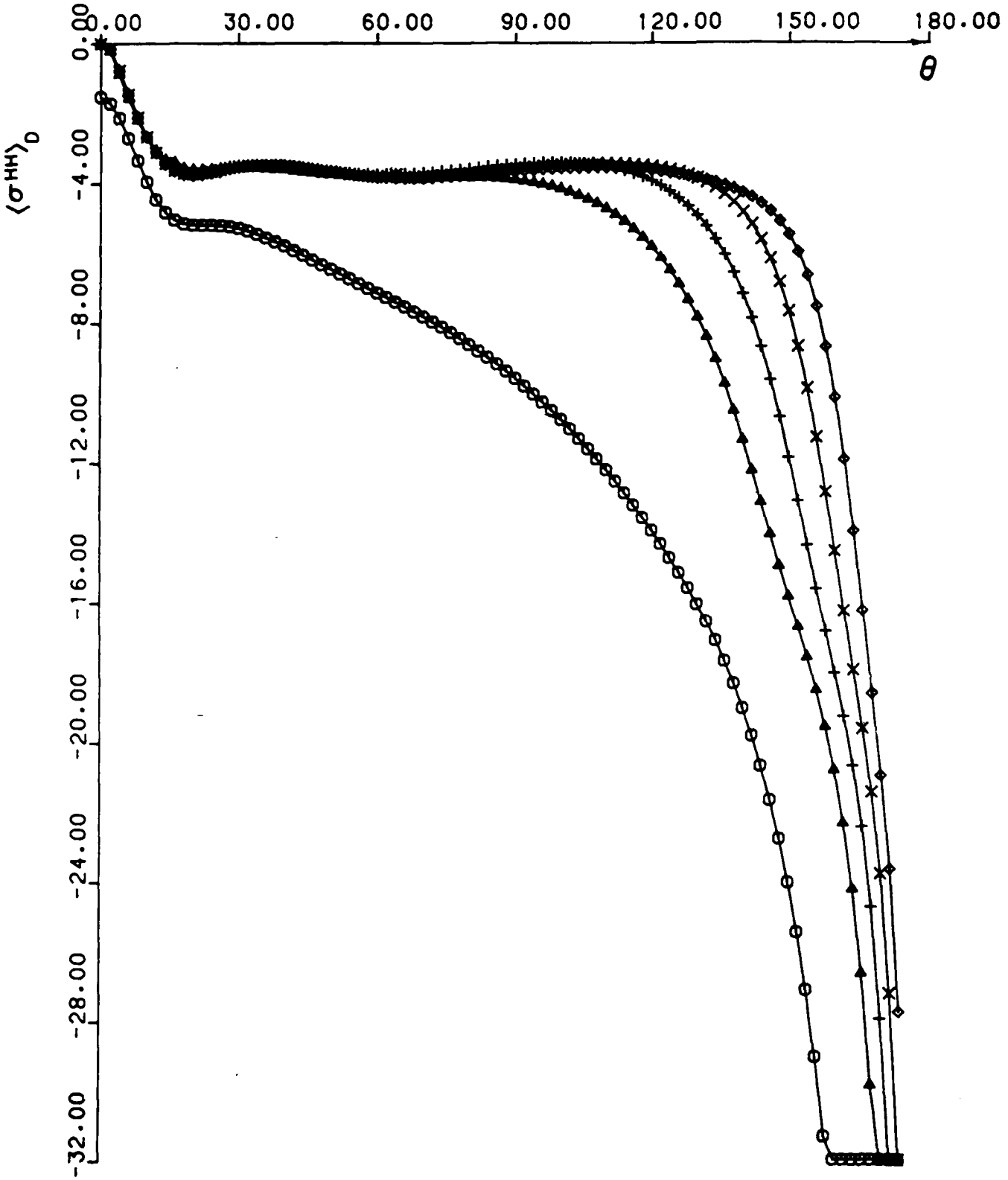
0.00
30.00
60.00
90.00
120.00
150.00
180.00
θ
0.00
-4.00
-8.00
-12.00
-16.00
-20.00
-24.00
-28.00
-32.00
⟨σ^HH⟩_D

Fig. 26

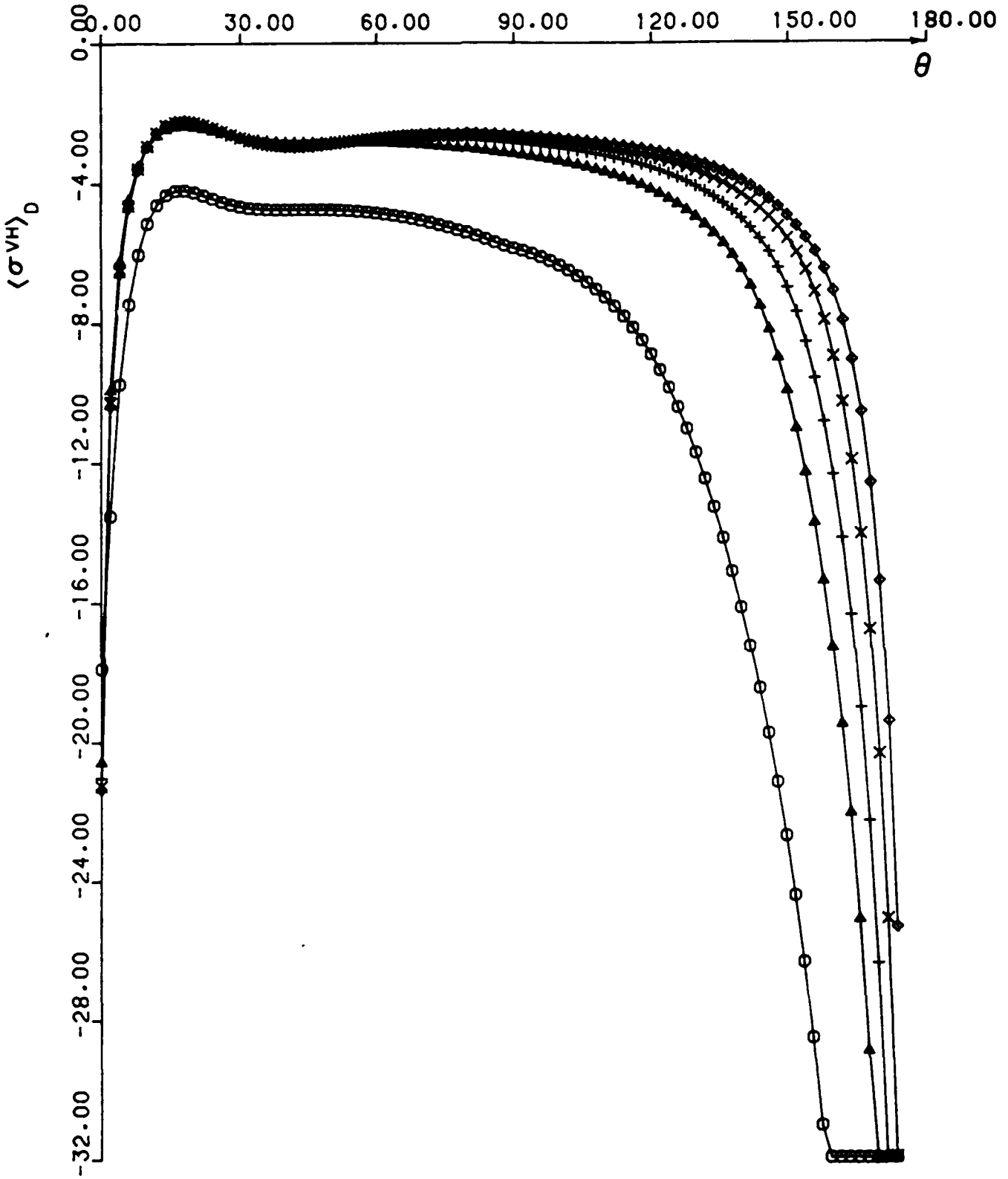

Fig. 27

APPENDIX B

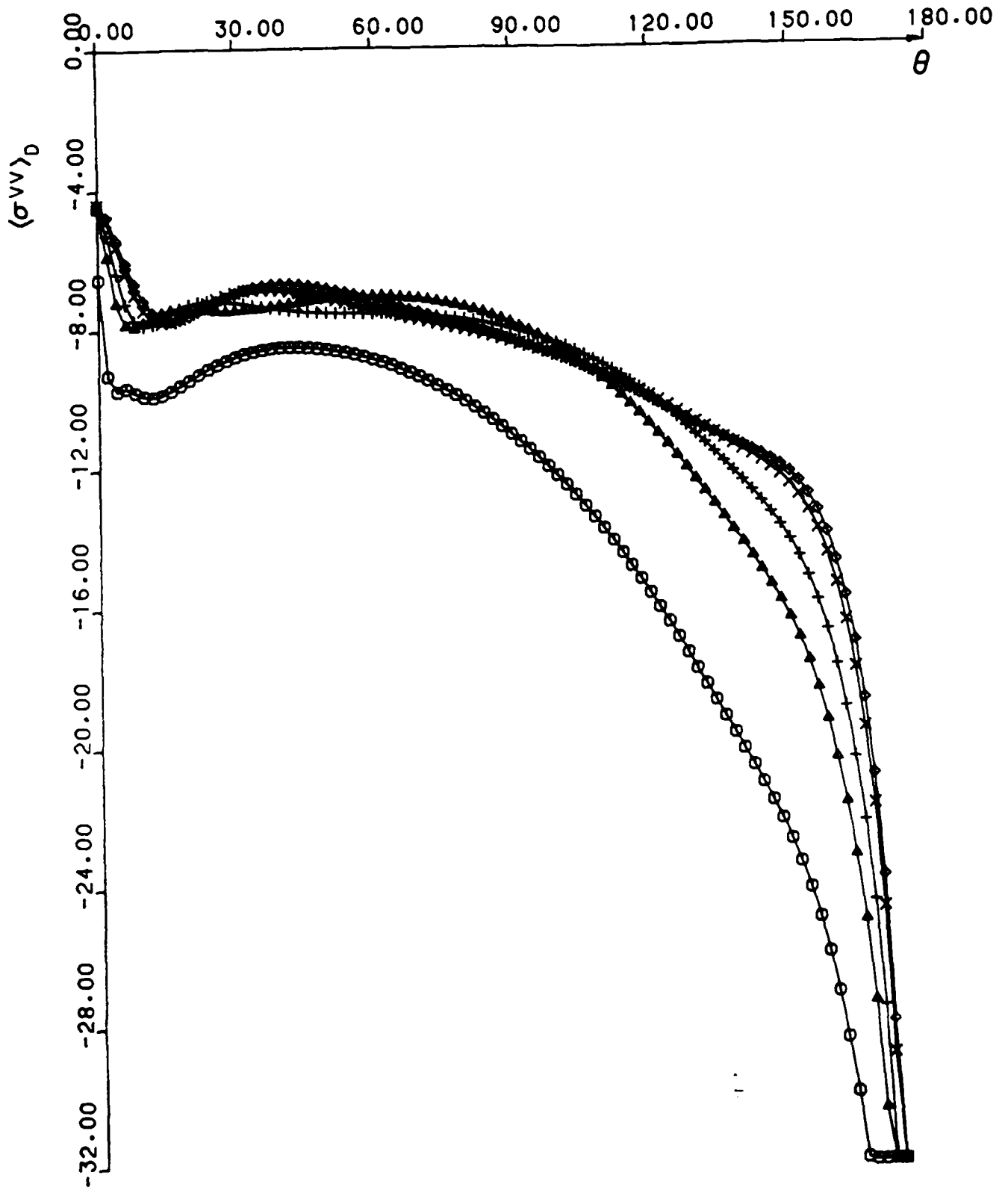

Fig. 28

APPENDIX B

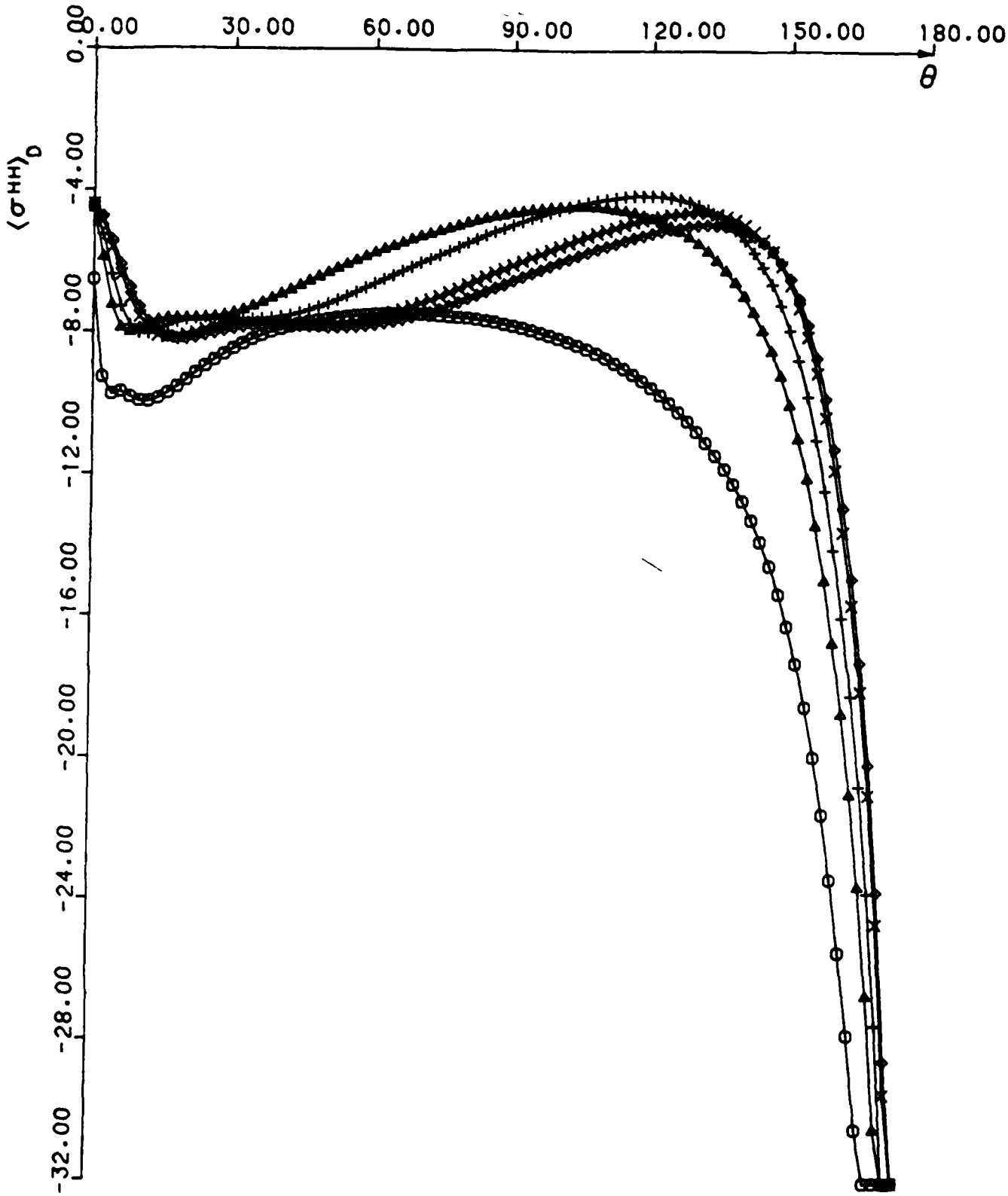

Fig. 29

APPENDIX B

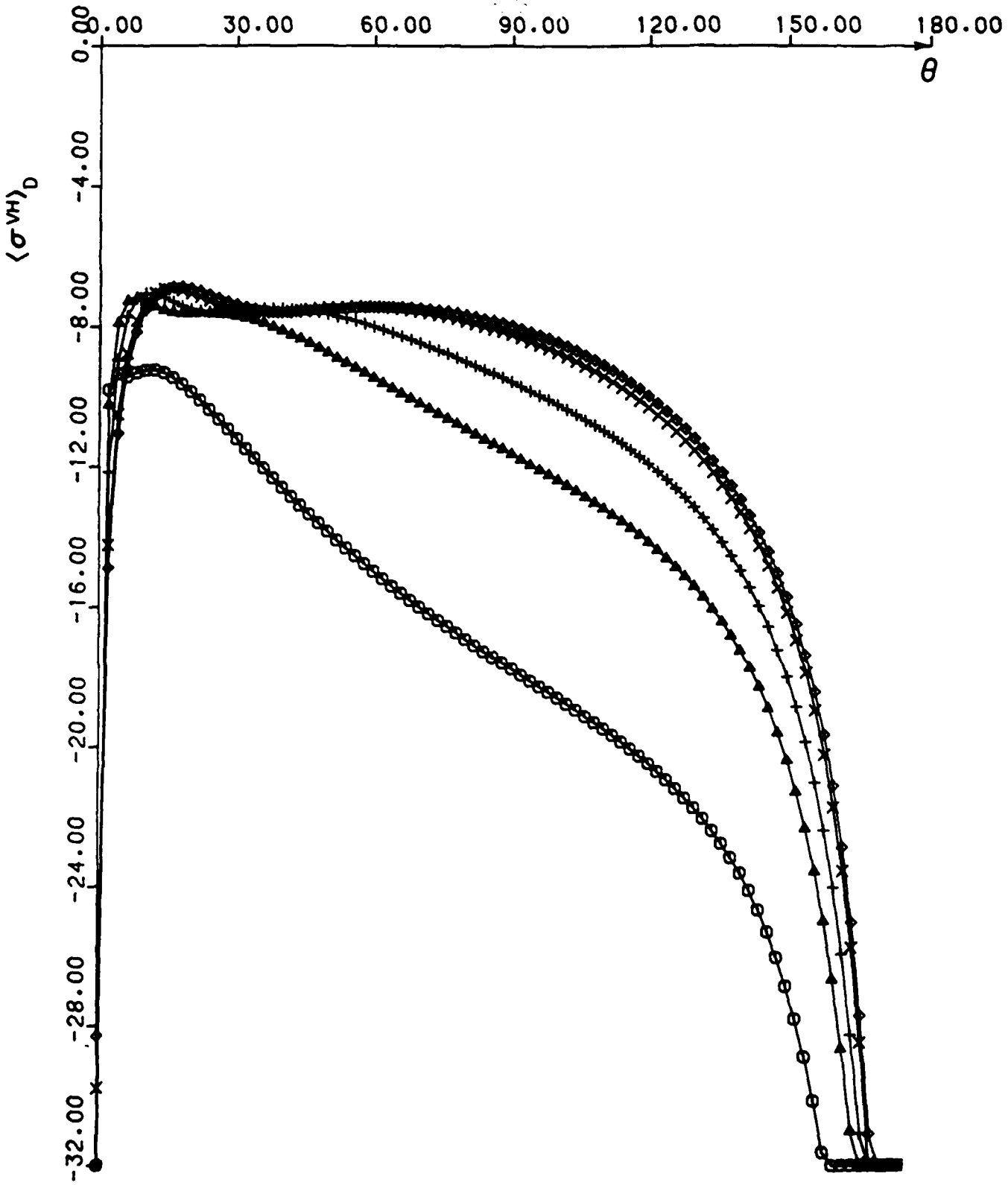

Fig. 30

APPENDIX B

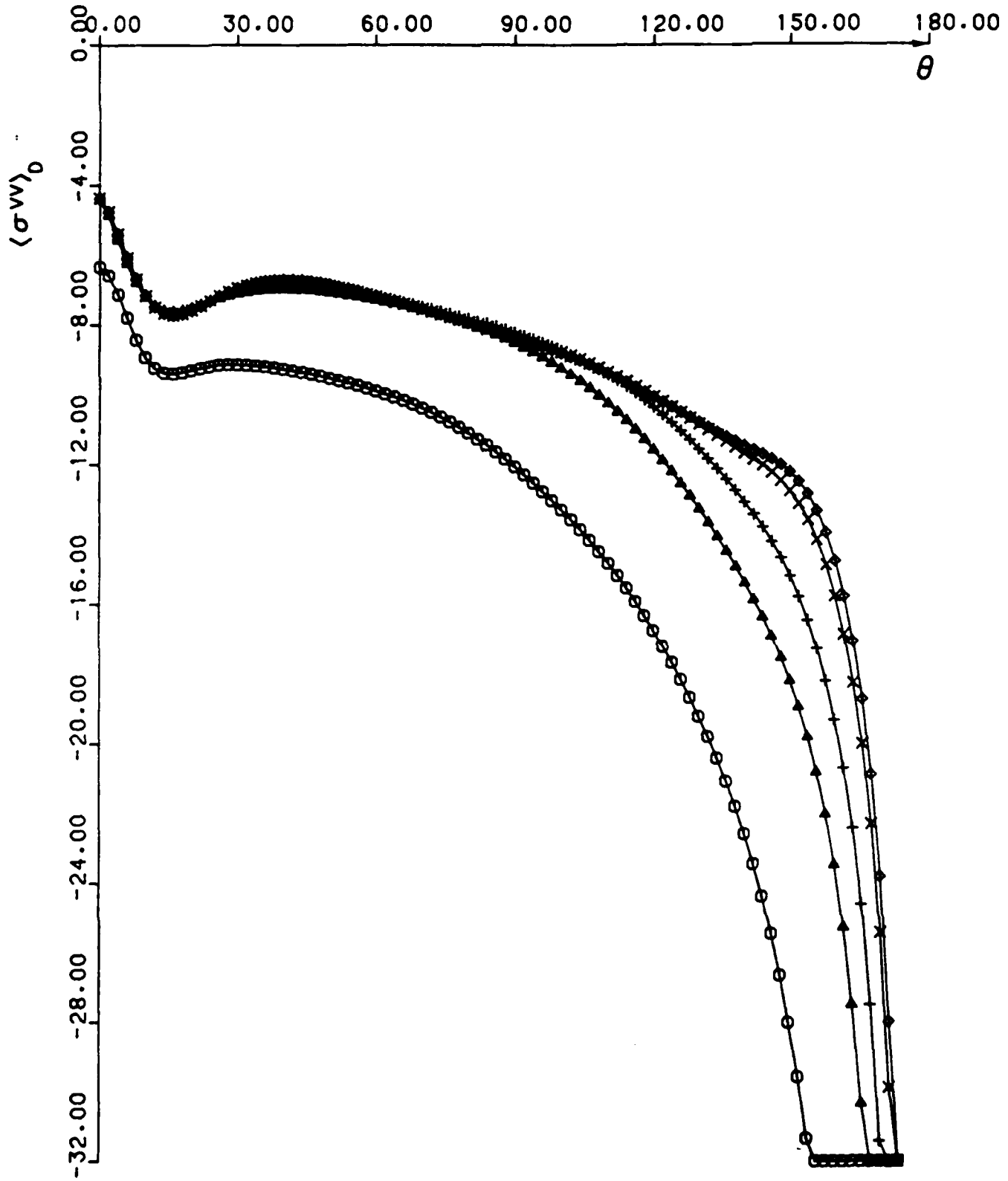

Fig. 31

APPENDIX B

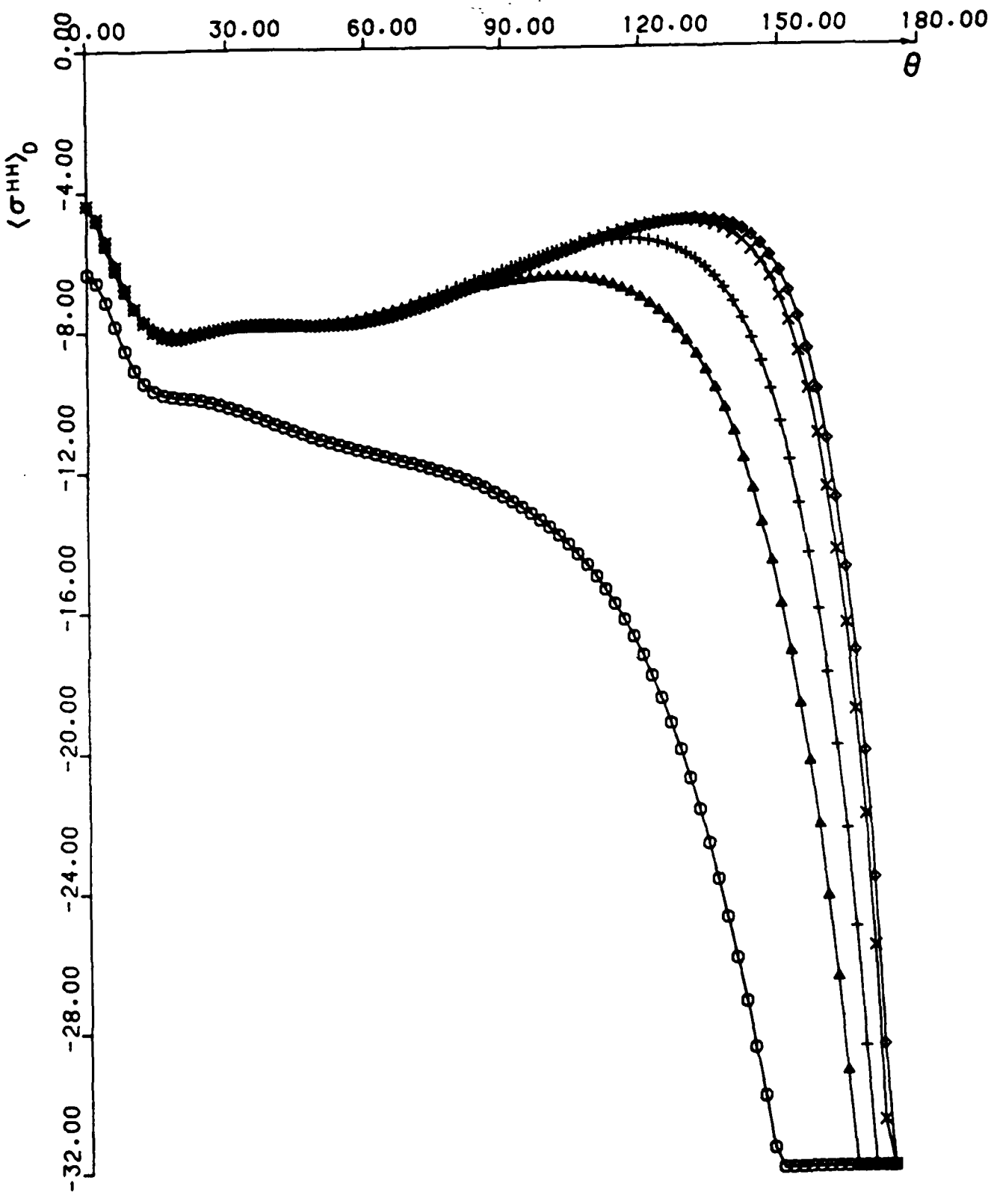
0.00
30.00
60.00
90.00
120.00
150.00
180.00
θ
$\langle\sigma^{HH}\rangle_0$
0.00
-4.00
-8.00
-12.00
-16.00
-20.00
-24.00
-28.00
-32.00

Fig. 32

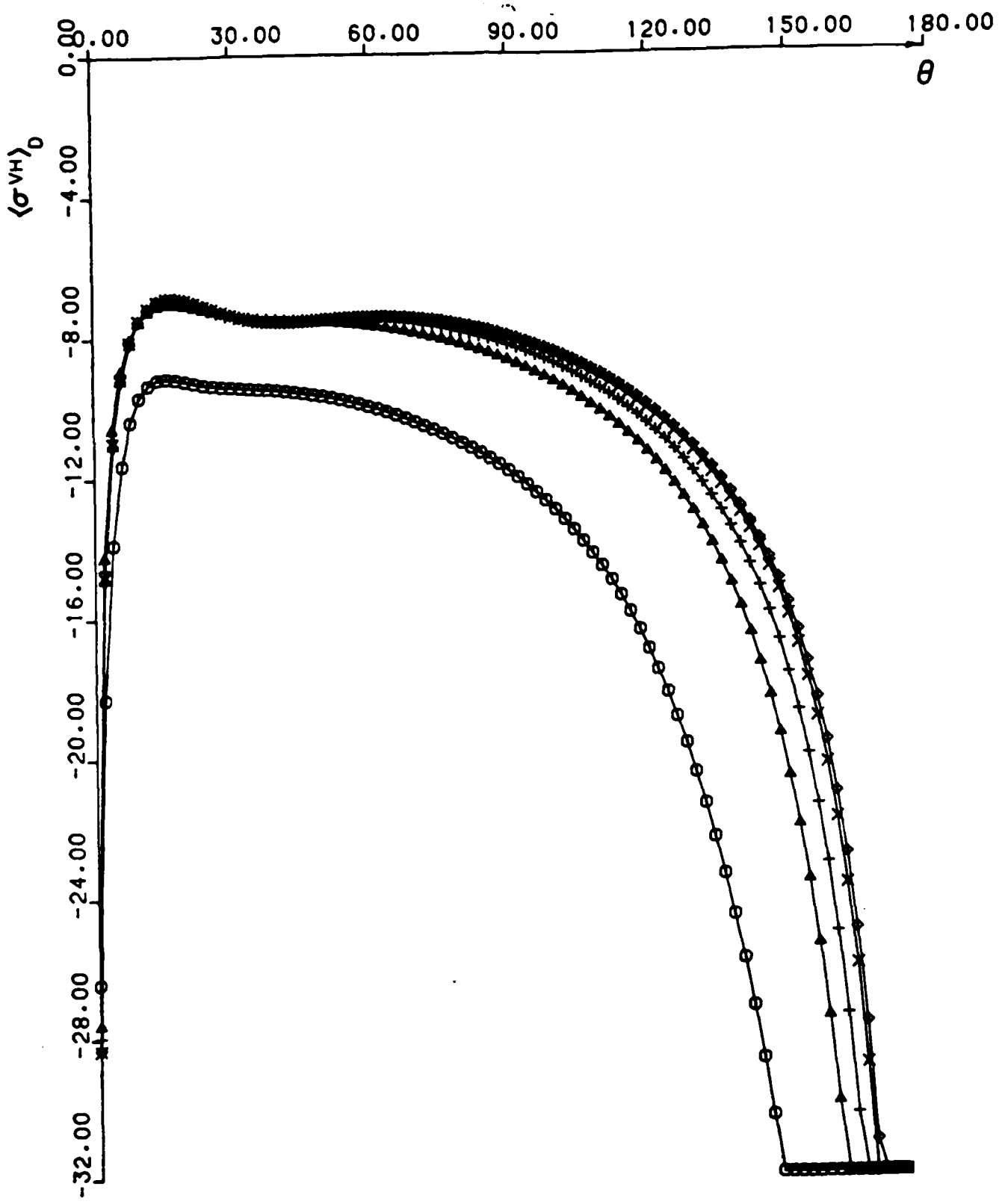

Fig. 33

APPENDIX B

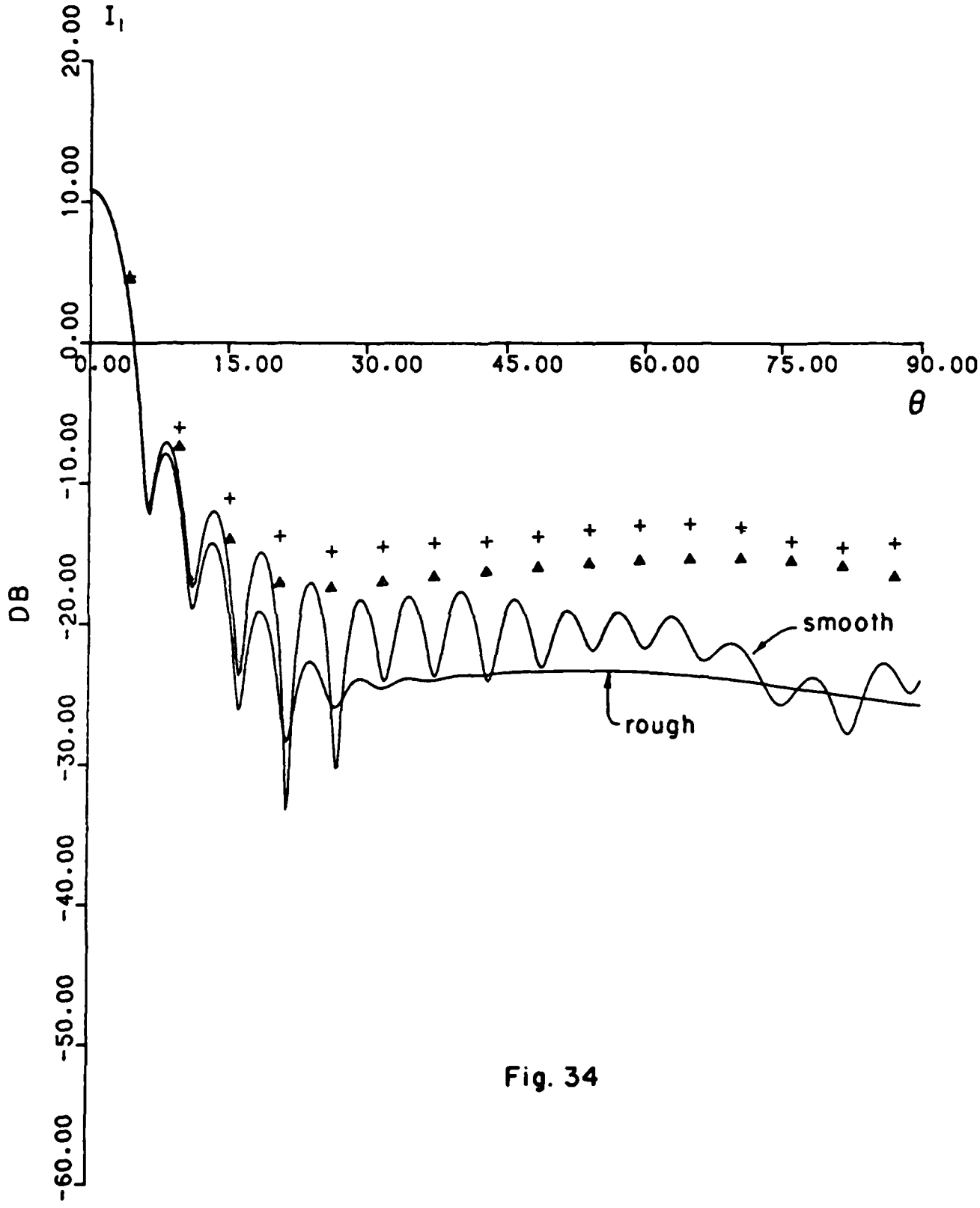

Fig. 34

APPENDIX B

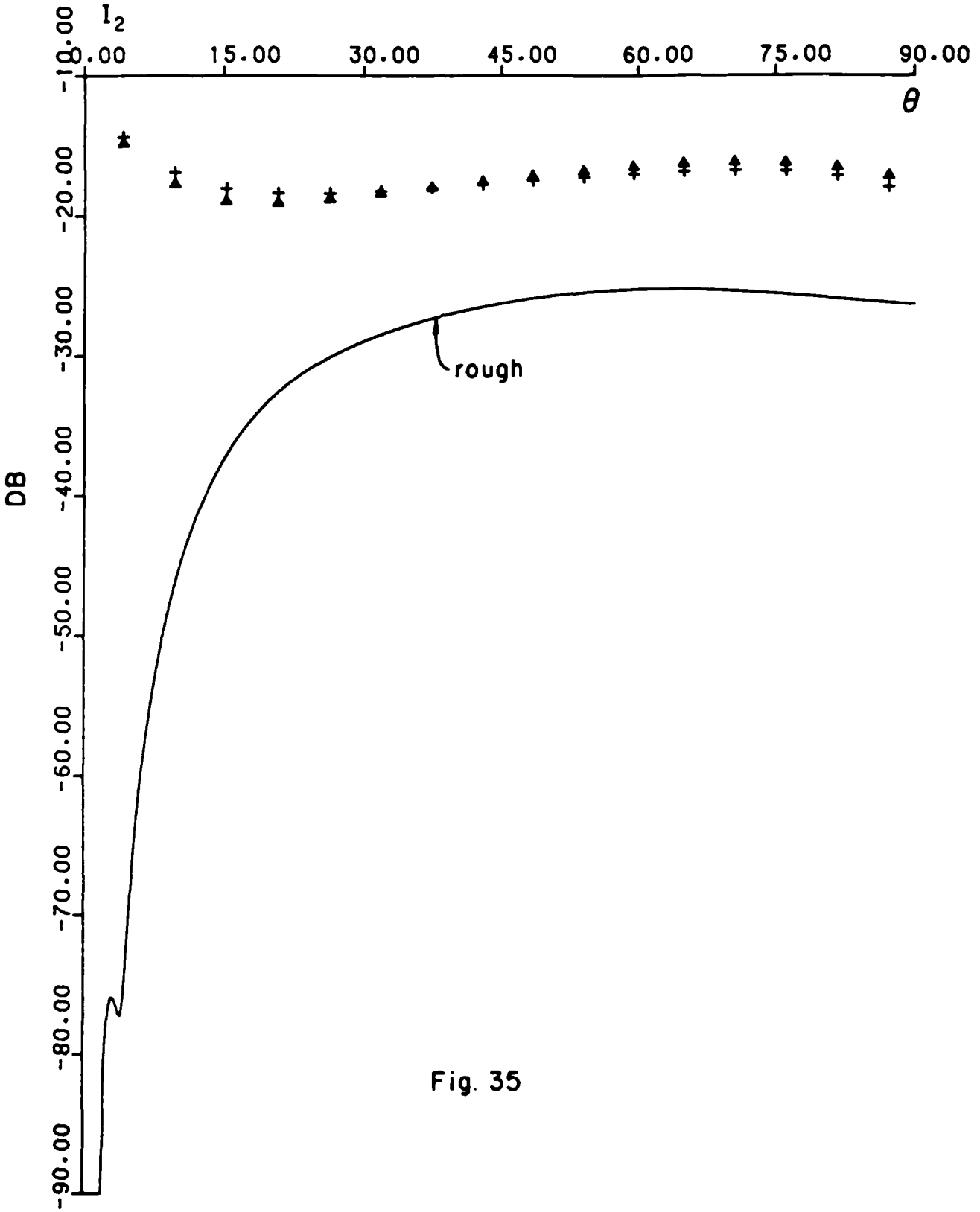

Fig. 35

APPENDIX B

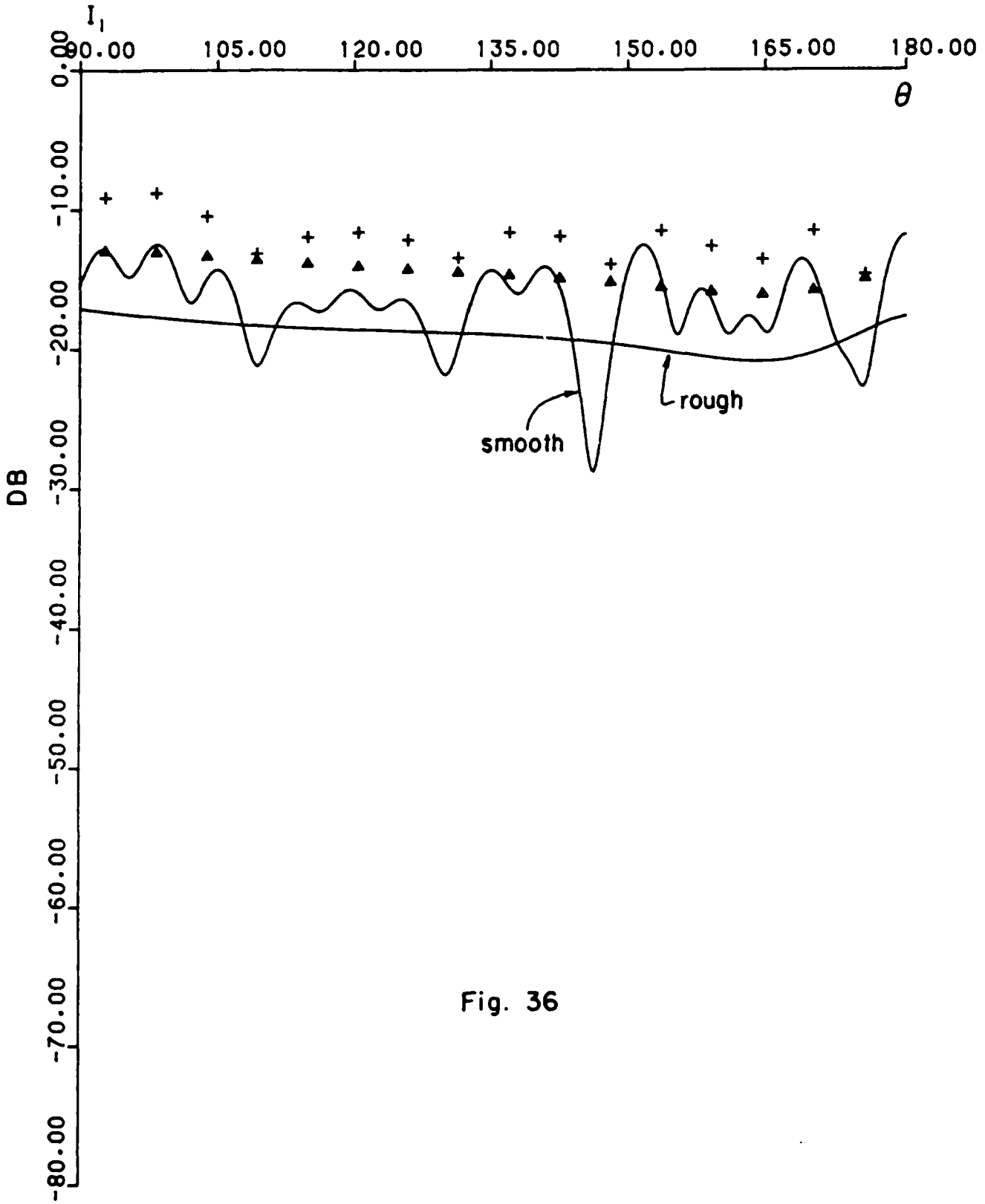
I_1
90.00
105.00
120.00
135.00
150.00
165.00
180.00
θ
0.00
-10.00
-20.00
-30.00
-40.00
-50.00
-60.00
-70.00
-80.00
DB
smooth
rough

Fig. 36

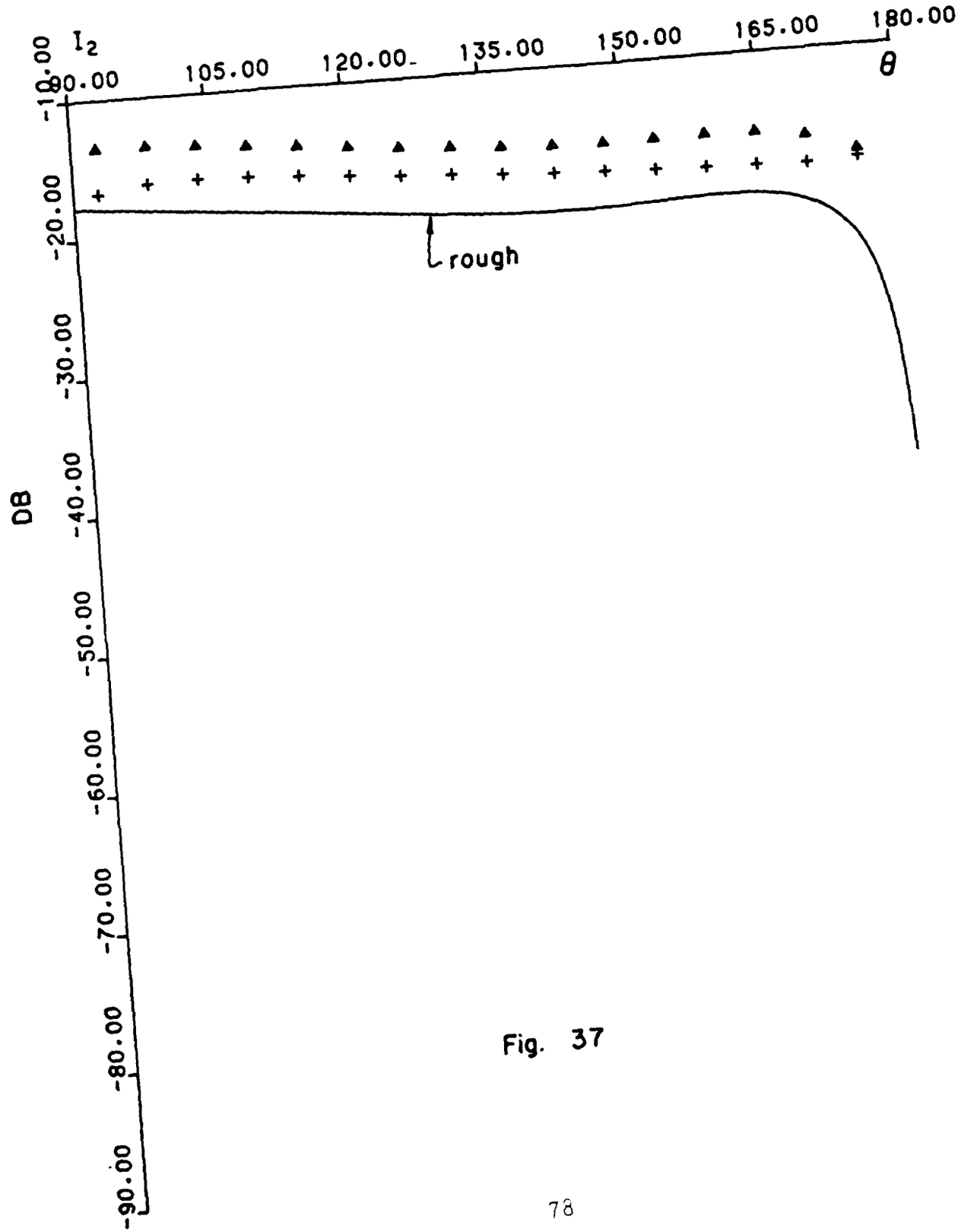

Fig. 37

APPENDIX B

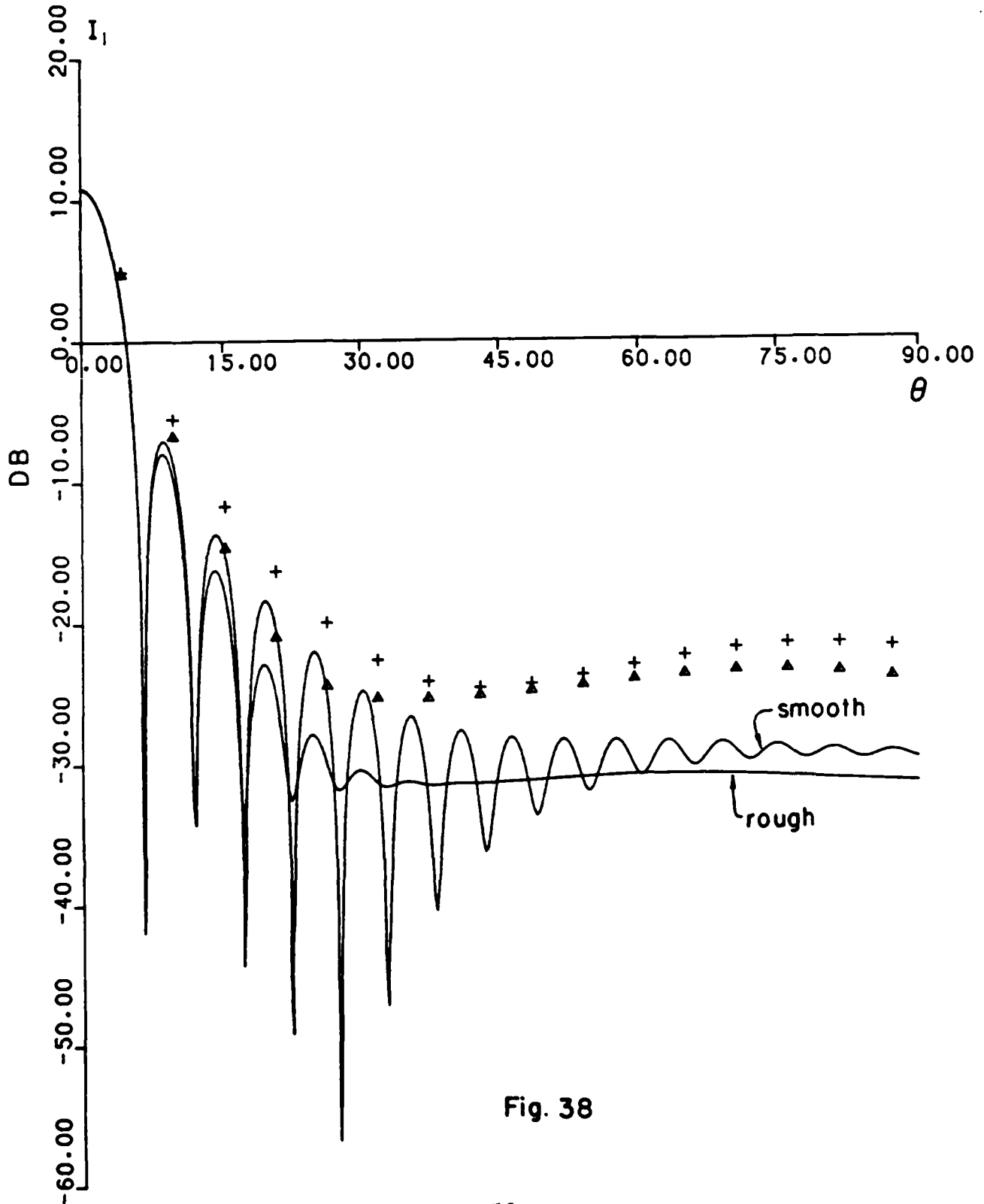
I_1
20.00
10.00
0.00
0.00
15.00
30.00
45.00
60.00
75.00
90.00
θ
DB
-10.00
-20.00
-30.00
-40.00
-50.00
-60.00
smooth
rough

Fig. 38

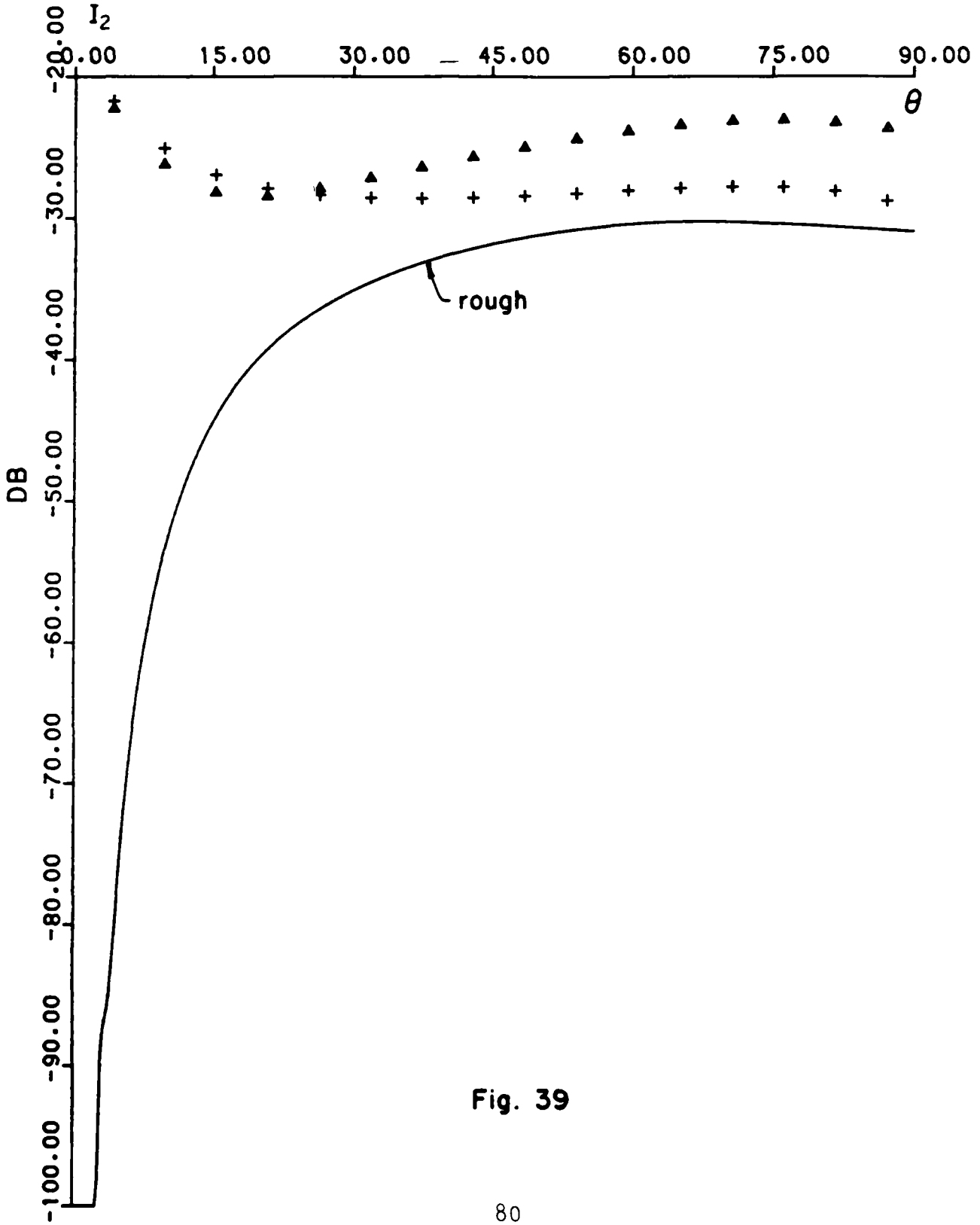

Fig. 39

APPENDIX B

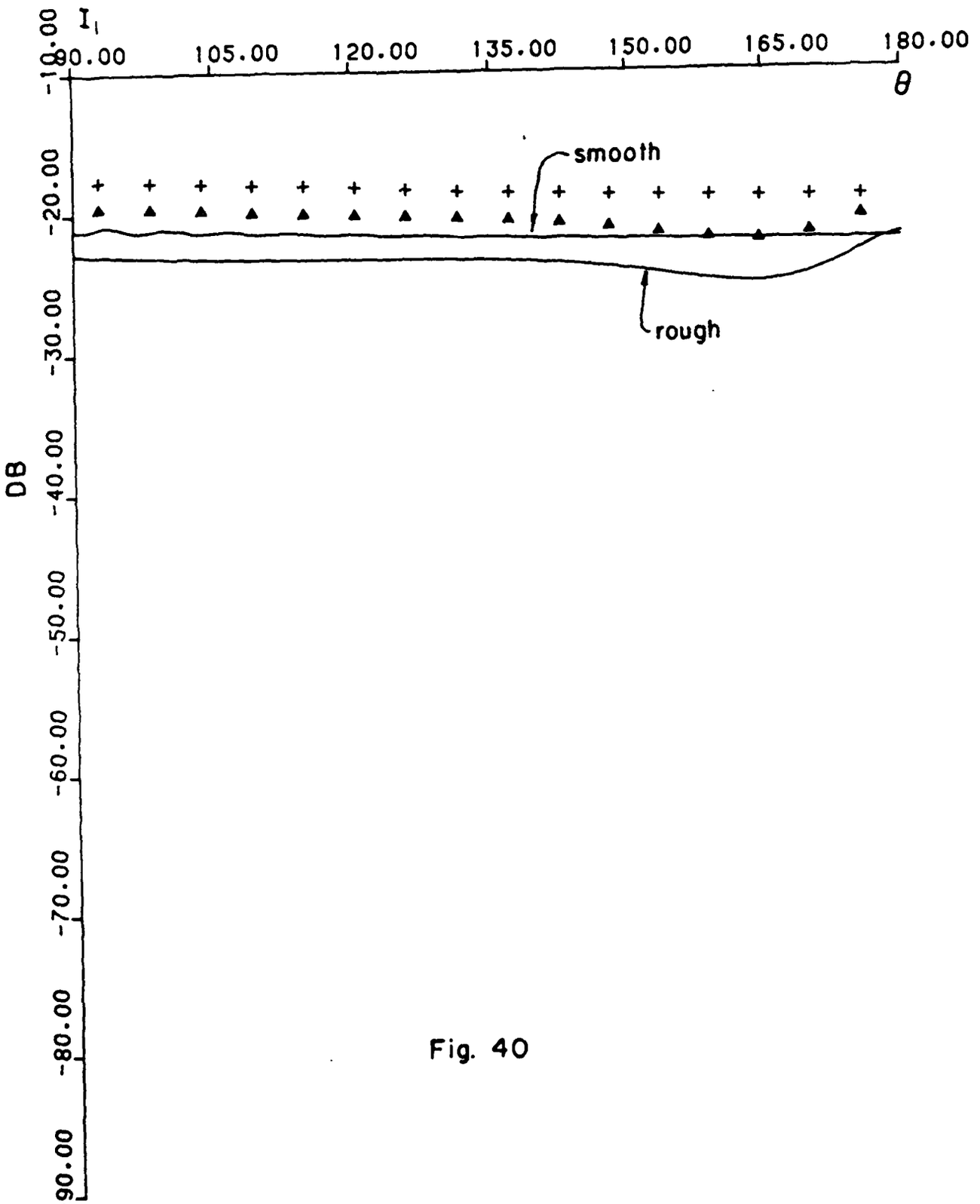

Fig. 40

APPENDIX B

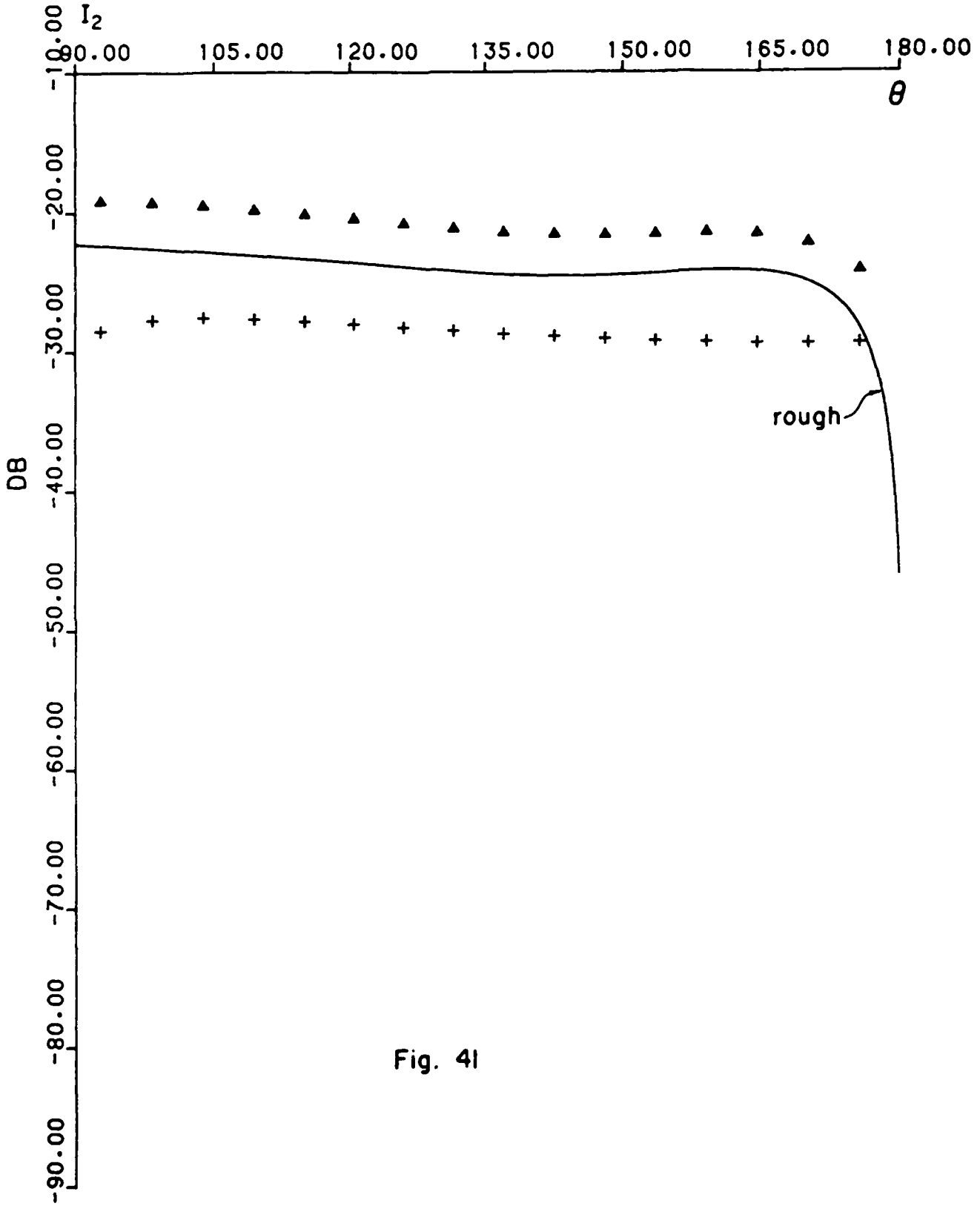

Fig. 41

APPENDIX B

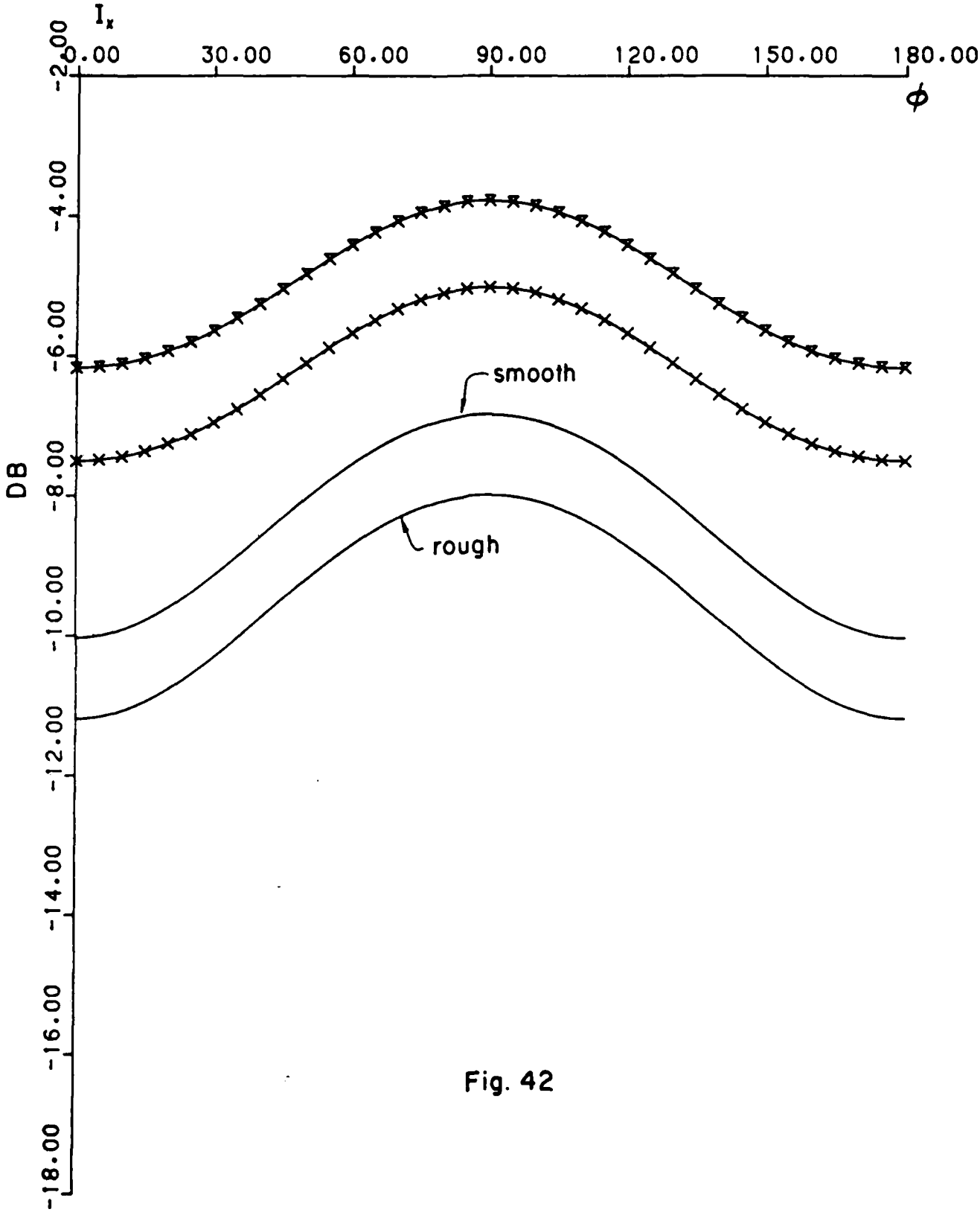

Fig. 42

APPENDIX B

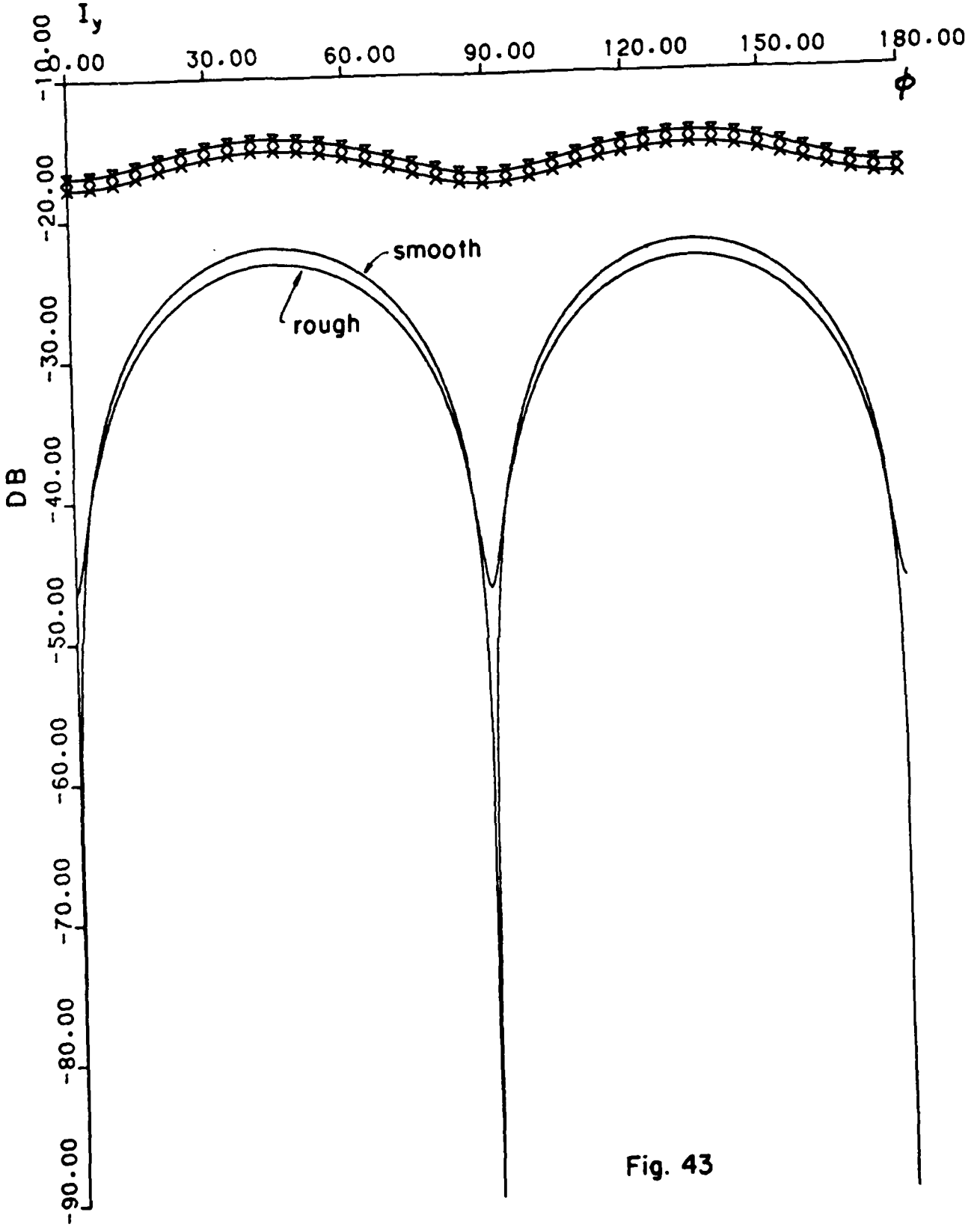
I_y
0.00
30.00
60.00
90.00
120.00
150.00
180.00
ϕ
-10.00
-20.00
-30.00
-40.00
-50.00
-60.00
-70.00
-80.00
-90.00
DB
smooth
rough

Fig. 43

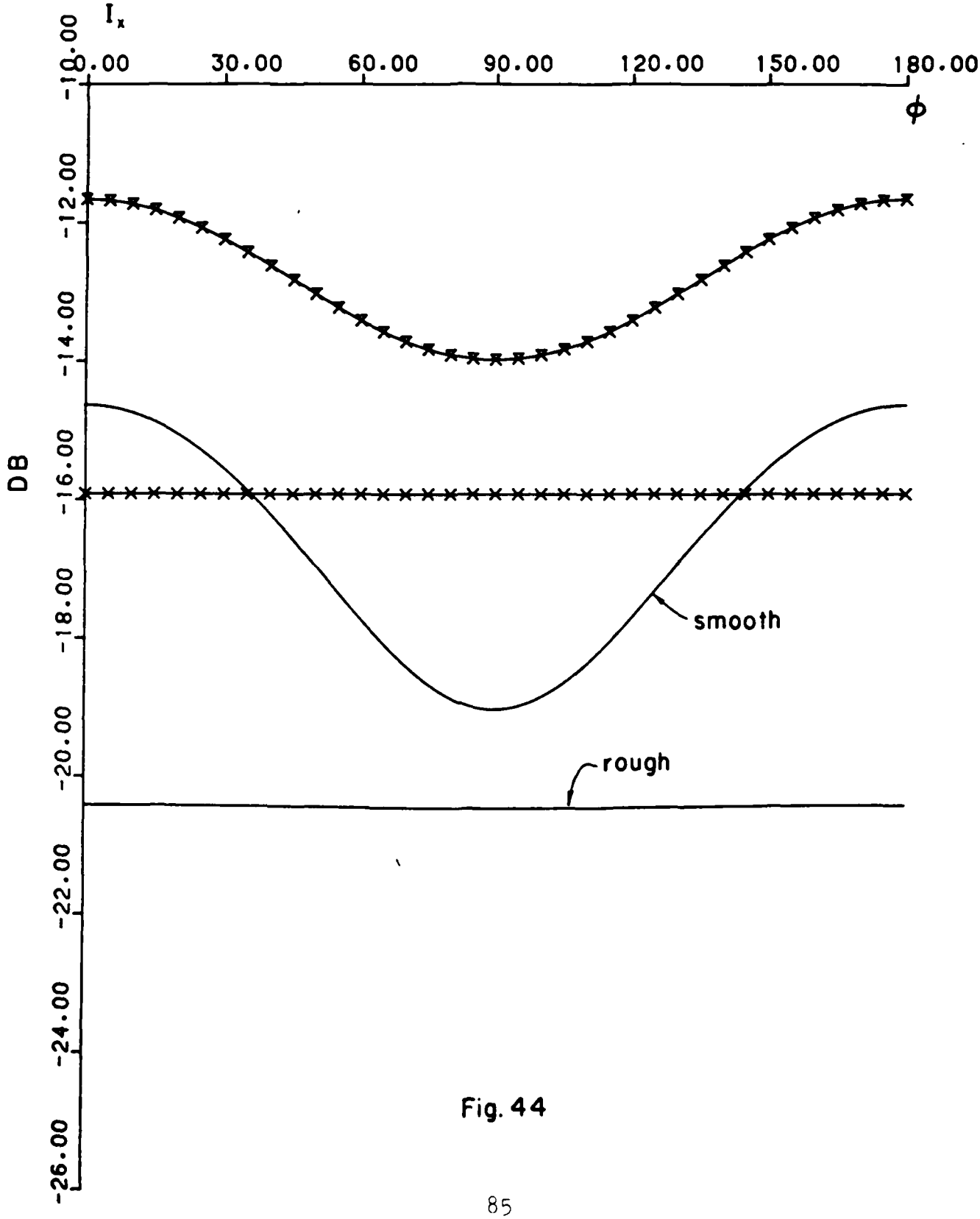

Fig. 44

APPENDIX B

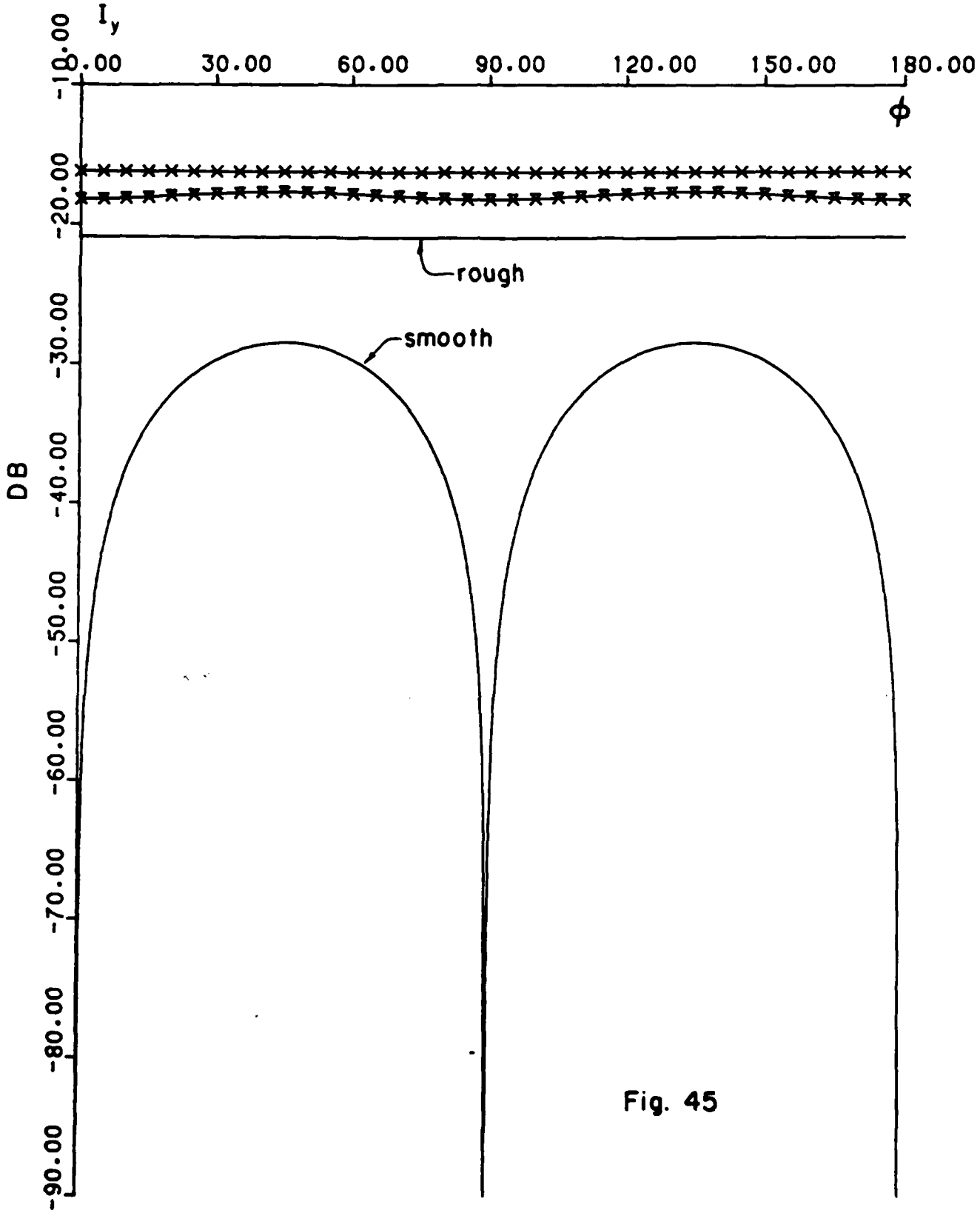
I_y
0.00
30.00
60.00
90.00
120.00
150.00
180.00
ϕ
-10.00
-20.00
-30.00
-40.00
-50.00
-60.00
-70.00
-80.00
-90.00
DB
rough
smooth

Fig. 45

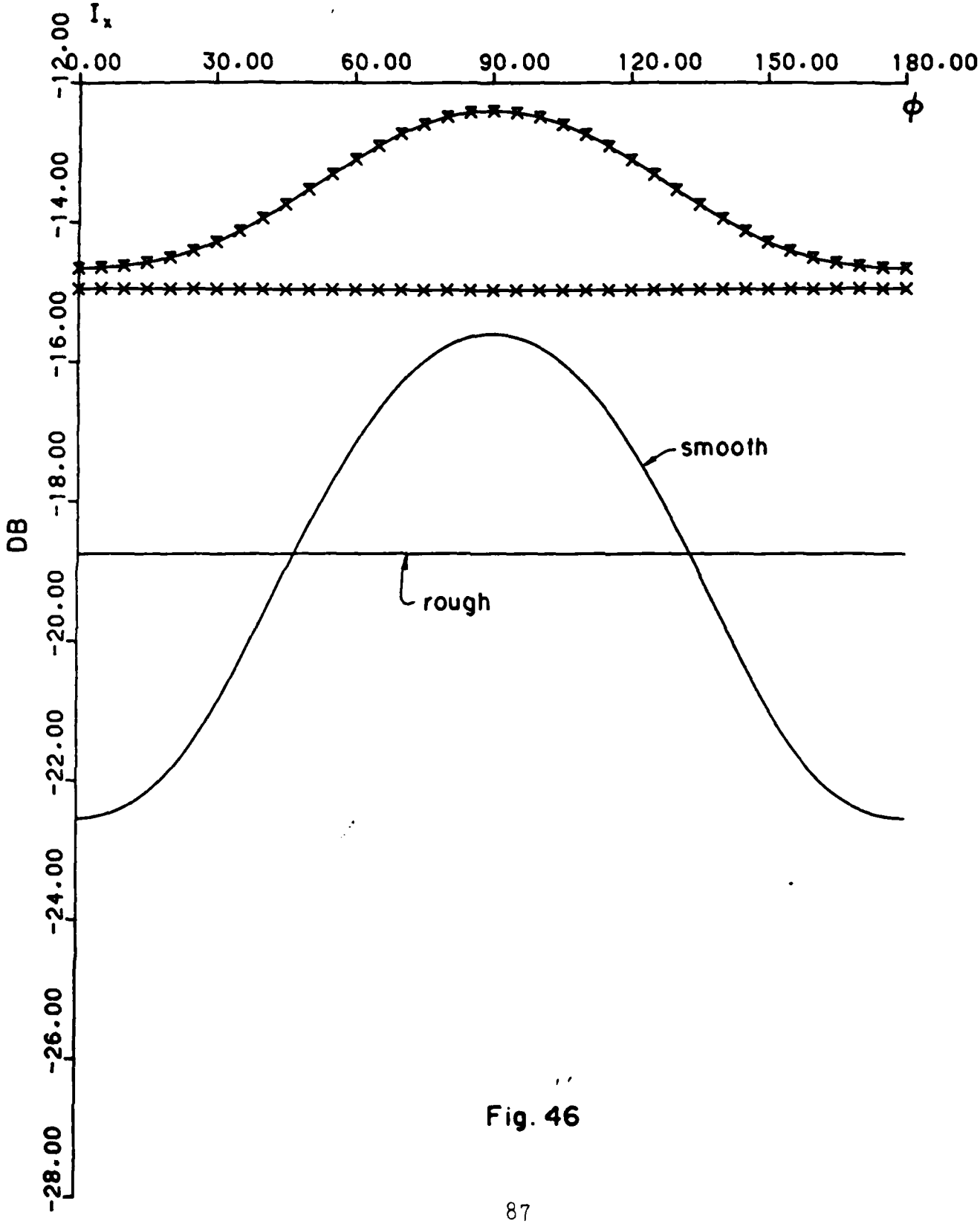

Fig. 46

APPENDIX B

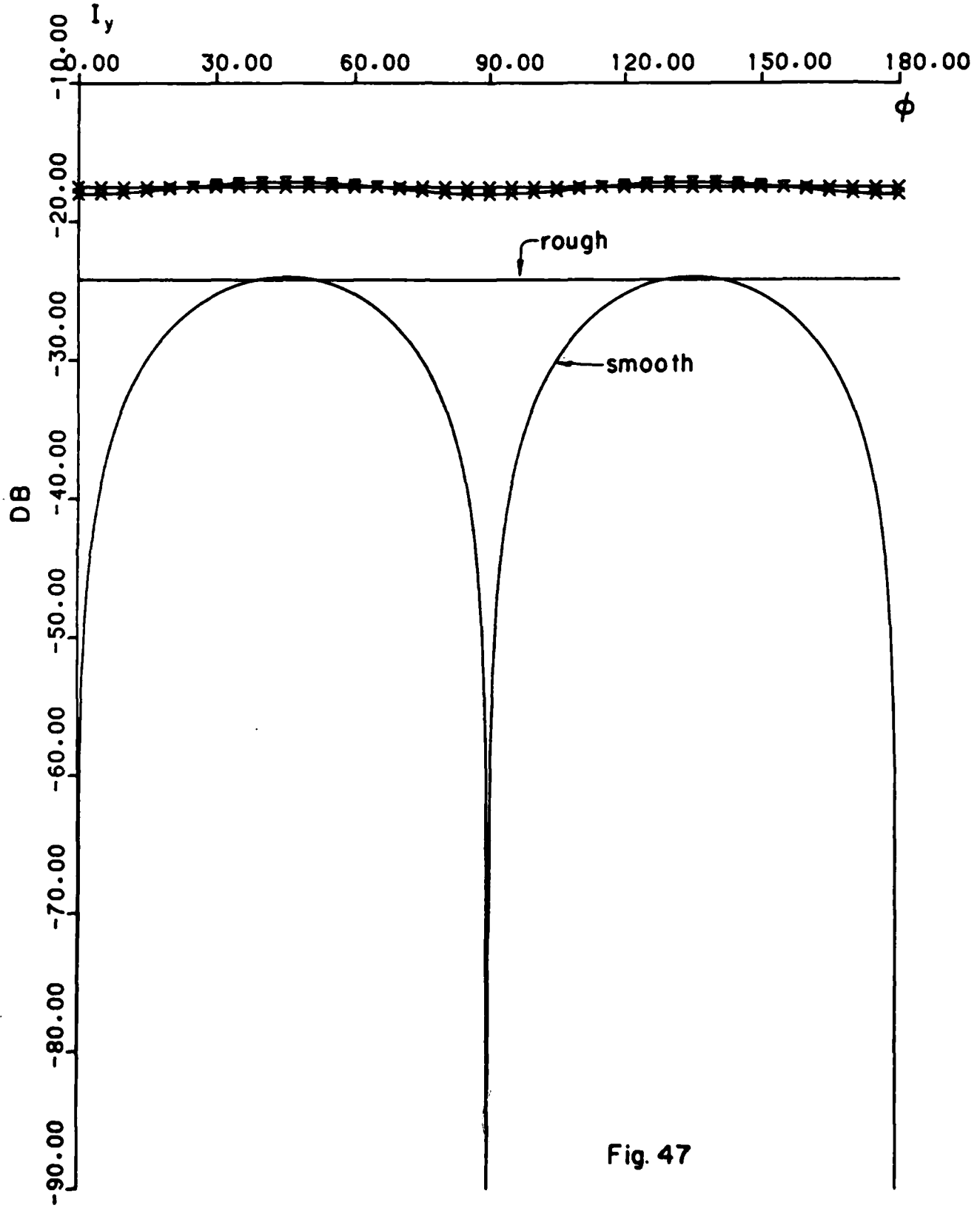

Fig. 47

APPENDIX B

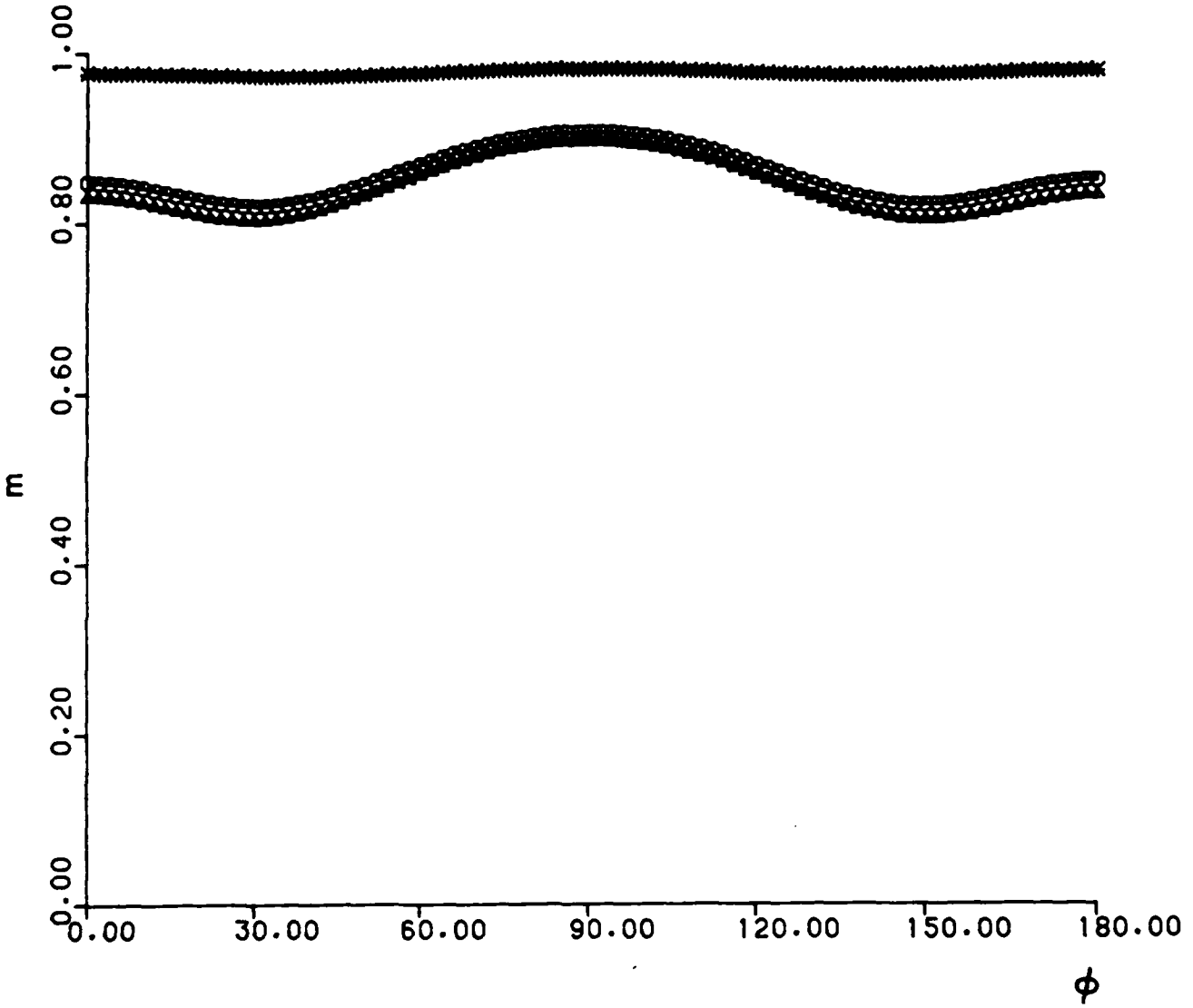

Fig. 48

APPENDIX B

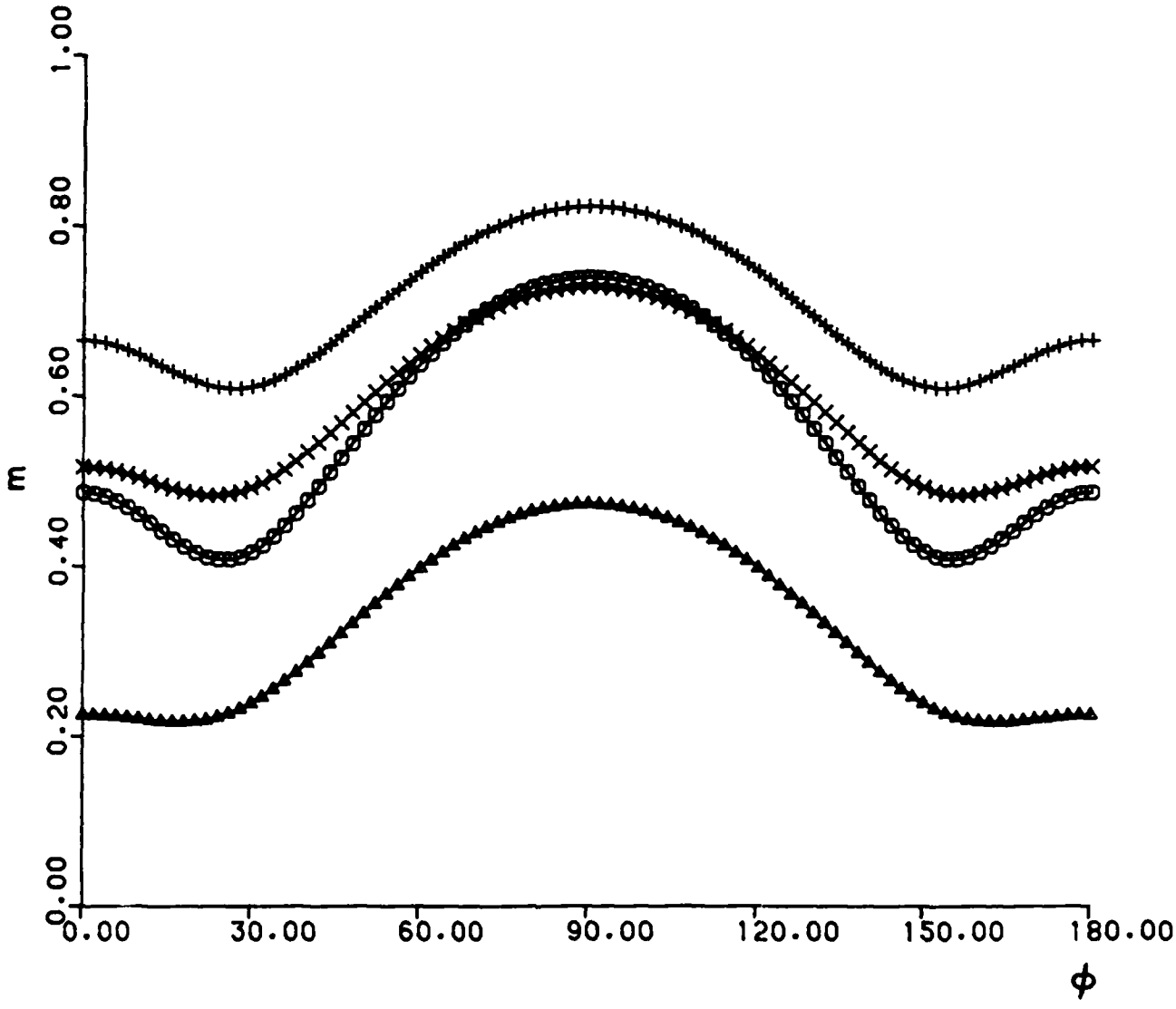
1.00
0.80
0.60
0.40
0.20
0.00
m
0.00
30.00
60.00
90.00
120.00
150.00
180.00
ϕ

Fig. 49

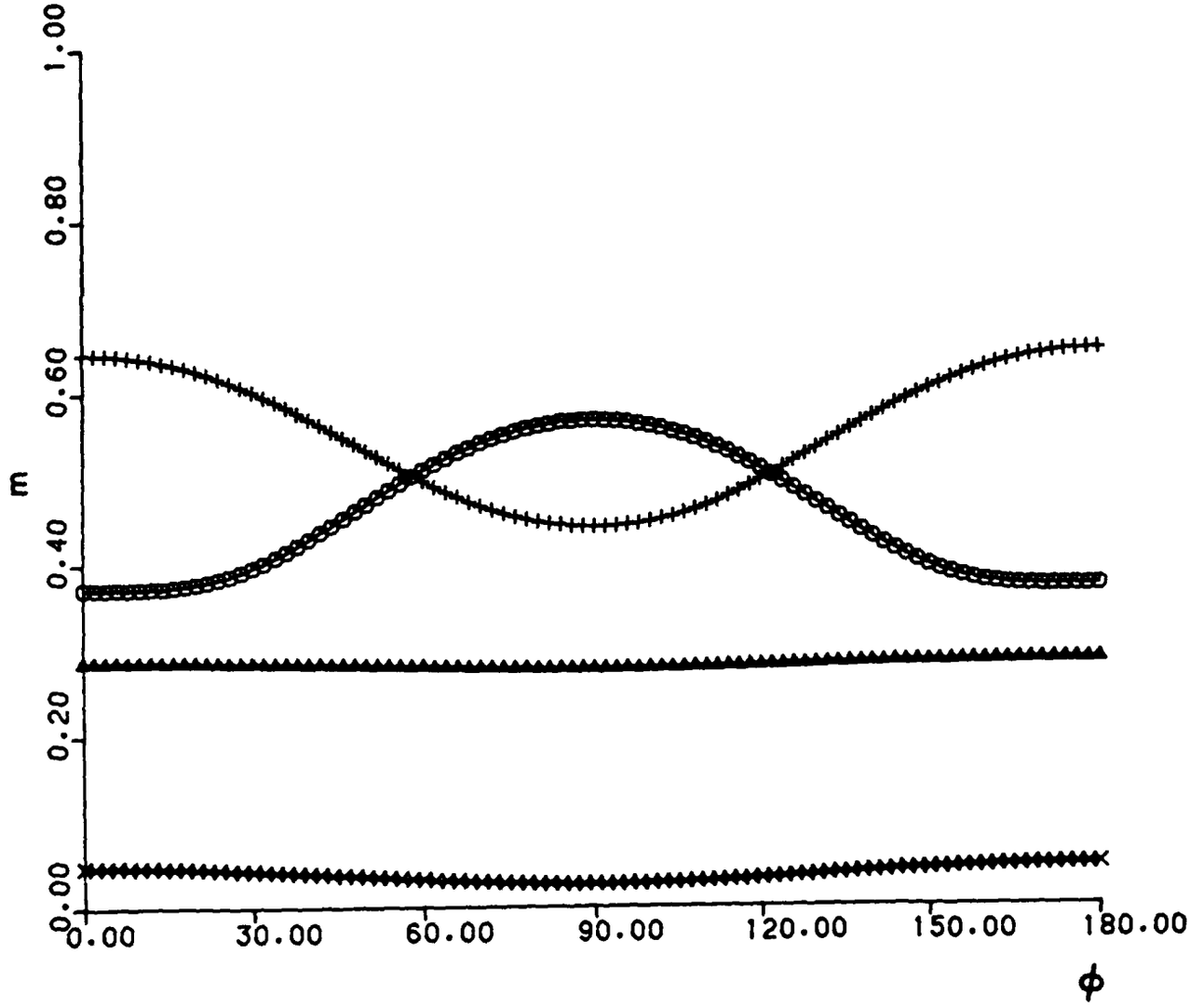
1.00
0.80
0.60
0.40
0.20
0.00
m
0.00
30.00
60.00
90.00
120.00
150.00
180.00
ϕ

Fig. 50

END

DTIC

8—86